RESTORING AUDITORY FUNCTION IN MAMMALS USING AAV-BASED GENE THERAPY

Ana E Amariutei

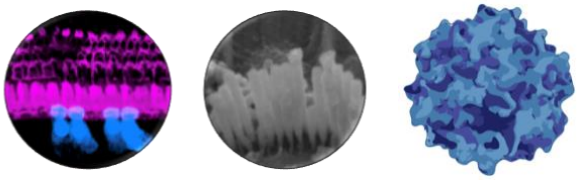

June 2023

The University of Sheffield
Faculty of Science
Department of Biosciences

Table of contents

Acknowledgements

I did not take any of the steps during my PhD alone, so I would like to thank those who guided and helped.

I will begin with my supervisor – Professor Walter Marcotti, who always provided me with support, fuelled me with ideas, knowledge and ambition and helped me develop from an academic and personal perspective. He is the person who cares so much about this topic that managed to inspire me during my Bachelor's degree to choose this field. I am aware that I could not have had a better research supervisor and manager. Thank you ever so much for absolutely everything!

Thanks to my most influential lecturers – Doctor Stuart Johnson, Doctor Laura Corns and Doctor Federico Ceriani who taught me to appreciate the hearing field and helped me understand science concepts. Your insights are to be found throughout this thesis.

To my work colleagues – Lara, Francesca and Niovi – you made the days of failed experiments bearable. Your laughter, humour and guidance contributed tremendously to my time in and outside of the lab. I am forever grateful for all your support.

To Michelle, for her care for the tiniest and biggest creatures. Your heart is the gentlest one I am yet to meet. Thank you for being there every day!

I also want to thank the community of patients that I am part of and I have been privileged to interact with. They inspired and motivated me to work hard and to research more. Without knowing it, they also contributed to this thesis.

I would also like to thank my family and my closest friends Teodora and Elena for all their support, for listening, for understanding and for being always patient with me. Lastly, but certainly not the least, I would like to thank Felix for the integral role he plays in absolutely everything I do and for being open to learn so much about hearing. It is not easy to do a PhD and be a good daughter, sister, partner, sister-in-law, aunt, and friend.

Thank you all for being there. This was quiet a journey, I do not regret any second of it, but I am aware that I would not have made it without you.

Declaration

I, the author, confirm that the Thesis is my own work, except in cases where it is clearly specified in the text and outlined below. All work that is not my own was reproduced with consent. I am aware of the University's Guidance on the Use of Unfair Means (www.sheffield.ac.uk/ssid/unfair-means). This work has not been previously presented for an award at this, or any other, university.

The plasmid and the small-scale viral production were carried out by Marie-Jose Lecomte and Saaid Safieddine at Institute Pasteur, Paris, France.

All scanning electron microscopy processing post-fixation was carried out by Anna Underhill and Adam Carlton.

Abstract

Hearing loss is the most common sensory disorder in humans, and it is estimated that approximately 2.5 billion people worldwide will be affected by 2050 (World Health Organisation). Profound deafness and progressive hearing loss have an impact on the quality of life of both children and adults. Despite the prevalence of hearing dysfunction in the population, there are no available treatments for it. In the auditory system, acoustic information is translated into electrical signals by the sensory hair cells in the cochlea, which are the primary target of genetic mutations leading to hearing loss. A key protein involved in the development and function of the hair cells is Myosin VIIa. *Shaker-1* mice have a mutation in *Myo7a* and the same mutation in the orthologous gene in humans leads to Usher syndrome type 1, which is a form of congenital hearing loss. In addition to this, mice that have *MYO7A* gene conditionally knocked-out (*Myosin VIIa*$^{fl/fl}$ *x Myosin15-CRE*$^{+/-}$) exhibit cochlear phenotypes that resemble those seen during progressive or age-related hearing loss. The above two mouse models were used in the current study to examine if the auditory function can be restored by AAV- *MYO7A* augmentation.

AAV8 and AAV9 vector serotypes were assessed to determine the transduction efficiency of the hair cells both *ex vivo* and *in vivo MYO7A*was delivered to the inner ear using dual-AAV- *MYO7A*vectors injected through the round window membrane. One-month after surgery, mice were tested for any recovery in their hearing ability using *in vivo* electrophysiology (auditory brainstem recordings). The potential morphological and functional recovery of the hair cells was tested using immunostaining and scanning electron microscopy. The results from the current project show that dual-AAV-*MYO7A* gene-based therapy leads to the partial restoration of hearing capability in the congenital deafness mouse model (*Shaker-1*) and in the progressive hearing loss murine model (*Myosin VIIa*$^{fl/fl}$ *x Myosin15-CRE*$^{+/-}$).

In both mouse models, some of the morphological and biophysical characteristics of the dysfunctional hair cells were reinstated after the transduction of the exogenous gene via AAVs. These results highlight that the inner ear retains its ability to be manipulated even in the adult cochlea. However, further pre-clinical research is needed to optimise the delivery and transduction efficiency of the AAVs into the inner ear, which is an essential step before gene-based therapy can be successfully applied to patients.

List of abbreviations

6J	C57BL/6J
6N	C57BL/6NTac
ABR	Auditory Brain stem responses
Ach	Acetylcholine
AChR	Acetylcholine receptor
AMPA	α-amino-3-hydroxy-5-methyl-4-isoxazolepropionic acid
ANOVA	Analysis of variance
ARHL	Age-related hearing loss
BK	Large conductance Ca2+-activated potassium channel
CAP	Compound action potential
EDTA	Ethylenediaminetetraacetic acid
EPS8	Epidermal Growth Factor Receptor Pathway Substrate 8
I_{Ca}	Calcium current
IHC	Inner hair cell
I_K	Potassium current
I_{Na}	Sodium current
KO	Knock-out
LOC	Lateral olivary complex
MET	Mechanoelectrical transduction
MOC	Medial olivocochlear neurons
MYO15	Myosin15
MYO7A	Myosin VIIa
OHC	Outer hair cell
PBS	Phospho-buffered saline
PCR	Polymerase chain reaction
PFA	Paraformaldehyde
RNA	Ribonucleic acid
SEM	Scanning electron microscopy
SGN	Spiral ganglion neuron
USH	Usher syndrome
VGLUT3	Vesicular glutamate transporter 3

Chapter 1: Introduction

OUTLINE

In the present introduction chapter, the following information related to the project will be addressed:

- the hearing mechanism and the development of hearing organ and function
- auditory system dysfunction with a focus on congenital and age-related hearing loss
- current treatments for hearing loss and unmet medical need
- brief overview of gene therapy approaches with a focus on AAV vectors
- the role of Myosin VIIa in hearing and in congenital and age-related hearing loss
- the scope of the current project.

1.1. The ear and the mechanism of hearing

Aristotle (384 – 322 BC) was credited as being the first to number the five human senses – sight, hearing, olfaction, taste, and touch. The main role of these sensory systems is to inform the central nervous system about stimuli that have their origin within us or are provided by the outside world.

The sense of hearing aids in our communication with the surrounding environment and our ability to understand speech and listen to sound. In addition to this, the ability of perceiving auditory information allows us to avoid dangerous situations and carry out our daily activities without any limitations. The sense of audition is strongly dependent on the hair cells that are located within the inner ear (Marcotti and Masetto, 2010). The hair cells are involved in the mechanoelectrical transduction of sound waves into electrical signals that are transmitted to the brain (Ó Maoiléidigh and Ricci, 2019). To do this, sound first reaches the outer ear, the pinna, which aids in the collection of sound that is then transmitted to the ear canal. The auditory canal funnels the sound originating from the environment and passes it towards the tympanic

membrane (**Figure 1.1**, Marcotti, 2012). Subsequently, the tympanic membrane vibrates in response to the sound waves and further transmits these vibrations to the middle ear. The middle ear is formed of three bones: the malleus, the incus, and the stapes which act as mechanical transformers that convert the acoustic energy into mechanical energy (**Figure 1.1**, Frolenkov et al., 2004). When sound information reaches these three bones it causes their movement.

Consequently, the motion of the stapes causes the oval window, one of the two openings of the mammalian cochlea, to further vibrate and in this way transfer sound energy inside the inner ear, which includes auditory and vestibular sensory epithelia (**Fig. 1.1**; Marcotti, 2012).

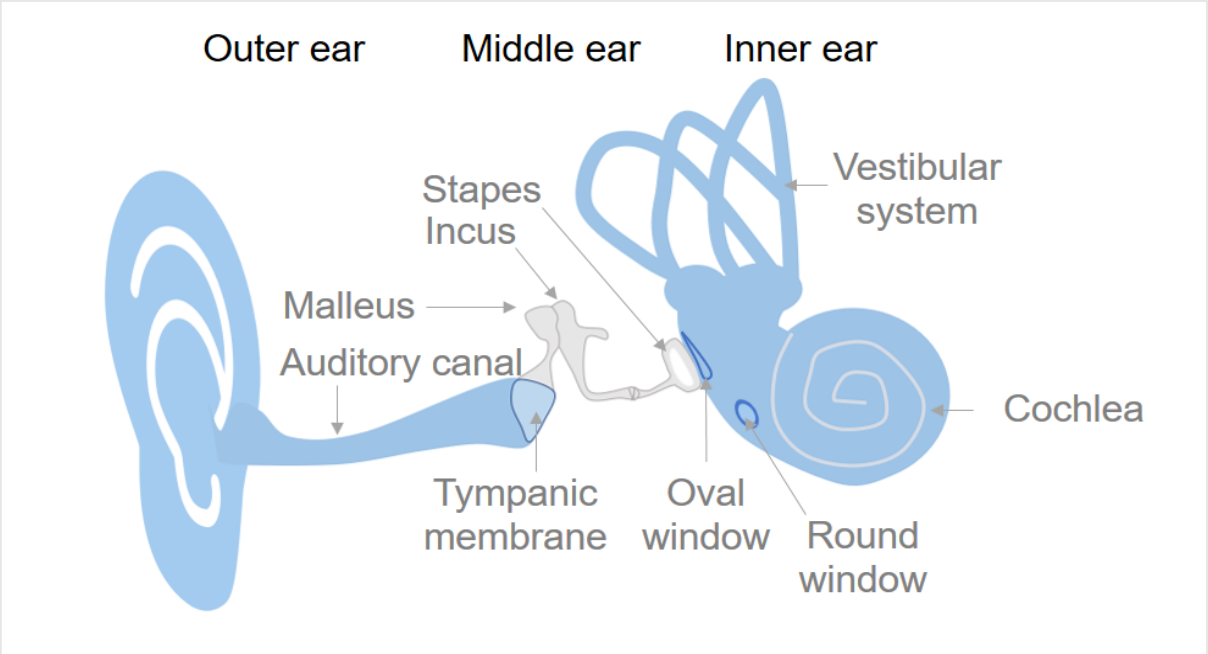

Figure 1.1: Anatomy of the human peripheral auditory system. The ear is divided in three parts: the outer, the middle and the inner ear. The outer ear consists of the pinna, the auditory canal and the tympanic membrane; the middle ear is composed of the malleus, incus and stapes bones; and the inner ear is composed of the vestibular system and the cochlea.

1.2. The role of the auditory hair cells in the process of mechanoelectrical transduction of sound information

The cochlea is a coiled structure that is tonotopically organized, with high frequency sounds detected by the hair cells located towards the basal region and low frequency

sounds detected towards the apical portion (Marcotti and Masetto, 2010). This tonotopicity begins in the cochlea and is maintained up to the auditory cortex in the temporal lobe of the brain. The sensory epithelium of the cochlea is called the organ of Corti and it is localised on top of the basilar membrane (a membrane that moves up and down in response to sound waves, **Figure 1.2**). The organ of Corti consists of one row of inner hair cells (IHCs) and three rows of outer hair cells (OHCs) as well as glia-like supporting cells that surround the hair cells and the nerve fibres (**Figure 1.2**). The IHCs are the primary sensory receptors and are responsible for the transmission of acoustic information to the brain (Hudspeth, 1989). On the other hand, the OHCs are responsible for the amplification of sound information. To achieve sound amplification, the OHCs express in their basolateral membrane a motor protein called prestin, which promotes the elongation and contraction of the cell in response to sound-induced membrane hyperpolarization and depolarization, respectively (Zhang et al., 2000).

The IHCs and OHCs are polarised epithelial cells with an apical and basal side. On the apical side the hair cells have actin-based stereocillia (Petit and Richardson, 2009). The stereocilia are arranged in 3 – 4 rows of increasing height forming hair bundles that are orientated towards the direction of mechanical sensitivity (Petit and Richardson, 2009). The tallest row of stereocilia of the OHCs is embedded or overlaid by the tectorial membrane which helps coordinate their movement and enables the deflection of the stereocilia. Sound causes the basilar membrane to move upwards, which correspond to the rarefaction phase of the sound wave, the hair cell stereocilia moves towards the longer stereocilia or excitatory direction (Fettiplace, 2017). During the compression phase of the sound waves, the basilar membrane moves downwards, and the hair bundles are displaced towards the shorter stereocilia or inhibitory directions. The displacement of the stereocilia of just a few nanometers leads to the

translation of sound information into electrical signals that are transmitted to the brain (Ó Maoiléidigh and Ricci, 2019).

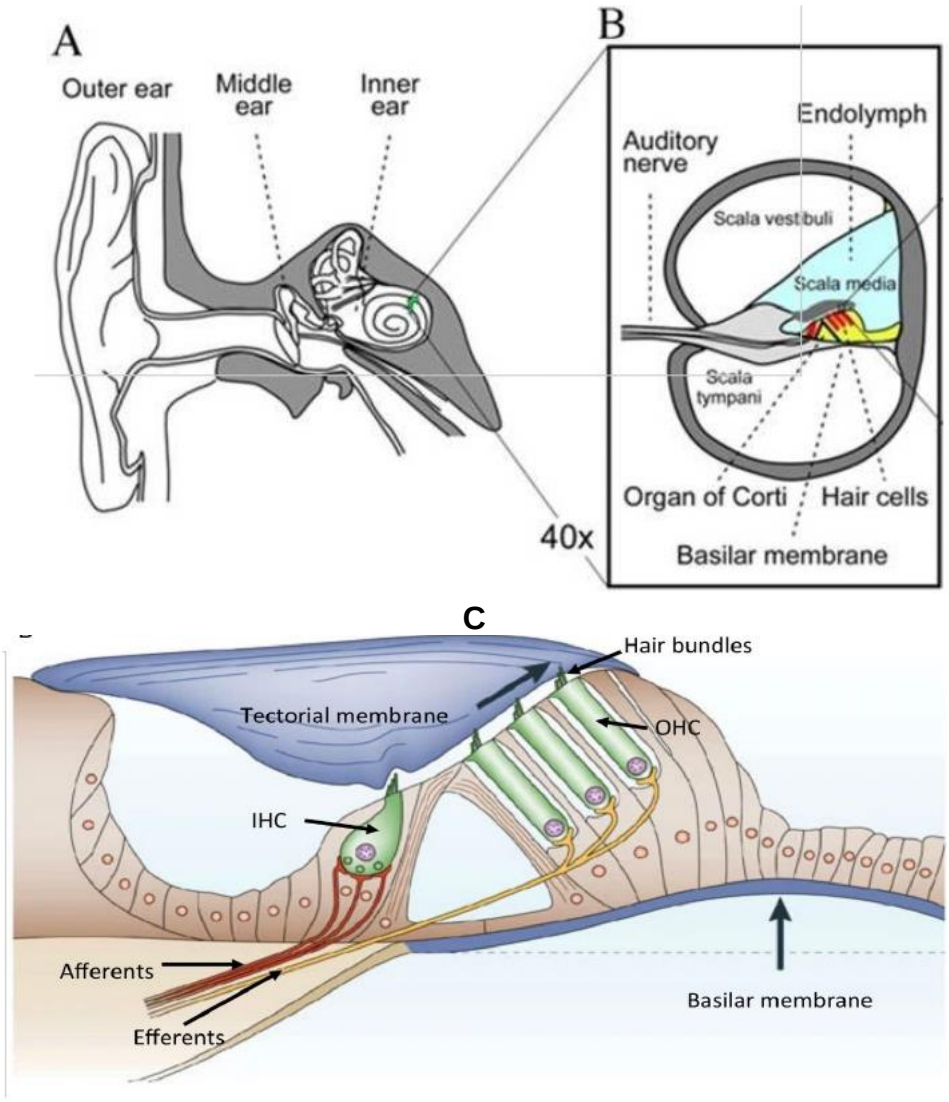

Figure 1.2: The inner ear. (A) Cross section of the ear illustrating the outer, middle and inner ear. **(B)** Figure showing a cross-section of the cochlea with the three chambers – *scala vestibuli, scala media and scala typmani*. The basilar membrane is immersed in perilymph (composition of the scala tympani) and the hair cell bundles are immersed in endolymph (composition of the *scala media*, Elliott and Shera, 2012).**(C)** The organ of Corti is located in the *scala media*. The organ of Corti lies on the basilar membrane and it is overlaid by the tectorial membrane. The organ of Corti is where the sensory hair cells reside – inner hair cells (IHCs, depicted in green) and outer hair cells (OHCs, depicted in green). In the mature cochlea, both IHCs and OHCs are innervated by the Type I and Type II spiral ganglion afferent neurons, respectively (depicted in red). At the same time, the Type I spiral ganglion afferent neurons innervating the IHCs are innervated by lateral olivocochlear efferent neurons (LOC, not shown in this image), while the OHCs are directly innervated by medial olivocochlear efferent neurons (MOC, depicted in yellow).

Sound transduction is also achieved because the mammalian cochlea is made of three compartments – *scala vestibuli*, *scala media* and *scala tympani*. *Scala vestibuli* is the uppermost duct of the cochlea, *scala media* represents the middle cochlear duct that contains the organ of Corti and *scala tympani* is the lowermost duct of the cochlea which is found under the basilar membrane (Duvall and Rhodes, 1967). *Scala vestibuli* and *scala tympani* are filled with perilymph, which is an extracellular fluid with high concentrations of sodium (Na^+, 140 mM) and calcium (Ca^{2+}, 1.3 mM) and low concentrations of potassium (K^+, 5.8 mM, **Table 1**). On the other hand, *scala media* is filled with endolymph that has high concentration of K^+ (150 mM), low concentration of Na^+ (1 mM) and an even lower concentration of Ca^{2+} (20-40 μM, **Table 1**, Raphael and Altschuler, 2003).

Table 1. Composition, pH, osmolarity and potential of the lymphatic components of the inner ear. Information reproduced from Wangemann and Schacht, 1996.

	Perilymph	**Endolymph**
	Scala vestibuli ***Scala tympani***	***Scala media***
Sodium - Na^+	140 mM	1 mM
Potassium - K^+	5.8 mM	150 mM
Calcium - Ca^{2+}	1.3 mM	0.02 – 0.04 mM
Proteins	1 g/L	0.15 g/L
Glucose	4 mM	0.5 mM
pH	7.4	7.4
Osmolarity	290 mosm/L	315 mosm/L
Potential	0 mV	80 – 100 mV

The different ion compositions cause the endolymphatic compartment, where the stereociliary bundles are localised, to reach a potential of about +80 mV compared to the perilymph, which is called endocochlear potential (**Table 1**). The difference between the endolymphatic potential (+80 mV) and the hair cells resting membrane

potential (approximately -60 mV), generates an electrical driving force of about 140 mV that drives cations to enter the hair cells (Fettiplace, 2017). Positive ions such as K^+ enter the hair cell through the mechanoelectrical transducer channel (MET) located at the tip of the shortest rows of stereocilia, and lead to the depolarization of the hair cells (Qiu and Müller, 2018). This depolarization primes the opening of Ca^{2+} channels ($Ca_v1.3$) localized at the basolateral membrane of the hair cells, which drive the calcium-dependent release of glutamate neurotransmitter from the ribbon synapse into the synaptic cleft (Nouvian et al., 2006; Johnson et al., 2019). Glutamate will then bind to AMPA and NMDA receptors localized on the afferent neuron terminals (Weigand and Enz, 2022). This causes the generation of action potentials in the auditory afferent neurons and the transfer of auditory information to the auditory cortex (Johnson et al., 2019).

1.3. Cochlear innervation

1.3.1. Auditory pathways to the brain

As mentioned above, sound information travels from the hair cells to the brain through afferent neurons, also known as the spiral ganglion neurons (SGNs), which represent a specialized population of bipolar neurons that are classified as type I or type II (Coate and Kelley, 2013). Type I SGN and type II SGN differ in their morphology, number, innervation, firing proprieties and synaptic targets. Type I myelinated SGNs innervate, in the mature cochlea, only IHCs while type II unmyelinated afferents innervate the OHCs (Zhang and Coate, 2017). About 90-95% of the existing SGNs are type I SGNs and each SGN contacts one IHC, however each IHCs is contacted by 10-20 type I SGNs (Barclay et al., 2011). On the other hand, type II SGNs innervate multiple OHCs, yet each OHC receives input from only one type II SGN (Zhang and Coate, 2017). Type I and type II SGNs have different roles – type I SGNs are involved in providing

sound information to the brain while type II SGN's function is currently unknown, but it is hypothesized that they may be involved in mediating noxious stimuli (Johnson et al., 2019). To do this, SGNs relay the transduced information received from the sensory hair cells to the cochlear nuclei in the brainstem (**Figure 1.3**). From the cochlear nuclei, the information is delivered to the superior olivary complex (**Figure 1.3**), which then converge in the inferior colliculus and in the medial geniculate body, both of which are localised in the thalamus (part of the midbrain, **Figure 1.3**, Felix et al., 2018). At this level, sound information is further refined and then is transmitted to the primary auditory cortex in the temporal lobe of the brain (**Figure 1.3**, Felix et al., 2018). Once the auditory information reaches the primary cortex sound is being assigned with a meaning.

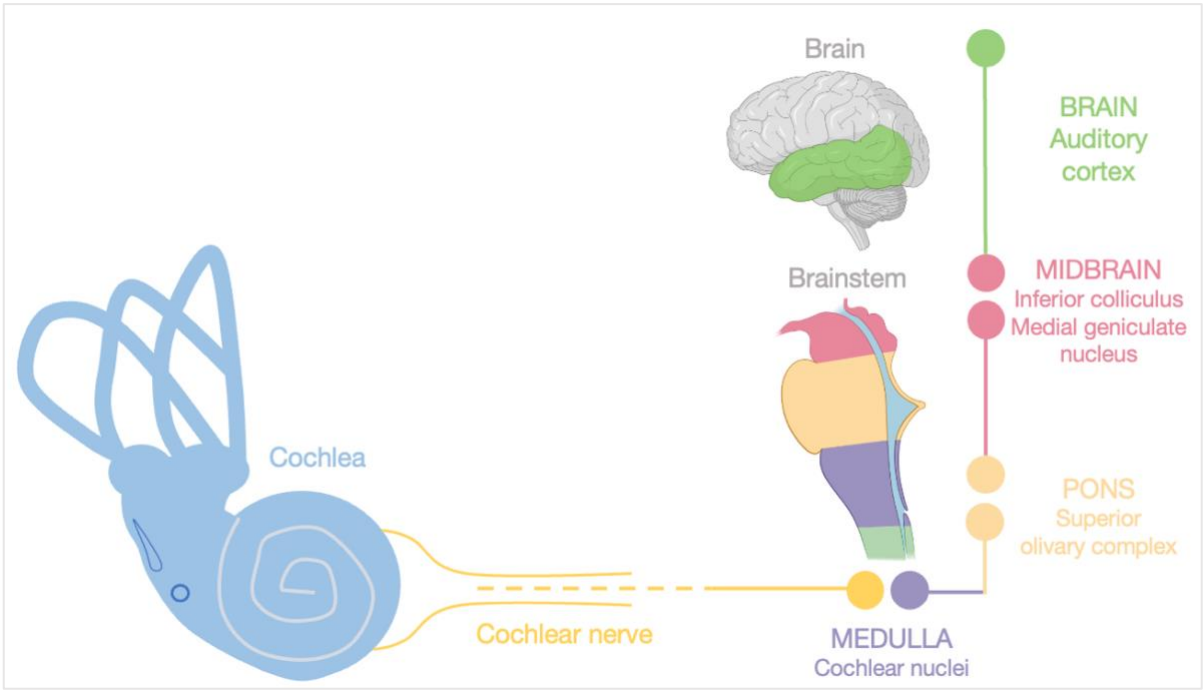

Figure 1.3: The auditory pathway to the brain. Schematic figure showing the cochlea and the cochlear nerve that carries the sense of audition to the cochlear nuclei of the medulla of the brainstem. The information ascends further to the superior olivary complex. At this level the information starts being processed and interpreted, and it is sent to the inferior colliculus and to the medial geniculate nucleus of the thalamus. The medial geniculate nucleus of the thalamus sends projections to the temporal lobe (depicted in green) of the brain. Within the temporal lobe of the brain is localised the auditory cortex where information is decoded and assigned with a meaning.

1.3.2. Auditory pathways from the brain

In addition to the glutamatergic afferent fibres, the cochlea is also innervated by efferent neurons that originate from the medial or lateral superior olivary nuclei in the brainstem (**Figure 1.4**). These efferent neurons, which in the mature cochlea innervate only the OHCs, are cholinergic since they primarily release the neurotransmitter acetylcholine (ACh). ACh opens the ionotropic α9α10 nACh receptors, which causes the influx of Ca^{2+} into the OHCs (Im, 2012). The entry of Ca^{2+} into the cells activates the Ca^{2+}-activated K^{+} channels (SK2) and the consequent hyperpolarization of the cells dampens their activity (Kong et al., 2008). In this way the responsiveness of the hair cells is reduced, and this provides auditory focus and receptiveness to wanted sounds and thus enhances our capability to discriminate sound in noisy environments. In the mature auditory system OHCs are the primary target of the thick, myelinated medial olivocochlear efferent fibres (MOC, **Figure 1.4**). MOC inhibit OHCs electromotile ability and reduce cochlear amplification (Wersinger and Fuchs, 2011). On the other hand, IHCs are only transiently innervated by the efferent fibres during the pre-hearing stages of development (Kearney et al., 2019), the role of which is to modulate the frequency of action potentials during pre-hearing stages (Frank and Goodrich, 2018). In this way, the efferent neurons play a key role in the refinement of the auditory pathway prior to maturation (Frank and Goodrich, 2018). In the mature cochlea, the thin, unmyelinated lateral olivocochlear efferent fibres (LOC) originating from the brainstem make postsynaptic contacts on the button-like terminals of the type I SGN fibres (Frank and Goodrich, 2018). Thus, the LOC fibres do not modulate directly the activity of the IHCs (**Figure 1.4**). The role of LOC efferent fibres is still unclear, but it is presumed that it prevents the afferent fibre from excitotoxicity and in this way reduce auditory neuropathy (Fuchs and Lauer, 2019). Additionally, it is

supposed that LOC fibres could potentially play a role in balancing the outputs of the right and left ear in order to achieve optimal binaural hearing (Irving et al., 2011).

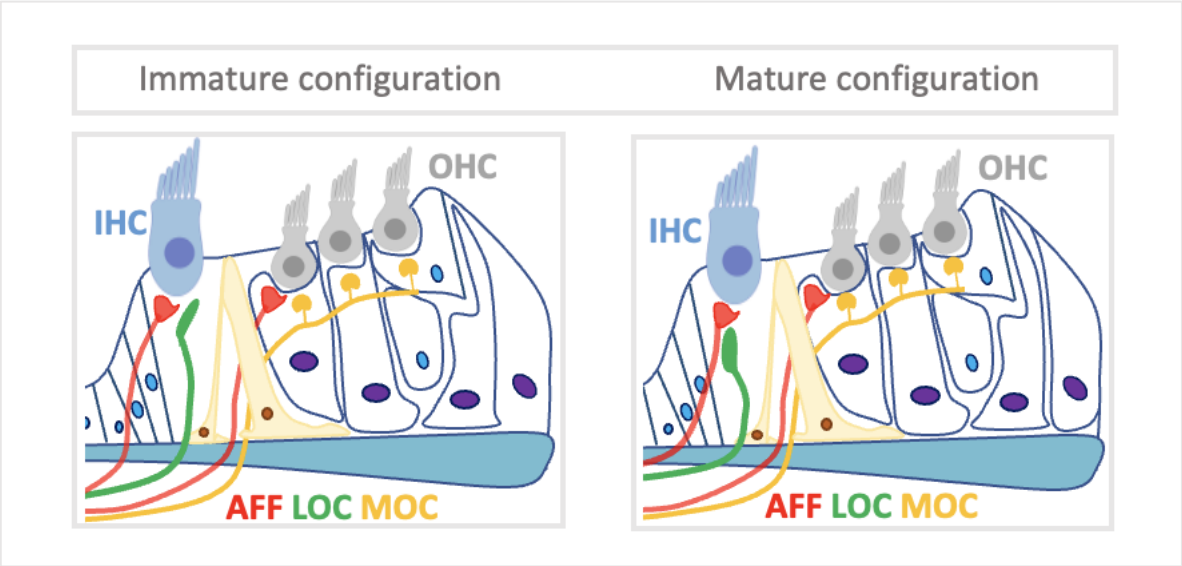

Figure 1.4: Organ of Corti afferent and efferent innervation of the hair cells. During the immature stages lateral olivocochlear efferents (LOC, depicted in green) innervate directly the IHCs (depicted in blue) and when the system matures the LOC make contact with the SGN (depicted in red). O the other hand, OHCs are innervated by medial olicocochlear fibres (MOC, depicted in yellow).

As mentioned above, the efferent system plays key roles both in the mature and developing cochlea and it is essential for the formation, refinement, and protection of the auditory pathways (Clause et al., 2014; Clause et al., 2017). Similarly, as the system ages, the pattern of innervation undergoes a process of re-organization that mimics the developmental period – this will be further addressed in the following sections.

1.4. Development of the auditory system

1.4.1. Development of the cochlea

The complexity of the function of the inner ear is defined by the multitude of cells and tissues present within the whole auditory organ. The system originates from the

surface of one of the embryonic cell layers – the ectoderm (**Figure 1.5A**, Anthwal and Thompson, 2015). The surface of the ectoderm is called the otic placode and in mice this structure forms around embryonic day 8 (E8) through the precise regulation of different signals that include GATA, DLX transcription factors and molecules such as Fibroblast Growth Factors (FGF, Wright and Mansour, 2003). Following induction, the ectodermal cells of the otic placode undergo a process of invagination that leads to the formation of the otic cup (**Figure 1.5B**, Kelley, 2006). By E9.5 the otic cup forms the otocyst (also called the otic vesicle, **Figure 1.5C**, Sai and Ladher, 2015). Subsequently, Notch and Wnt are activated and control together with Sonic Hedgehog (SHH) the patterning of the otocyst (**Figure 1.5C**, Whitfield, 2015). This leads to a series of morphogenetics events that promote the formation of the two main parts of the otocyst – the dorsal and the ventral pouches (**Figure 1.5D**, Whitfield, 2015). The dorsal pouch of the otocyst gives rise to the endolymphatic duct and the vestibular system, while the ventral pouch elongates and forms the cochlea (**Figure 1.5E**, Whitfield, 2015). The formation of the dorsal pouch of the otocyst is dependent on the expression of GBX2, DLX5/6, Bone Morphogenetic Protein 4 (BMP4) and GLI3 signalling pathways (Ohta et al., 2016). On the other hand, the formation and cell specification of the ventral pouch of the otocyst is dependent on SHH (Riccomagno et al., 2002). After cell specification, the identity of the ventral pouch is maintained by GATA3 and OTX2 (Wu and Kelley, 2012).

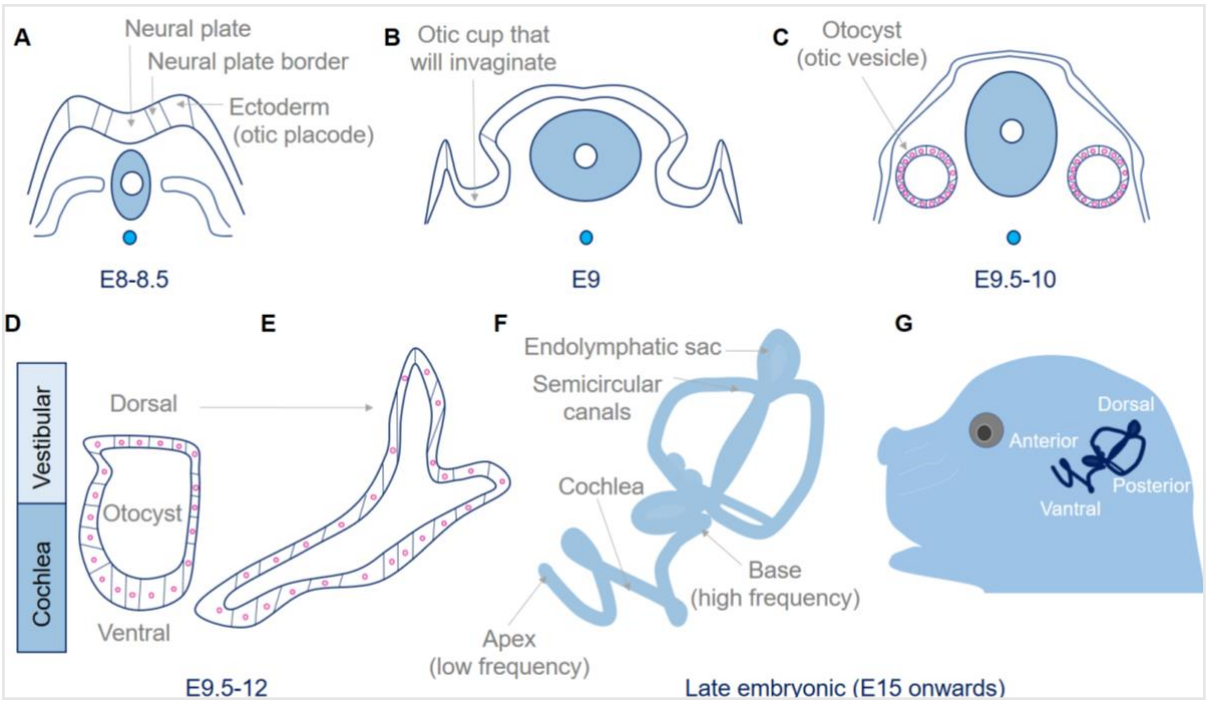

Figure 1.5: Development of the cochlea. Schematic illustration to show the development of the inner ear in the mouse. **(A)** Formation of the otic placode and **(B)** of the otic cup that will invaginate to form the **(C)** otocyst – all these structures originate from the ectoderm which is illustrated in the first panel. **(D)** The dorsal part of the otocyst will give rise to the endolymphatic duct and the vestibular system, while the ventral part of the otocyst will give rise to the cochlea. **(E)** The otocyst elongates and at E9.5 is positioned to receive extrinsic secreted signals that originate from adjacent structures (hindbrain, notochord). **(F)** During development the auditory and vestibular systems are patterned, specified and formed. **(G)** View of the mouse ear inside the skull.

The otocyst acts as an autonomous structure that contains all the signalling information required for the development of the inner ear, including proliferation, differentiation and cell specification. The otocyst gives rise to both non-sensory and prosensory domains which are necessary for the development and function of the cochlear cells. Around E9.5-10 the prosensory cells migrate and start proliferating under the expression of SOX2 (**Figure 1.6A**, Jacques et al., 2012). During this period, Notch signalling is involved in maintaining the identity of the prosensory cells (**Figure 1.6A**, Kiernan, 2013). The prosensory cells will keep dividing until E12-14.5 when the cell-cycle arrest factor p27 starts being expressed (**Figure 1.6B**, Lee et al., 2006). The expression of p27 will first emerge at the apex of the cochlea and then will be present in the middle and basal coils of the cochlea – it is known that the cells that will first exit

the cell cycle will be the ones to differentiate last (apically localised hair cells, Pujol et al., 1998). Subsequently, the prosensory cells will become either sensory or non-sensory cells (Whitfield, 2015). Between E13 and E14.5 Atoh1 starts being expressed in the middle and basal regions of the cochlea and promotes the differentiation of the prosensory cells into hair cells (**Figure 1.6B**, Pan et al., 2011). In the following 2-4 days, the expression of Atoh1 spreads apically from the basal and middle coils and in this way a longitudinal gradient of Atoh1 transcription factor is established and promotes the differentiation of cells into cochlear hair cells (Cheng, 2019). On the other hand, Notch, Hes1, Hes5, FGF and Kremen1 will aid into the differentiation of the cells into non-sensory supporting cells (Maass et al., 2016).

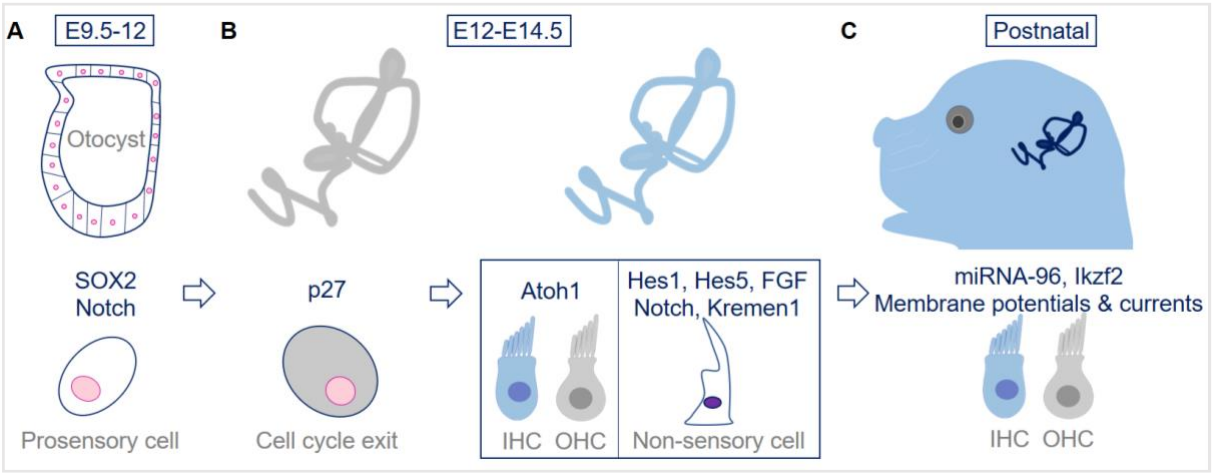

Figure 1.6: Development of the mammalian inner ear sensory and non-sensory cells. Schematic illustration to show the cell fate decisions made during development to develop the inner ear cells. **(A)** The scheme illustrates the otocyst and the signaling factors (SOX2 and Notch) that aid in the specification of the prosensory cells. **(B)** At E12-E14.5 the prosensory cells exit the cell cycle (terminal mitosis) under the influence of p27. Consequently, the cells then start differentiating into either sensory or non-sensory cells. The expression of Atoh1 leads to the differentiation of prosensory cells into IHC and OHC, while the expression of Hes1, Hes5, FGF, Notch and Kremen1 promote the differentiation of the cells into non-sensory supporting cells. **(C)** During the postnatal period, the cells mature and become fully functional.

By the end of the embryonic period (E20) the number of IHCs and OHCs is established and during the postnatal stages the hair cells will increase in their dimension and

mature from a functional point of view (Ehret, 1983; Kros et al., 1998). At postnatal day 0 (P0), miRNA-96 starts being expressed in the cochlea and further supports the functional differentiation of both IHCs and OHCs (**Figure 1.6C**, Kuhn et al., 2011). miRNA-96 is a non-coding RNA, and its role is to decrease the level of the complementary genes and assist in the maturation of the hair cell bundle as well as in the refinement of the cochlear innervation (Kuhn et al., 2011). In addition to these factors, the zinc finger transcription factor GATA3, which initially supports the formation of the otic placode, contributes in IHC maturation and growth (Bardhan et al., 2019) and gap junction channels (connexins) also aid in the functional maturation of the IHCs (Johnson et al., 2017). Similarly, around P4 Ikzf2 transcription factor starts being expressed in the OHCs and promotes their maturation through the expression of prestin and oncomodulin (**Figure 1.6C,** Chessum et al., 2018).

1.4.2. Development of hair cell function

Once the prosensory cells differentiate into hair cells, the IHCs start expressing a small delayed-rectifier K^+ current (I_K) that sets the resting membrane potential at -50 mV within the hair cells. Later, at E16.5 the hair cells present with a second inward-K^+ rectifier current (I_{K1}) which further increases in size until the onset of hearing function at P10 – P15 (Marcotti et al., 2003). In addition to this, the IHCs express I_{Ca} that together with I_K aid in the generation of spontaneous Ca^{2+} - dependent action potentials which play key roles in the establishment of tonotopicity, in setting-up the appropriate gene expression profile, in synaptic refinement and also supports the normal acquisition of mature basolateral membrane currents (Jeng et al., 2020). At the same time, it is known that voltage-gated sodium currents (I_{Na}) also contribute from embryonic stages to facilitate the generation of spontaneous action potentials that play key roles during hair cell development (Eckrich et al., 2012; McPherson, 2018; Corns

et al., 2018). Another current required for the appropriate functionality and maturation of the system is the MET current, which is first detected in hair cells at around the day of birth in mice. The functional maturation of the IHCs coincides with the expression of a large conductance outward K^+ current named I_{Kf}, which allows the cells to respond with fast, graded, receptor potentials to sound information (Kros et al., 1998, Marcotti et al., 2003). The current literature suggests that this fast K^+ current is conveyed by BK channels (Marcotti et al., 2004). This channel is expressed in the neck region of the IHCs.

Other changes that guide the functional development of the hair cells occur during the postnatal period starting around P3 when IHCs present a hyperpolarizing response to ACh (Pujol et al., 1998, Marcotti et al., 2004a). This response is observed in immature IHCs and mature OHCs where efferent stimulation leads to an increase in intracellular Ca^{2+} that activates SK2 which subsequently leads to K^+ leaving the cell and leading to its hyperpolarization (Marcotti et al., 2004a). As already mentioned, the hyperpolarization of the IHCs by ACh is aiding in the inhibition of action potentials and during development plays a role in the in the activation of small-conductance SK2 channels that carry the small conductance Ca^{2+} activated K^+ current (I_{SK2}). Therefore, the development of hair cell function is marked by the transition from spiking activity that is essential during early development stages, to graded receptor potentials, which are necessary for the mature function of auditory hair cells. The transition from spiking to graded potentials is influenced by the maturation of the efferent system, where the IHC around P3 start displaying a hyperpolarizing response to Ach which is a response mediated by the activation of SK2 channels. The hyperpolarisation effectively inhibits

further action potential generation and in this way leads to the predominance of graded receptor potentials.

Additional channels, their expression onset and their characteristics are listed in **Table 2**.

Table 2. Ion channel changes present throughout development.

Channel	Expression onset	Characteristics / functions
I_K	E14.5	K^+ current Will be I_{Ks} Outward delayed rectifier Increase in amplitude up to P12 Stops being expressed shortly after P12
I_{K1}	E15.5	K^+ current Inward rectifier Increase in amplitude up to P12 Disappears between P12-P15 (once hair cell becomes mature)
I_{Kf}	P12	K^+ current BK channel Large conductance Fast kinetics Present in the IHCs once the cells are mature Expressed in the neck region of the cell
I_{Ks}		K^+ current KCNQ4 channel Slow kinetics
I_{Kn}	P8 - P12	K^+ current KCNQ4 / Kv7.4 channel Aids in the increase of open probability of the channel at rest Aids in the functional maturation of the hair cells Present once hair cell is mature
I_{Ca}	E16.5	Ca^{2+} current Mainly $Cav_{1.3}$ channel Increase in amplitude up to P6 Expression persists throughout development and maturity of the cells
I_{SK2}	P0: OHCs P12: IHCs	Ca^{2+} activated K^+ current SK2 / KCNN2 Increase in amplitude up to P12 Expressed in IHCs during development and in the OHCs during maturity
I_T	P0 – P7	MET current Involved in hair cell development & maturation Involved in channel adaptation Expression persists during development and maturity of the cells
I_{Na}	E16.5	Na^+ current $Na_v1.1$ and $Na_v1.6$ or $Na_v1.7$ channels Increase in amplitude up to P6 Expression persists during development and maturity of the cells

1.5. Damage of the auditory system

Considering the intricate composition and function of the auditory system is not surprising that both the hair cells and the associated neurons can be irreversibly damaged during aging, due to gene mutations or because of environmental increased noise exposure as well as treatment with ototoxic drugs (Coffin et al.,2010). Damage of the mechanosensory hair cells leads to malfunctional sensory receptors and hearing loss (Wu et al., 2019). It is known that deafness affects five percent of the world's population (approximately 466 million people, out of which 34 million are children, World Health Organization, Zanzibar commemorates World Hearing Day | WHO | Regional Office for Africa, 2019); these numbers are projected to double over the next 20 years since the population expands and ages. The current estimates by the World Health Organization list that by 2050 2.5 billion people worldwide will have some degree of hearing impairment and disability (World Health Organization, 2023).

Hearing loss can be classified into three categories – (1) conductive hearing loss, (2) sensorineural hearing loss and (3) mixed hearing loss.

Conductive hearing loss is caused by changes that take place at the level of the outer or middle ear. For example, within the outer ear a build-up of ear wax or excessive skin production can impact the hearing ability of an individual. At the same time, within the middle ear, accumulation of fluid caused by infection, ossification of the ossicles or rupture of the tympanic membrane can cause conductive hearing loss. On the other hand, sensorineural hearing loss is characterised by damaged hair cells or neurons and represents the most common type of loss in hearing function which is irreversible and permanent. Sensorineural hearing loss can be caused by aging, exposure to loud noise, injury, disease, application of ototoxic compounds as well as genetic alterations. This type of hearing loss can be present at birth (congenital) or can be acquired

meaning that it may develop in children or adults later in life. Lastly, mixed hearing loss is caused by both conductive and sensorineural hearing loss.

For the purpose of the current work, the information within this section will focus on sensorineural hearing loss with emphasis on congenital and age-related hearing loss.

Congenital hearing loss appears in 1 – 3 out of 1000 live births and can greatly delay or impair the ability to develop speech, language, emotional and social abilities and significantly reduces the overall quality of life (Korver et al., 2017). Congenital hearing loss can be caused by environmental factors and congenital infections (cytomegalovirus). However, for most of the patients the cause for congenital hearing loss relates to genetic mutations that impair the functionality of different components of the hearing pathway. The most common mutations that lead to congenital hearing loss affect the process of mechano-electrical transduction and the inner ear homeostasis such as the production and preservation of endolymph (Korver et al., 2017). Since in the majority of the patients that suffer from congenital hearing loss the cause is initiated by genetic alterations, the management options that are available for this population are limited to antimicrobial therapies (antibiotics), surgical treatment, usage of hearing aids and intervention programmes that assist the patient and the carers. Thus, these patients are not provided with a cure, and children suffering from congenital hearing loss are put at a greater risk of having a delay in acquiring communication skills and developing mental health problems that include but are not limited to anxiety and depression.

At the same time, in adults, the most common hearing deficit is represented by age-related hearing loss (ARHL; Holt and Vandenberghe, 2012). ARHL is a chronic condition normally present in people aged 45 and older and is characterised by impaired hearing sensitivity, defective sound localization and inability to understand speech (Jafari et al., 2019). As such, deafness has debilitating effects on the patient's mental health and social status (Shukla et al., 2021). Hence, ARHL causes a huge quality life burden not only for the affected individual, but also for the patient's family. Patients suffering from ARHL usually present with phenotypes that illustrate the loss or improper functionality of the cells responsible for high frequency sound information and are unable to recognise speech or appreciate music. Similar to congenital hearing loss, ARHL has no cure, although cochlear implants and amplification devices address some of the symptoms.

Regardless of the therapeutic options and assisted hearing devices that are currently available for patients suffering from hearing loss, these treatments do not provide the affected ones with the required sensitivity of a functional ear, and most importantly do not provide them with a cure.

1.6. Listening to their needs – current unmet medical need

At the present time there are no FDA/EMA-approved drugs for addressing the needs of hearing loss patients. This is because, as already noted, hearing loss and deafness are mainly characterised by the malfunction or degeneration of the hair cells and / or adjacent neurons. In addition to this, it is known that about half of the diagnosed patients suffer from genetic mutations that impair the functionality of the auditory organ. Currently, there are two potential approaches for the recovery of hearing function: stem cell therapy and gene therapy. Stem cell therapy aims to regenerate

completely the missing or non-functional HCs, while gene therapy aids in the regulation of genes involved in hearing function. Since both congenital and ARHL are caused by multiple factors including genetic alterations, current research mainly focuses on gene therapy as this technique is deemed safer and has the potential to provide a curative option to patients diagnosed with hearing loss.

In the current project, the gene therapy approach was used both as a study technique for the identification of a possible therapeutic method as well as for assessing whether the auditory system retains the ability to be manipulated and can reinstate normal function in the transduced cells.

1.7. Gene therapy for hearing loss

There are different forms of gene-based therapy, including gene suppression (antisense oligonucleotides, RNA interference), gene editing (CRISPR/Cas9), and gene replacement (using adenovirus, herpes simplex virus, lentivirus or AAVs). Gene replacement is the most straightforward form of gene-based therapy, and it is characterised by the substitution of a defective gene with a normal wild-type copy through the use of a vector that carries the normal gene to the target tissue.

AAVs are normally used as gene transfer vectors as they have numerous advantages over other vectors. These include longer gene expression, a reduced immune response and decreased toxicity (Lee et al., 2020). Added to that, AAVs have a small size (approximately 20-25 nm, Colella et al., 2018) which means that their diffusion across cellular barriers is facilitated and this in turn promotes the expression of the gene to the native location (Colella et al., 2018).

The capability, efficiency and stability of gene transduction within the mammalian ear mainly depends on the AAV serotype, the route of delivery and surgical procedure, the target cell, the time of delivery of the gene construct as well as the animal model (Ahmed et al., 2017). Since there are no standardized cochlear gene therapy protocols, the following sections will outline some of the recent discoveries in terms of (1) vector components, (2) AAV infection strategies as well as (3) the most common used serotypes within the hearing field.

1.7.1. AAV vector components

The AAV is a member of the *parvoviridae* family which was discovered initially in 1965 as a contaminant of an adenovirus stock. The virus is non-enveloped and consists of two main components which are the genome and the capsid (**Fig. 1.7**). The genome is represented by the single-stranded DNA and comprises the promoter, transgene and the polyA sequence. At both ends of the genome are the inverted terminal repeats (ITRs). The ITRs are indispensable for the replication and packaging of the virus into the capsid (Maguire and Corey, 2020). The AAV capsid is required for genome protection and intracellular trafficking processes that ultimately lead to the expression of the desired gene.

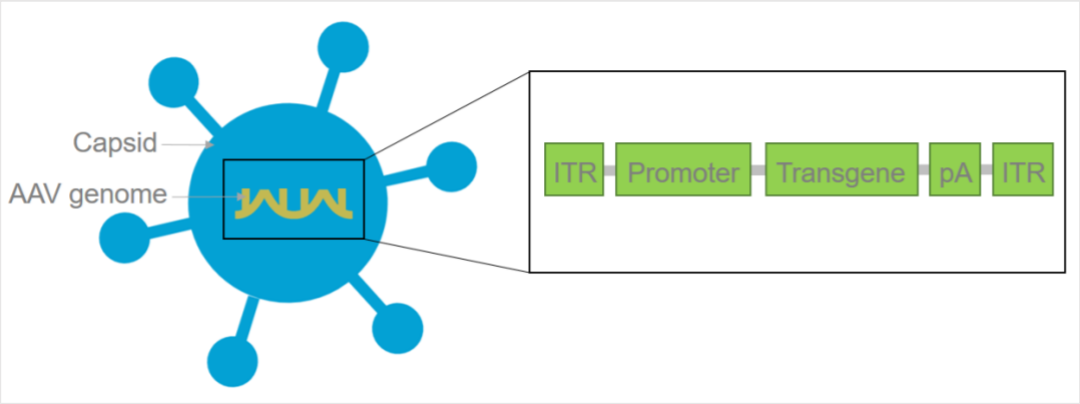

Figure 1.7: Schematic representation of AAV vector. The AAV vector consists of the capsid which carries the AAV genome (in most of the cases it is a single-stranded DNA genome). The AAV genome is 4.7 kb and it consists of the transgene or therapeutic gene (of approximately 4.4 kb), the promoter that drives the expression of the AAV transgene, the polyadenylation or polyA (pA) signal that aids in the export of RNA and RNA translation and the inverted terminal repeats (ITR) sequences that are required for genome rescue, replication, packaging and to confer persistence to AAV genomes upon transduction (Earley et al., 2020).

One major limitation of the AAV vectors is their packaging capacity that allows the expression of a 4.7 kb transgene cassette only. This is of relevance since there are numerous hearing phenotypes caused by mutations in genes that have coding sequences exceeding 4.7 kb (Wu et al., 2010; McClements and MacLaren, 2017). This means that an insert size higher than 4.7 kb is unstable and will not efficiently transduce the cells of interest. Nonetheless, it has been shown that dual vector (capacity of approximatively 9 kb) and even triple vector (capacity of approximately 12.5 kb) can be used to deliver larger genes (Ghosh et al., 2011; Dyka et al., 2014; Al-Moyed et al., 2018; Akil et al., 2019). In the dual-AAV system each of the two vectors carries a fragment of the gene and the two vectors reassemble after the injection to reconstitute the full-length expression cassette within the hair cell (Ghosh et al., 2008). There are different approaches to achieve this – listed in **Table 7, Chapter 2**. For example, through the trans-splicing approach, the AAV genomes can undergo intermolecular ITR-mediated head-to-tail concatemerization (Trapani et al.,

2013). To do this, a splicing donor is placed at the 3'-end of the 5'-half of the target gene and a splicing acceptor at the 5'-end of the 3'-half of the target gene. Both halves of the target gene have a binding sequence and upon transduction the mature mRNA is produced and leads to the synthesis of the full-length protein. In two recent studies, the trans-splicing-mediated dual gene delivery was used for the otoferlin cDNA and showed that auditory function can be restored in otoferlin knock-out mice (Al-Moyed et al., 2019; Akil et al., 2019). Otoferlin is a protein coded by the OTOF gene and it is calcium-sensitive protein that plays roles in the exocytosis of synaptic vesicles at the ribbon synapses of cochlear IHCs. Mutations in the OTOF gene are linked to non-syndromic hearing loss as the function of Otoferlin is essential for the synaptic release of neurotransmitters in response to sound stimuli. Added to that, in another study, *MYO7A* cDNA was transduced within the retinal cells of a mouse model for Usher syndrome type 1B (Colella et al., 2013). The gene was transduced using an AAV2/5 vector that had the capacity to accommodate the whole *MYO7A* gene. The study showed that AAV2/5-*MYO7A* gene transfer to the eye improved retinal activity (Colella et al., 2013). Overall, such studies illustrate that dual AAV vector system can be adapted and can reconstitute the target gene cDNA coding sequence through recombination in the target cell. However, another significant aspect required for the efficient AAV transduction into the auditory hair cells relates to the delivery of the AAV to the inner ear – the following section will address this.

1.7.2. Routes of vector administration to the inner ear and AAV cellular transduction

The anatomical structure of the inner ear makes the delivery of repair genes difficult and represents a major determinant of the efficiency and specificity of transgene delivery in the cochlea. For vector application to the cochlea, a huge challenge has been the establishment of protocols that deliver the gene of interest to the inner ear without further impairing the functionality of the auditory system. In order to achieve this, various surgical approaches have been developed by different groups in order to deliver AAV vectors to the inner ear of different animal models. Some of the most basic procedures included the administration of injections into the amniotic cavities, temporal veins and intraperitoneal injections. Later, more precise approaches involved the delivery of viral vectors locally. To do this, viral vectors were targeted to the inner ear by doing either intra or trans-tympanic injections. The trans-tympanic route is minimally invasive and is already performed in humans (Lee et al., 2020). This method of administration involves the injection of agents into the middle ear and their diffusion through the round window into the inner ear. However, one of the main disadvantages of the trans-tympanic injections is that the concentration of the virus cannot be precisely controlled and the virus entry into the inner ear is dependent on the permeability of the round window (Lee et al., 2020). The intratympanic delivery method is a direct approach carried out either through the oval window, round window, cochlea or through one of the semi-circular canals (**Figure 1.8**, Ren et al., 2019). The intratympanic approach seems to be the preferred route since in this way the vector does not have to diffuse from the middle ear into the inner ear (Ren et al., 2019). However, to reach any of these routes, surgical operations are necessary, and these are likely to induce significant additional damage (Ahmed et al., 2017). Nonetheless, there are numerous recent publications that showed promising results in adult mice

where the AAV vectors were delivered to the cochlear hair cells through the round window membrane (RWM) without causing additional damage (Akil et al., 2012; Landegger et al., 2017; Pan et al., 2017; Yoshimura et al., 2018; Al-Moyed et al., 2018; Akil et al., 2019; Tan et al., 2019). Furthermore, recent publications showed that RWM injections can be combined with additional canal fenestrations in order to improve viral-mediated cochlear gene delivery (Yoshimura et al., 2018). In this way, gene vector delivery can be manipulated to achieve higher transgene expression in a more precise spatial and temporal manner (Hudry et al., 2018).

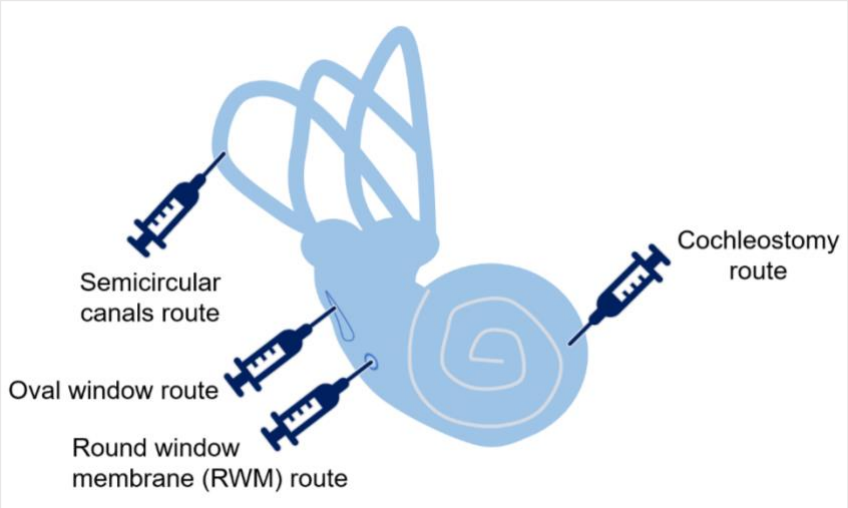

Figure 1.8: Intratympanic delivery routes of AAV. Schematic diagram illustrating several routes of delivery for injecting vectors and genes into the inner ear in order to target the cochlear hair cells.

In addition to this, upon the virus entrance into the inner ear, the AAV construct has to transduce different populations of cells. To do that the AAVs mainly bind to the cell surface receptors (glycan receptor binding) or enter the intracellular space through clathrin-mediated endocytosis, integrin-mediated cell entry or through micropinocytosis (Berry and Asokan, 2016). The mechanisms of vector entry into the cell are still being studied and explored, but there are particular components that have been identified to play essential roles in AAV infection. For example, a recent study showed that GPR108 (member of the G protein-coupled receptor superfamily), which is conserved between mice and humans was shown to be one of the factors that is

required for AAV-entry and cell transduction (Dudek et al., 2020). Following cell entry, the AAV is trafficked intracellularly to the early, late or recycling endosomes and from there to the Golgi apparatus where the virus binds to the AAV receptor (AAVR). AAVR is synthesized from the KIAA0319L gene and is a cellular factor that is essential for AAV infection (Pillay et al., 2016). From the Golgi apparatus, AAV is transferred to the trans-Golgi network (TGN) and then to the nucleus . The AAV enters the nucleus through the nuclear pore complex (NCP) and afterwards undergoes a process of uncoating and subsequently the genome is released . Following this, the single-stranded DNA is converted into double-stranded DNA and the process ends with the synthesis of the desired sequence and production of the target protein.

Nonetheless, different AAV serotypes will employ different mechanisms of cell entry, and this will further influence the transduction efficiencies.

1.7.3. AAV vector serotypes

Because different vector serotypes show different transduction efficiencies, initial studies focused on expanding the biodiversity of AAVs and analysed the efficiency of the vectors to transduce both the auditory hair cells as well as the support cells (Bankoti et al., 2021). Up to date, 13 district human and non-human primate AAV serotypes (from 1 – 13) have been sequenced and analysed and transduced in different organ systems. Each serotype has different receptors localised on the capsid and this explains why certain serotypes bind with higher affinity to particular cell types that express the complementary vector receptor. Synthetic capsid variants that provide better penetration into the cell of interest and with reduced antibody neutralization can be designed. For example, the AAV capsid can be engineered by introducing tyrosine-to-phenylalanine and threonine-to-valine point mutations, which reduce phosphorylation and promote the accumulation of viral DNA into the target cell nucleus and in this way increase the expression of the transgene (Petrs-Silva et al., 2011). Since AAV is not an enveloped virus, the capsid can be engineered to change its cellular tropism and target with higher efficiency the hair cells.

A variety of studies analysed the precision and efficiency of different AAV serotypes in the immature and mature mammalian cochlea. As such, different AAV serotypes showed promising results in mice injected with a viral vector starting from postnatal day 0 (P0) up to 6 months (Suzuki et al., 2017; Yoshimura et al., 2018; Isgrig et al., 2019). The first successful cochlear gene therapy study used AAV1 vector to treat homozygous *VGLUT3* mutant mice. Mice that lack *VGLUT3* are deaf due to the inability to release glutamate at the IHC afferent synapse. The release of glutamate from inner hair cells onto the dendrites of SGNs and in this way represents a key step in auditory neurotransmission. The study showed that the transgene expression of *VGLUT3* in the IHC enable them to regain their functionality and partial hearing

recovery based on auditory brainstem response (ABR) (Akil et al., 2012; Holt and Vandenberghe, 2012). In addition to this, an “ancestor” of the AAV serotypes 1, 2, 8 and 9 – Anc80L65 was used in numerous studies in the field. Anc80L65 is an *in silico* AAV and was found to transduced efficiently almost 100% of the mature IHCs and OHCs at a dose that was significantly lower than the dose used for the natural AAVs (Landegger et al., 2017; Suzuki et al., 2017). This vector was used in a mouse model for Usher Syndrome Type 1C to transduce harmonin (Pan et al., 2017). Anc80L65-harmonin injections were done at P0-P1 and the data showed that the hair cell mechanotransduction was restored, and both the auditory and the vestibular function were significantly improved (Pan et al., 2017). Anc80L65 is currently the most powerful vector used for hair cell transduction in the cochlea. The disadvantage of the three studies presented above is that the injections were done between P0 and P1 suggesting that there could be a small age-dependent window of opportunity for such therapies to work prior to the onset of hearing. Nonetheless, Chen and colleagues, showed that some AAV serotypes can be used in older animal models (Chen et al., 2018). AAV8 was used as a vector for the NT-3 gene transduction (Chen et al., 2018). The injections were done in 2-3 months old guinea pigs prior to noise exposure in order to prevent cochlear synaptopathy (Chen et al., 2018). The guinea pigs had normal ABR thresholds and also had fewer damaged synapses compared to the non-treated subjects (Chen et al., 2018). Therefore, this suggests that AAV8 can successfully transduce hair cells after the hearing onset in different mammalian models, and this, of course, is of clinically translatable relevance.

Further studies showed that the cells of the inner ear were efficiently transduced by AAV1, AAV2, AAV3, AAV4, AAV7, AAV8, AAV9 (Akil et al., 2012; Askew et al., 2015; Ahmed et al., 2017; György et al., 2017; Tao et al., 2018) and that the best serotypes

for targeting the IHC are: AAV1, AAV2, AAV3, AAV5, AAV6, AAV8 and AAV9 (Ahmed et al., 2017; György et al., 2017). Additional information from different studies on the AAV serotypes used, the timing of the injections, the delivery method and the transduction efficiency are listed in **Table 3** (at the end of the chapter).

Overall, such proof-of-concept studies elevate the prospects for gene transduction in the human inner ear and increase the confidence in gene therapy approaches. Added to that, two studies using AAV-vector approaches to target the cochlear hair cells are already used in clinical trials (ClinicalTrials.gov Identifier: NCT05788536 and NCT03996824) which further suggests that such approaches hold the promise of providing patients with treatment options for hearing loss.

The following sub-sections will focus on the role of Myosin VIIa in hearing function and dysfunction, and the phenotypes observed when *MYO7A* is mutated and the chapter will end detailing the scope of the present project.

1.8. Mysin7a role in hearing and deafness

The focus of the current project is on *MYO7A* that encodes the Myosin VIIa protein which is an unconventional myosin. Myosins represent a diverse family of motor proteins that are categorised into conventional and unconventional myosins. Conventional myosins, such as Myosin II, have coiled-coil domains that enable them to form thick filaments that are required for muscle contraction and cytokinesis (Hartman and Spudich, 2012). On the other hand, unconventional myosins that include various classes from myosin I to myosin XVII, do not form thick filaments and are often involved in the transportation of cellular cargo, maintainance of cell shape and cell motility (Hartman and Spudich, 2012). Myosin VIIa is a unique member of the unconventional myosin superfamily which plays key roles in sensory function. Myosin VIIa is involved in maintaining the tension of the tip link – a filamentous structure that

connects the tips of adjacent stereocilia – this is essential for the sensitivity and adaptation of the MET channels to stimuli. Mutations in *MYO7A* reproduce the phenotypes observed in patients diagnosed with congenital hearing loss (Usher Syndrome Type 1B) and conditional *MYO7A* knockout mouse models recapitulate some of the changes occurring in the hair cells during ageing. In relation to Usher syndrome, *MYO7A* mutations disrupt the delicate arrangement, leading to mislocalisation of key molecules and proteins within the hair bundle. These include harmonin, cadherin 23, and protocadherin 15, all of which are part of the tip link complex and are critical for MET function. The correct localization of these molecules by Myosin VIIa is paramount for the structural integrity of the hair bundles and proper function of the MET channels. Myosin VIIa is an unconventional functional myosin that in the inner ear is specifically expressed in the hair cell body and hair cell bundle. Within the auditory organ, Myosin VIIa is involved in (1) development and maintenance of the stereocilia, (2) maintenance of membrane tension in the stereocilia, and (3) intracellular transport of molecules (Prosser et al., 2007). The roles of Myosin VIIa within the hair cell suggest its importance in hearing. Myosin VIIa plays roles in the process of mechanoelectrical transduction (MET) process, which involves the conversion of mechanical stimuli into electrical signals. Furthermore, it is believed that Myosin VIIa is involved in the process of MET adaptation by maintaining the tension within the hair cell stereocilia. Through tension adjustment, Myosin VIIa modulates the sensitivity of the MET channel to additional stimuli.

To carry out its function, Myosin VIIa has three operating domains – a motor domain, a neck domain, and a tail domain (**Figure 1.10A**, Yu et al., 2017). The motor head domain represents the binding site for actin and is the domain that generates force through ATP hydrolysis. The second domain is represented by the neck region, and it

is the main site that allows the interaction of Myosin VIIa with other proteins, this domain consists of five isoleucine – glutamine (IQ) subdomains which are calmodulin binding motifs (**Figure 1.10B**, Heissler and Manstein, 2012). At the same time, the C-terminal tail domain acts as an anchor and it is made of the coil-coil subdomain (CC, also known as the α-helix domain) two myosin tail homology 4-4.1 (MyTH4) subregions, an SRC homology 3 (SH3) domain and two FERM subdomains (**Figure 1.10B**, Heissler and Manstein, 2012). The tail domain has sequences that are known to interact with components of the cytoskeleton, such as actin filaments (Heissler and Manstein, 2012).

To carry its activity, the motor head domain interacts with the tail (Yang et al., 2009) suggesting that mutations in any of these regions can be linked to unstable and dysfunctional Myosin VIIa and hence deafness. Most of the point, missense and deletion defects in *MYO7A* were identified in the head region and affect the functionality of Myosin VIIa protein (**Figure 1.10C**, Schwander et al., 2009; Miller et al., 2012). At the same time, mutations in the tail domain of the protein mainly affect its stability (Schwander et al., 2009).

Morphological assessment of these mutations in murine animal models shows that the hair cell bundles are disorganised or completely deteriorate and that the kinocilium, which represents a single true cilium that is present during development and disappears by P12, is often misplaced (Senften et al., 2006; Wang and Zhou, 2021). Furthermore, biophysical experiments carried out in *MYO7A* mutant mice show that Myosin VIIa directly affects the opening of the MET channel and its dependence on Ca2+ (Kros et al., 2002, Holme and Steel, 2002; Prosser et al., 2007; Lefevre et al., 2008; Grati and Kachar, 2011; Li et al., 2020). The current literature suggests that

these defects are likely cause by inadequate control of actin dynamics and by the impaired transport of vesicles and actin polymerization regulators within the hair cell (Durrbach et al., 1996; Govindan et al., 1995, Holme and Steel, 2002; Prosser et al., 2007; Lefevre et al., 2008).

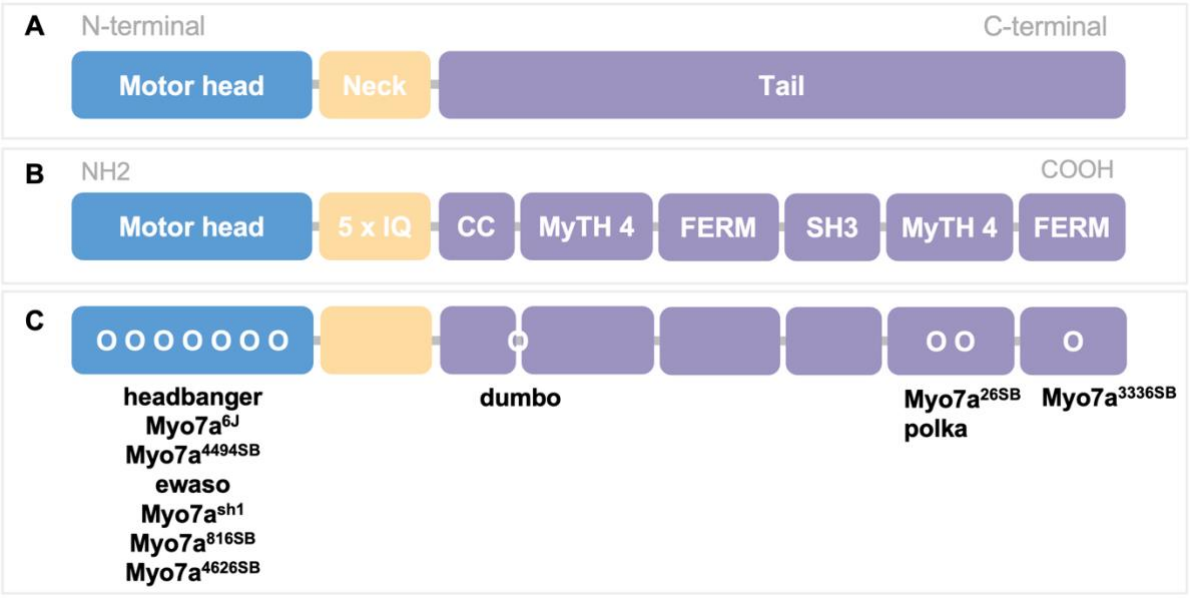

Figure 1.10: Schematic diagram of the Myosin VIIa protein domains. (A) Myosin VIIa domains which are composed of the motor, the neck and the tail. **(B)** Figure to show the subdomains of the motor head, the neck and the tail. **(C)** Diagram showing some of the *MYO7A* mutations that are associated with human disease – it can be observed that most of the mutations are in the motor head domain and are associated with Usher Syndrome Type 1 (headbanger, ewaso, 6J etc.). Conversely, some of the mutations that are associated with non-syndromic hearing loss are in the neck domain (dumbo). Graphic representation reproduced after Miller et al., 2012.

Overall, Myosin7a is involved in the process of mechanoelectrical transduction and serves as a key regulator that fine-tunes the responsiveness of the hair cells. Myosin VIIa also contributes to MET adaptation which aids in recalibrating the sensitivity of the hair cells to sustained mechanical stimuli and in this way maintaining the fidelity of auditory signal transduction over a range of sound intensities. The protein's function in adjusting the MET channel resting open probability is essential for setting the baseline sensory state for the hair cells, thus defining their readiness to respond to

sound waves. The resting open probability has direct implication for the hair cell receptor potential and following neural firing rates.

Therefore, mutations in *MYO7A* lead to impairments in the hair cell bundle development and maintenance, molecule transport within the cell and affect the functionality of the MET channel all of which consequently leads to different forms of hearing loss (**Figure 1.11**).

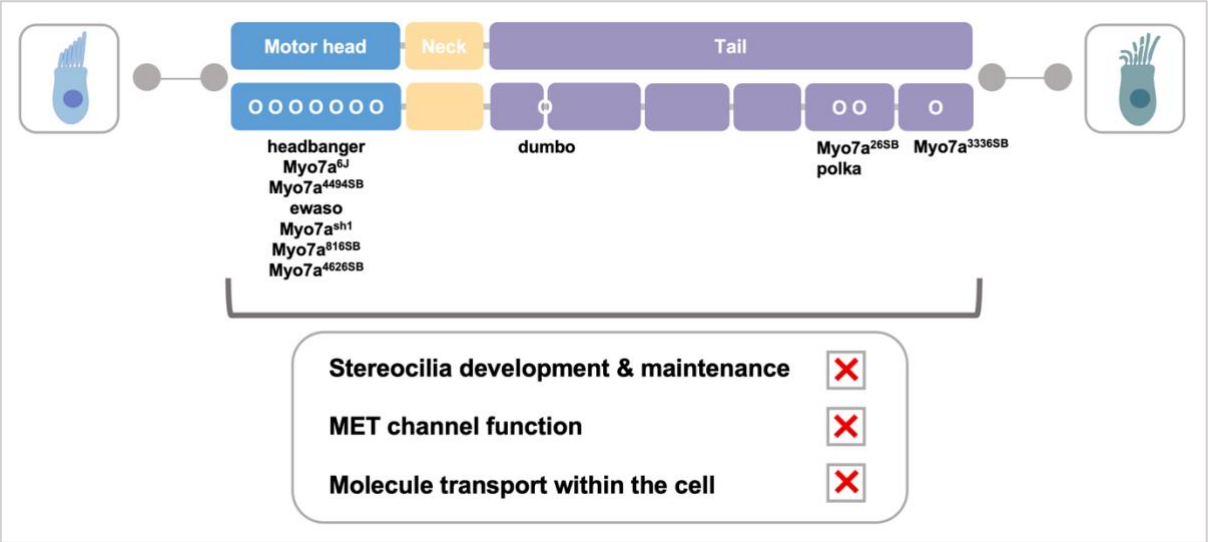

Figure 1.11: Schematic representation of *MYO7A* mutations effect on hair cells. Figure to show how *MYO7A* mutations impair the development and maintenance of stereocilia, affect the function of the MET channel and lead to the dysfunction of the transport of molecules within the hair cells.

1.9. Myosin VIIa and congenital hearing loss and scope of the current project

The first *MYO7A* mutation was described in the *Shaker-1* mouse and it was characterised in 1929 (Lord and Gates, 1929). The *Shaker-1* mice present with circling behaviours, deafness, head-tossing and hyperactivity (Lord and Gates, 1929). This genetic condition and the described phenotypes are also observed in patients suffering from Usher syndrome type 1 (Gibson et al., 1995; Self et al., 1998).

There are three forms of Usher syndrome – type 1, 2 and 3, and this disorder is known to represent 3-6% of all the cases of childhood deafness (Pan et al., 2017). Patients suffering from Usher syndrome present with congenital severe-to-profound bilateral sensorineural hearing loss, vestibular defects, and progressive blindness (retinitis pigmentosa). The table below describes the genes mutated in the three forms of Usher syndrome (**Table 4**). The table illustrates the relationship between Myosin VIIa dysfunction and the pathophysiology of Usher syndrome, highlighting the importance of the protein both for the structure and function of the bundles.

Table 4. Genes associated with Usher syndrome and the signs and symptoms of the disease.

<table>
<tr><th colspan="4">Usher Type 1</th></tr>
<tr><th rowspan="2">Gene</th><th rowspan="2">Subtype</th><th colspan="3">Signs and symptoms</th></tr>
<tr><th>Hearing</th><th>Vision</th><th>Balance</th></tr>
<tr><td>MYO7A</td><td>USH1B</td><td rowspan="6">Congenital severe-to-profound hearing loss</td><td rowspan="6">Progressive loss of vision starting from childhood</td><td rowspan="6">▪ Delayed sitting ability
▪ Delayed walking ability
▪ Ongoing balance issues</td></tr>
<tr><td>USH1C</td><td>USH1C</td></tr>
<tr><td>CDH23</td><td>USH1D</td></tr>
<tr><td>PCDH15</td><td>USH1F</td></tr>
<tr><td>USH1G</td><td>USH1G</td></tr>
<tr><td>CIB2</td><td>USH1J</td></tr>
<tr><th colspan="4">Usher Type 2</th></tr>
<tr><th rowspan="2">Gene</th><th rowspan="2">Subtype</th><th colspan="3">Phenotypes</th></tr>
<tr><th>Hearing</th><th>Vision</th><th>Balance</th></tr>
<tr><td>USH2A</td><td>USH2A</td><td rowspan="3">Congenital mild-to-severe hearing loss</td><td rowspan="3">Progressive loss of vision in adolescents / young adults</td><td rowspan="3">No phenotype present</td></tr>
<tr><td>GPR98</td><td>USH2C</td></tr>
<tr><td>WHRN</td><td>USH2D</td></tr>
<tr><th colspan="4">Usher Type 3</th></tr>
<tr><th rowspan="2">Gene</th><th rowspan="2">Subtype</th><th colspan="3">Phenotypes</th></tr>
<tr><th>Hearing</th><th>Vision</th><th>Balance</th></tr>
<tr><td>CLRN1</td><td>USH3A</td><td rowspan="2">▪ No congenital hearing loss
▪ Progressive hearing loss developing from adolescence</td><td rowspan="2">Progressive loss of vision in adolescents / young adults</td><td rowspan="2">Variable vestibular abnormalities (usually mild)</td></tr>
<tr><td>HARS</td><td>USH3B</td></tr>
</table>

The most common types of Usher Syndrome are types 1 and 2 and for both these types the mutated genes are involved in the production of proteins associated with the hair cell bundle. For type 2 Usher Syndrome the mutated genes are involved in the production of ankle links proteins, while for type 1 the modified genes are responsible for the production of proteins related to tip links, lateral links and top links or connectors (Castiglione and Möller, 2022). At the same time, the most common gene presenting with modifications in patients with Usher Syndrome type 1 is *MYO7A*.

Murine models for the *MYO7A* human point mutation (R502P, *Shaker-1* model) had been previously assessed and presented with a delay in hair cell maturation, with hair cell bundles that had only two rows of stereocilia instead of three (Self et al., 1998) and with hair cells that began to reduce in size upon hearing onset at P12. At the same time, the tectorial membrane altered its shape and twisted and later on the cells degenerated (Deol, 1956; Saw et al., 1997; Brown and Ruben, 1969).

Therefore, one of the aims of the current project was to assess whether gene therapy approaches could restore the hearing function present in the murine model for Usher Syndrome type 1B (*Shaker-1*). It was hypothesized that AAV-*MYO7A* surgical inoculation in *Shaker-1* mice would (1) prevent or restore hair cell bundle morphology and that the transduced cells would have the normal three rows of stereocilia and (2) the mice would not present hearing defects and would have a certain degree of hearing ability.

1.10. Mysin7a and age-related hearing loss

In addition to the point mutation *MYO7A* mouse model, which replicates congenital hearing loss, the conditional knockout of the gene with Myosin15-CRE$^{+/-}$ line (*Myosin VIIa$^{fl/fl}$ x Myosin15-CRE$^{+/-}$*) leads to morphological and functional changes in the hair cells that mimic those present during age-related hearing loss. In Myosin VIIa$^{fl/fl}$ x Myosin15-CRE$^{+/-}$, the MET channels are non-functional. Research carried out in this mouse line, as well as in aged wild-type mice (C57BL/6), showed that IHCs are re-innervated by the efferent system (Corns et al., 2018; Fuchs and Lauer, 2018). As already mentioned in the previous Chapters, the efferent cholinergic neurons originate in the brainstem and their role is in selective attention, distinguishing sounds in noisy environments, sound localization and in reducing cochlear damage. In the aged

cochlea, the efferent neurons that normally innervate the afferent fibres, made direct contacts with the IHCs (**Figure 1.12**). The identity of the efferent neurons that make direct contact with the IHCs is currently not confirmed, but immunostaining data suggests that they are LOC efferents (Jeng et al., 2021). It is currently unknown whether in the aged, deafened cochlea the efferent re-wiring shifts from mature to immature in order to recapitulate cochlear development and try to repair the damaged auditory machinery or whether this process of efferent re-wiring has a negative impact on the auditory system.

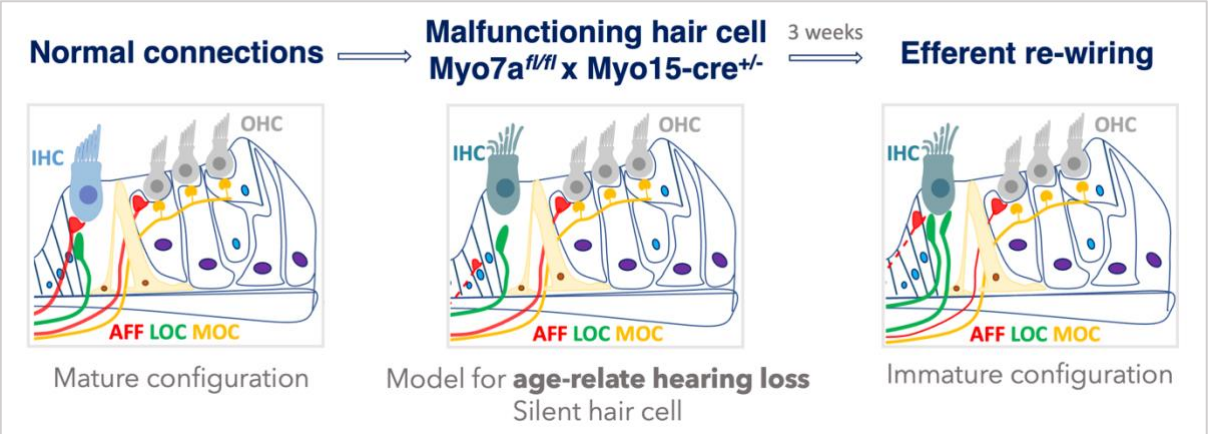

Figure 1.12: Cholinergic efferent innervation is re-established in aged mouse models and can be induced by silencing the hair cell. In the mature cochlea (left panel), the IHC (blue) are innervated directly by the afferent neurons (red) and indirectly by the efferent neurons (green). However, recent data showed that when the IHC is malfunctional (dark blue) and the MET current is abolished (left and middle panels), the cholinergic afferent neurons (green) innervate the IHC directly, similarly to the pre-hearing stages. The exact identity of the efferent fibre that innervates the IHC during the rewiring programme is currently unknown (LOC or MOC) and similarly it is unknown whether the afferent fibre is present adjacent to the IHC or whether it retracts.

Since the recently published data illustrates that the absence of *MYO7A* and MET function promotes the re-innervation of the efferent system (Corns et al., 2018), the aim of this study was to understand whether gene therapy approaches can revert the reorganization of the efferent system back to a normal state. It was hypothesized that AAV-*MYO7A* surgical inoculation in *Myosin VIIa*$^{fl/fl}$ *x Myosin15-CRE*$^{+/-}$ murine models

would (1) aid in the restoration of hair cell function that would consequently (2) promote efferent system to revert to its mature configuration and that this would overall (3) aid in the recovery of hearing activity. Therefore, through this approach we would determine whether the system is plastic and can be manipulated to recover its function.

1.11. Overall scope of the project

Throughout the introduction general information related to the mammalian auditory system function and dysfunction was presented.

Figure 1.13. describes the overall scope of the present project which is to assess whether gene therapy approaches can aid in restoring the normal morphological features and hearing function in two *MYO7A* murine models that recapitulate phenotypes for congenital hearing loss (*Shaker-1*) and age-related hearing loss (*Myosin VIIa*$^{fl/fl}$ *x Myosin15-CRE*$^{+/-}$).

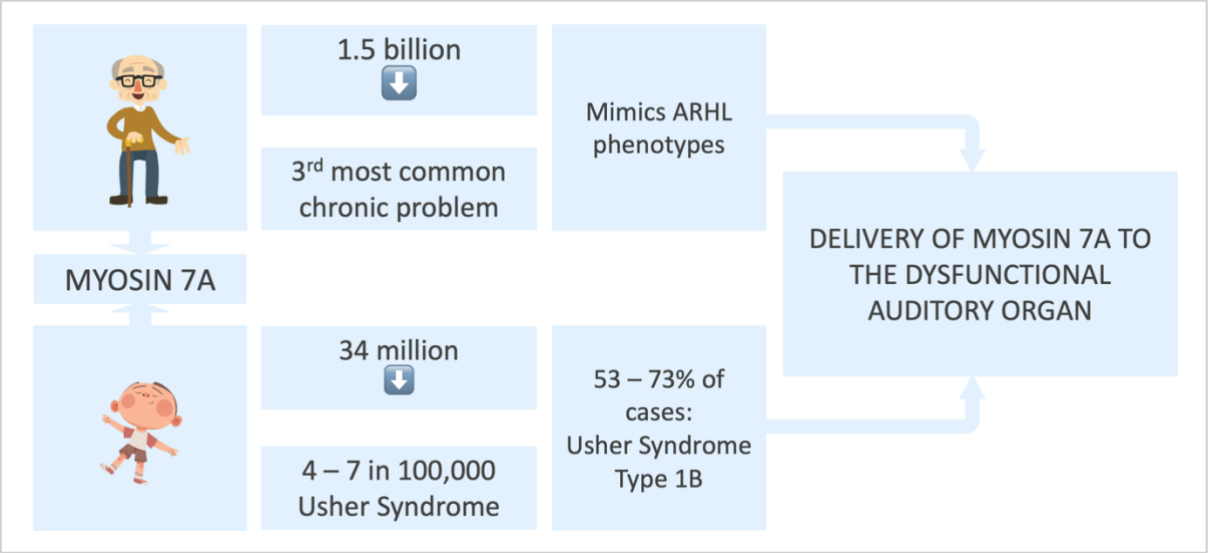

Figure 1.13: Myosin VIIa – model for two diseases. At the present time 1.5 billion adults live with hearing loss and deafness represents the third most common chronic problem. It is known that the chance of developing hearing loss dramatically increases with age. At the same time, 34 million children suffer from deafness, and it is known that Usher syndrome affects approximately 4 – 7 in 100,000 people worldwide. Out of all Usher Syndrome cases, 53 – 73% of the patients suffer from Usher Syndrome Type 1B. Therefore, it is of importance to better understand whether the auditory system can be manipulated, revert the hearing loss phenotype and achieve a therapeutic benefit in models that mimic age-related and congenital hearing loss. This will be achieved through the delivery of *MYO7A* to the dysfunctional cochlea of two *MYO7A* mutant mouse models briefly described in this chapter - *Myosin VIIa*$^{fl/fl}$ *x Myosin15-CRE*$^{+/-}$ and *Shaker-1*.

Table 3. Some examples of data published until June 2019 related to restoration of auditory function in mammalian models through AAV-based gene therapy. (Where the gene name is not present, the data illustrates the serotype used, the delivery method and transfection efficiency for that particular AAV.) RWM=round window membrane; P=postnatal.

Gene	Animal Model	AAV serotype	Delivery method	Transduction efficiency IHC	Transduction efficiency OHC	Titration (GC/mL)	Injection age	Follow-up age	Recovery	Reference
Vglut3	Mouse	AAV1	RWM	100%	-	2.3×10^{10}	P1-P3	P483-P489	✓	Akil et al., 2012
				40%	-		P10 – P12	P483-P489	✗	
Reporter	Mouse	Anc80L65	RWM	Apex, Base: 100%	Apex, Base: 95%	1.7×10^{12}	P0-P2	5-29 days after surgery	-	Landegger et al., 2017
		AAV8		Apex, Base: aprox. 20%	Apex, Base: 0%	1.3×10^{12}				
Harmonin	Mouse	AAV2/Anc80L65	RWM	69%	65%	9.0×10^{12}	P1	6 weeks	✓	Pan et al., 2017
Reporter	Mouse	AAV2/9	RWM	30.26%	-	3.90×10^{13}	P15 – P16	2 weeks after surgery	-	Yoshimura et al., 2018
		AAV2/9	RWM + canal fenestration	95.2%		3.90×10^{13}				
		AAV2/9		17.36%		1.40×10^{12}	P56 – P60			
NT3	Guinea pig	AAV8	Cochleo-stomy	Apex, Base: 0-100%	-	6.92×10^{13}	2-3 months old	2 weeks after surgery	✓	Chen et al., 2018
Otof	Mouse	AAV8	RWM	80%	50%	3.34×10^{13}	P1-P3	P15-P21	✓	Tertrais et al., 2018
Otof	Mouse	AAV2/6	RWM	77%	-	$(1.2\text{-}1.38)\times10^{13}$	P1-P2	3-4 weeks after surgery	✓	Al-Moyed et al., 2018
				-	-		P6-P7		✗	

Otof	Mouse	AAV2	RWM	60%	-	6.3×10^{12} 4.5×10^{12}	P10 P17 P30	8 weeks after surgery	✓	Akil et al., 2019
NT3	Mouse	AAV2/Anc80L65	Semicircular canal	-	-	2.3×10^{12} 3.1×10^{12}	6-9 weeks	11 weeks	✓	Hashimoto et al., 2019
Reporter	Mouse	AAV2.7m8	Semicircular canal	84.1%	83.1%	9.75×10^{12}	1-6 months	4 weeks after surgery	-	Isgrig et al., 2019
		AAV8BP2		55.7%	44.1%	1.10×10^{12}				
		AAV2		43.6%	54.5%	5.69×10^{12}				
		AAV8		86.%	51.7%	1.16×10^{12}				
Atoh1	Mouse	AAV-ie	RWM	Support cells: 90%		1.0×10^{10}	P3	P17 – P30	✓	Tan et al., 2019

Chapter 2: Materials and methods

OUTLINE

In the methodology chapter, the following information related to the current project will be addressed:

- ethics statement
- management of anaesthesia and analgesia
- species and strains
- genotyping protocol
- plasmid and small-scale viral production
- organotypic cultures for *in vitro* AAV testing
- auditory brainstem response recordings
- scanning electron microscopy
- immunolabelling and confocal microscopy
- statistical analysis.

2.1. Ethics and anaesthesia

2.1.1. Ethics statement

All animal procedures were approved by the University of Sheffield, United Kingdom and were licensed by the Home Office under the Animals Scientific Procedures Act (ASPA) 1986 (Personal Project Licence: PCC8E9E53) and were carried out in compliance with the guidelines of the University of Sheffield Ethical Review Committee.

2.1.2. Anaesthesia and analgesia management

Prior to surgical procedure animals had subcutaneous injections done with the analgesic Metacam (2-3mg/kg; Boehringer Ingelheim, **Table 10**). Early postnatal mice or gerbils (P0 – P5) and adult animals (P15 – P40) were anaesthetized with gaseous Isoflurane (conditions listed in **Table 10**). The entire surgery was carried out on heat a mat set at 37℃ to maintain the adequate body temperature. Adult mice had Lubrithal lubricator gel (Dechra) applied on the eyes in order to moisturise and maintain the tear layer of the eye during the procedure. The surgical wound was closed using GLUture (Zoetis) tissue glue that offered a flexible seal and a strong bond on the surgery site. Upon finishing the surgical procedure, mice or gerbils were placed into separate cages on a heated pad at 37℃ and monitored until they were moving and responded as non-procedure littermates. The following day, animals were given 50 μL of Metacam oral analgesic (Boehringer Ingelheim, **Table 10**) and, when required, EMLA local analgesic cream that was topically applied (prilocaine and lidocaine; AstraZeneca, **Table 10**). Subsequent experiments were carried out at least 2 – 4 weeks post-injection for the early postnatal and adult injections.

Table 10. Anaesthesia and analgesia management options and drugs used.

General anaesthesia: Isoflurane	**Oxygen (gas carrier)**	**Isoflurane**
Induction	2 L / min	5.0 %
Maintenance	0.8 L / min	2.0 – 3.0 %
Pain management / analgesia	**Administration route**	
Metacam	Subcutaneous injection (prior to procedure)	
Metacam	Oral (after procedure)	
EMLA	Local / topical (after procedure)	

After surgical procedure hearing function was tested through auditory brainstem responses (ABRs) that were carried out on mice anaesthetized with Ketamine (100mg/kg; Fort Dodge Animal Health) and Xylazine (10mg/kg; Rompun 2%; Bayer).

2.2. Animal used

Experiments were performed on two rodent species – *Mus musculus* mouse and Mongolian gerbil of both sexes. The choice to use gerbils in hearing research is grounded in the physiological similarities between the gerbil and human inner ears. Gerbils are recognised for their sensitivity to high-frequency sounds, which is in line with human hearing capabilities. Due to this reason the gerbils represent models that can replicate aspects of human auditory processing that are limited in other rodents and in this way supports the translation of research findings easier to humans. The background strain for the *Shaker-1* was 85% CBA and 15% mixed (unspecified) and for *Myo7a*$^{fl/fl}$ *x Myo15-CRE*$^{+/-}$ the background strain was C57BL/6N. **Table 5** includes information on the species and strains used in the present experiments.

Table 5. Animal species used in the present project and brief description of each model.

Species	Strains	Model
Mouse *(Mus musculus)*	*Myo7a*$^{fl/fl}$ *x Myo15-CRE*$^{+/-}$	Progressive hearing loss Age-related hearing loss
	Shaker-1	Congenital hearing loss Usher syndrome type 1B
	C57BL/6J (6J)	Wild-type used with AAV-reporter
	C57BL/6NTac (6N)	Wild-type used with AAV-reporter
	C3H-HeJ	Wild-type used with AAV-reporter
Mongolian gerbil *(Meriones unguicalatus)*	Not applicable	Wild-type used with AAV-reporter

As already listed in *Chapter 1*, *Shaker-1* mice have a point mutation in *MYO7A* and recapitulates the hair cell morphological and functional defects observed in Usher syndrome type 1B (Self et al., 1998; Hasson et al., 1998; Lillo et al., 2003). The *Myo7a*$^{fl/fl}$ *x Myo15-CRE*$^{+/-}$ strain is a hair cell conditional knockout model, in which *MYO7A* is knocked out once *MYO15* starts being expressed at around P4. For *MYO7A* exons 10 and 11 were floxed and the cre-recombinase gene expression was driven

by the hair cell specific *MYO15* promoter. The cre-LoxP system recognises and deletes the *MYO7A* sequence that is located between the loxP sites (Caberlotto et al., 2011; Corns et al., 2018). In this way, the cre-LoxP system allows the hair cells to develop normally until the *MYO15* promoter expression and *MYO7A* is subsequently knocked out.

In addition to these models, both Mongolian wild-type gerbils and mice (*C57BL and C3H*) were also used in the project with AAV-reporters.

Animals were housed at the University of Sheffield in well ventilated cages, on 12-hour light - dark cycles, in rooms at a temperature of 20 – 24℃ with *ad libitum* food and water.

2.3. Genotyping

The mice were genotyped by carrying out polymeric chain reactions (PCR) to amplify the DNA which was then sequenced for the *Shaker-1* model or genotyped for the *Myo7a*$^{fl/fl}$ *x Myo15-CRE*$^{+/-}$ model (**Table 6**).

To do the PCR reaction, lysis buffer (25 mM NaOH, 2 mM Ehylenediamine tetra aetic acid – EDTA, Sigma, 102433425) was used to extract the DNA from ear clips (done at P14 or P21) or tail samples (done at P0). The ear or tail clips were incubated at 95℃ for 1h. Subsequently, 40 mM of Tris hydrochloride buffer was added to each sample. The PCR reactions were carried out with 1 μL of the forward primer and 1 μL of the reverse primer (**Table 6**), 10 μL of 2 x GoTaq master mix, 7 μL dH_2O and 1 μL of DNA or 1 μL of water to act as a negative control. After this, 10 μL of the PCR products were loaded onto a 2 % agarose gel and the gel was run for 1 hour at 120 V.

Table 6. Primers, primer sequences, protocol, and band sizes for genotyping of the two strains used in the project.

Strain	Primers	Primer sequence 5' end – 3' end	Protocol	Band size
Shaker-1	Sh1_F	GAG CAT CGA CTG GTT GCA CA	1. 95°C x 5 min 2. 95°C x 30 sec 3. 60°C x 30 sec 4. 72°C x 30 sec 5. Repeat 2 – 4 (35 times) 6. 72°C x 5 min 7. 12°C hold	WT / MUT: 130 bp
	SH1_R	CCA CCT TGG GGA ACT TGC TC		
Myo7a$^{fl/fl}$	MYO7A_F	GGG AGA GAA AGC AGG GTG TG	1. 95°C x 5 min 2. 95°C x 30 sec 3. 65°C x 30 sec 4. 72°C x 45 sec 5. Repeat 2 – 4 (35 times) 6. 72°C x 7 min 12°C hold	WT: 360 bp MUT: 510 bp
	MYO7A_R	AAG CTG GAC TCT CTG GTG GC		
Myo15-CRE$^{+/-}$	MYO15_P1	AGG GAC CTG ACT CCA CTT TGG G	1. 95°C x 5 min 2. 95°C x 30 sec 3. 65°C x 30 sec 4. 72°C x 30 sec 5. Repeat 2 – 4 (35 times) 6. 72°C x 5 min 12°C hold	WT: no band MUT: 500 bp
	MYO15_P2	TGG TGC ACA GTC AGC AGG TTG G		

2.4. Plasmid and small-scale viral production

In order to test whether a normal copy of Myosin VIIa was sufficient to restore the typical morphology and function of the hair cells in the *Shaker-1* and *Myo7a*$^{fl/fl}$ *x Myo15-CRE*$^{+/-}$ mouse models, the cDNA had to be cloned into AAV vectors. This procedure was carried out by collaborators (Saaid Safieddine & Marie-Jose Lecomte) at Institute Pasteur (Paris, France). Hence this section will only briefly describe the process and the approaches used to obtain the AAV-MYO7A.

Recent published data showed that AAV vectors are efficient at transducing corrective genes into the auditory hair cells and are also able to restore hearing function in mouse models of human deafness (**Table 3, Chapter 1**). Nonetheless, as already mentioned in the previous chapter, the packaging capacity of AAV is 4.7 kb, which limits their use for the delivery of large genes such as *MYO7A* (6.6 kb, Ginger and Samulski, 2005;

McClements and Maclaren, 2017). In addition to this, considering that the transgene expression cassette consists of the promoter, the polyadenylation site and additional post-transcriptional regulatory elements, the cDNA of the transgene cannot be larger than 3.5 kb (Duan et al., 2003). To address this issue, previous studies have used either adenoviruses or lentiviruses that have higher packaging capacities. However, both adenoviruses or lentiviruses have a similar transduction efficiency of AAVs, but have lower safety profiles (Anson, 2004). Therefore, recent publications have used a dual-AAV systems where the transgene is split into two vectors. To obtain the full gene expression from the dual system, several approaches have been used (**Table 7**). For the current project, a trans-splicing approach was used to reconstitute the expression of Myosin VIIa, with the dual-AAV vectors carry non-overlapping halves of *MYO7A* (the 5' fragment and the 3' fragment: **Figure 2.1A**). The 5' and 3' fragments of *MYO7A* were cloned into AAV vectors and each had a recombinogenic bridging sequence. The AAV-MYO7A-Nterm (5' fragment) consisted of the promoter, the first half of the *MYO7A* gene and was followed by a splice donor site (**Figure 2.1A**). At the same time, the AAV-MYO7A-Cterm (3' fragment) consisted of the acceptor site, followed by the second half of the *MYO7A* gene, and was followed by the polyadenylation sequence (polyA, **Figure 2.1A**). Both AAV vectors have their transgene cassette flanked by ITR sequences which undergo non-homologous end-joining concatemerization (**Figure 2.1B**). Upon co-injection of the two separate AAV vectors encoding the 5' and 3' fragments of Myosin VIIa, the full-length *MYO7A* mRNA will be expressed in the target cells, which will be translated into the functional Myosin VIIa protein (**Figure 2.1B**).

Table 7. Strategies for split-AAVs that facilitate the expression of large transgenes. All techniques have been used to deliver large genes into a variety of tissues. Nonetheless, the results of studies that assess their efficiency are conflicting.

Strategy		Characteristics
1	Trans-splicing	Several transgene copies link through non-homologous end-joining of the ITR regions (process also called concatemerization).
2	Overlap	The 5' and 3' fragments contain overlapping homologous transgene cDNA sites. The full-length gene is expressed through the process of homologous recombination of the overlapping regions. In this case the transgenes share a region of homology.
3	Hybrid splicing	The transgenes of each AAV vector contain both overlapping sequences, as well as site donor and site acceptor regions. In this case, the transgene expression is achieved through concatemerization (1) and homologous recombination (2).
4	Miniature gene	Oversized transgenes can be modified to retain the relevant and crucial domains of the protein and fit these within one singe AAV vector. In this approach, there is a single AAV vector that carries a mini-gene. However, through this approach it is sometimes difficult to restore full function.

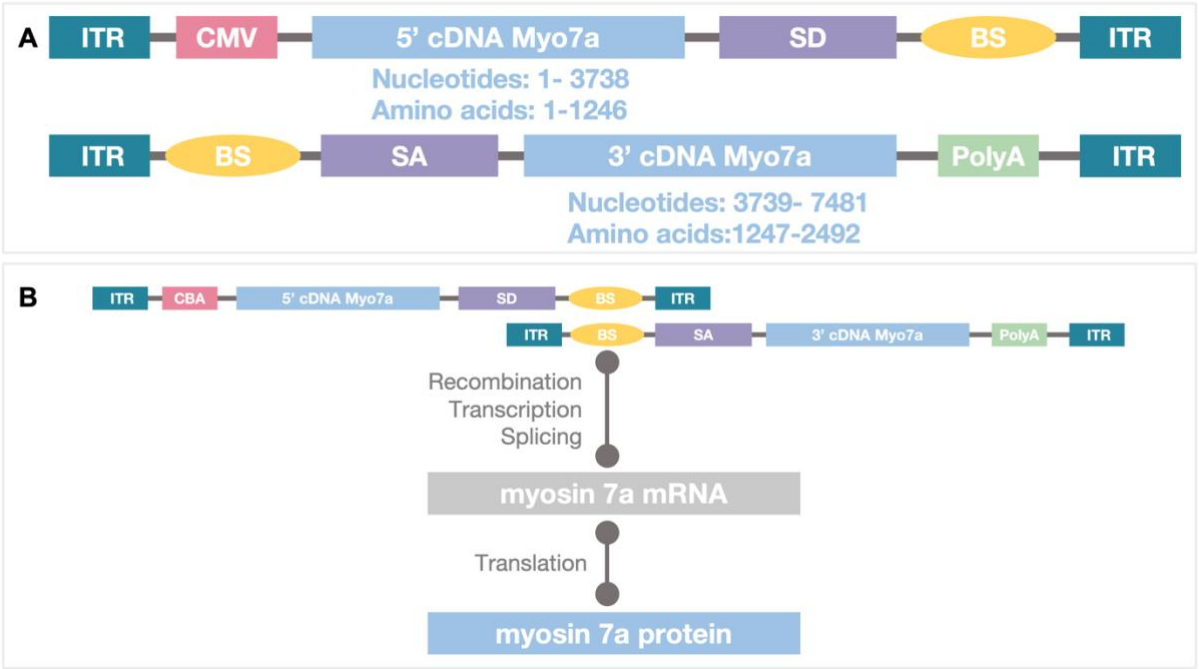

Figure 2.1: Dual-AAV vector construct. (A) The AAV design for *MYO7A* N – and C – terminals containing the 5' and 3' parts of the Myosin VIIa cDNA. The 5' part of the cDNA is followed by the splice donor (SD) site and the 3' part is preceded by the spice acceptor (SA) site. **(B)** The Myosin VIIa protein is generated when the two vectors form concatemers aided by the ITR sites. ITR: inverted terminal repeat; CMV: promoter; BS: binding sequence; SD: splice donor; SA: splice acceptor; polyA: polyadenylation signal.

In the present study two capsids were studied – AAV8 and AAV9. The capsids were chosen based on previous studies that assessed the tissue serotype preference and transduction efficiency in the auditory system. For example, AAV8 and AAV9 were shown to have high infection rates in tissues that include the retina and central nervous system, which have cells that are similar to the inner ear hair cells (Tao et al., 2018; Omichi et al., 2020; Verdoodt et al., 2021; Isgrig et al., 2022). The different serotypes receptos, co-receptors and tissue preference are listed in **Table 8**.

Table 8. AAV serotypes, the attachment receptors, co-receptors and tissue preferences.

Serotype	Receptor	Co-receptor	Examples of preferred tissues	References
AAV1	N-linked sialic acid	AAVR	CNS, retina	Choudhury et al., 2016; Nance and Duan, 2015
AAV2	Heparan sulfate proteoglycan	LamR, AAVR, FGFR1, $\alpha 5\beta 1$-integrin, HFGFR	CNS, liver, kidney	Perabo et al., 2006
AAV3	Heparan sulfate proteoglycan Laminin	LamR, AAVR, HFGFR, FGFR	Inner ear, skeletal muscle	Nance and Duan, 2015
AAV4	O-linked sialic acid	Unknown	CNS, retina	Verdera et al., 2020
AAV5	N-linked sialic acid	AAVR, PDGFR	CNS, retina	Pietersz et al., 2021; Wiley et al., 2018
AAV6	Heparan sulfate proteoglycan, N-linked sialic acid	AAVR, EGFR	Heart, skeletal muscle, bone marrow	Nance and Duan, 2015.
AAV7	Unknown	Unknown	CNS	Samaranch et al., 2013
AAV8	Unknown	LamR, AAVR	CNS, retina, pancreas, heart, liver	Nance and Duan, 2015
AAV9	N-linked galactose	LamR	Inner ear, CNS, pancreas, kidney, lung, liver, heart	Samaranch et al., 2013; Nance and Duan, 2015
AAV10	Unknown	LamR	CNS, retina	Belova et al., 2022
AAV11	Unknown	Unknown	Muscle, kindney	Belova et al., 2022
AAV12	Unknown	Unknown	Salivary glands, muscle	Belova et al., 2022
AAV13	Heparan sulfate proteoglycan	Growth factor receptor	CNS	Han et al., 2022

The chosen capsids contained reporters (GFP or mCherry) or the *MYO7A* cDNA. Each construct had different titrations and the concentrations for surgery were adjusted based on both constructs. **Table 9** lists the capsids, the plasmids, the reporters and the titration for each viral construct, as well as the characteristics of the construct, the promoter and the manufacturer or provider. **Table 9** lists all viral constructs that were used in the present project.

Table 9. AAV serotypes, the reporter or cDNA packaging, promoters and titrations, as well as the manufacturer or provider of each construct used in the present project.

Construct	Promoter	Titration	Characteristics	Manufacturer Provider
AAV8-GFP	CMV	1.2 x 10^{12} vg/mL	AAV8 with GFP reporter	Addgene (Catalog # 105530 – AAV8)
AAV9-GFP	CMV	6.1 x 10^{12} vg/mL	AAV9 with GFP reporter	SITraN (Prof. M. Azzouz)
dsAAV9-GFP	CMV	7.9 x 10^{12} vg/mL	Self-complementary AAV9 (double stranded) with GFP reporter	
AAV9-mCherry	CMV	1.0 x 10^{13} vg/mL	AAV9 with mCherry reporter	
AAV8-MYO7A-Nterm (C1)	CMV	2.68 x 10^{13} vg/mL	AAV8 with 5' part of murine Myo7a cDNA (first batch)	Institut Pasteur (Dr. S. Safieddine, Marie-José Lecomte)
AAV8- MYO7A-Cterm (C1)	CMV	1.64 x 10^{13} vg/mL	AAV8 with 3' part of murine Myo7a cDNA (first batch)	
AAV8- MYO7A-Nterm (C2)	CMV	1.0 x 10^{13} vg/mL	AAV8 with 5' part of murine Myo7a cDNA (second batch)	
AAV8- MYO7A-Cterm (C2)	CMV	6.3 x 10^{12} vg/mL	AAV8 with 3' part of murine Myo7a cDNA (second batch)	
AAV8- MYO7A-Nterm (C3)	CMV	2.08 x 10^{13} vg/mL	AAV8 with 5' part of murine Myo7a cDNA (third batch)	
AAV8- MYO7A-Cterm (C3)	CMV	6.3 x 10^{12} vg/mL	AAV8 with 3' part of murine Myo7a cDNA (third batch)	
AAV9-PHP.eB-MYO7A-Nterm (vMJL29)	CMV	1.5 x 10^{13} vg/mL	Vector pair corresponding to the same dual vectors used for AAV8-MYO7A produced with PHP.eB capsid	
AAV9-PHP.eB-MYO7A-Cterm (vMJL21)	CMV	6.8 x 10^{12} vg/mL		
AAV9-PHP.eB-MYO7A-Nterm (vMJL41)	CMV	1.0 x 10^{13} vg/mL	Vector pair corresponding to murine MYO7A dual vector designed with a new site junction produced with PHP.eB capsid	
AAV9-PHP.eB-MYO7A-Cterm (vMJL42)	CMV	1.8 x 10^{12} vg/mL		

Since the viral vectors were produced by our collaborators, the process of production is only briefly described in **Figure 2.2**.

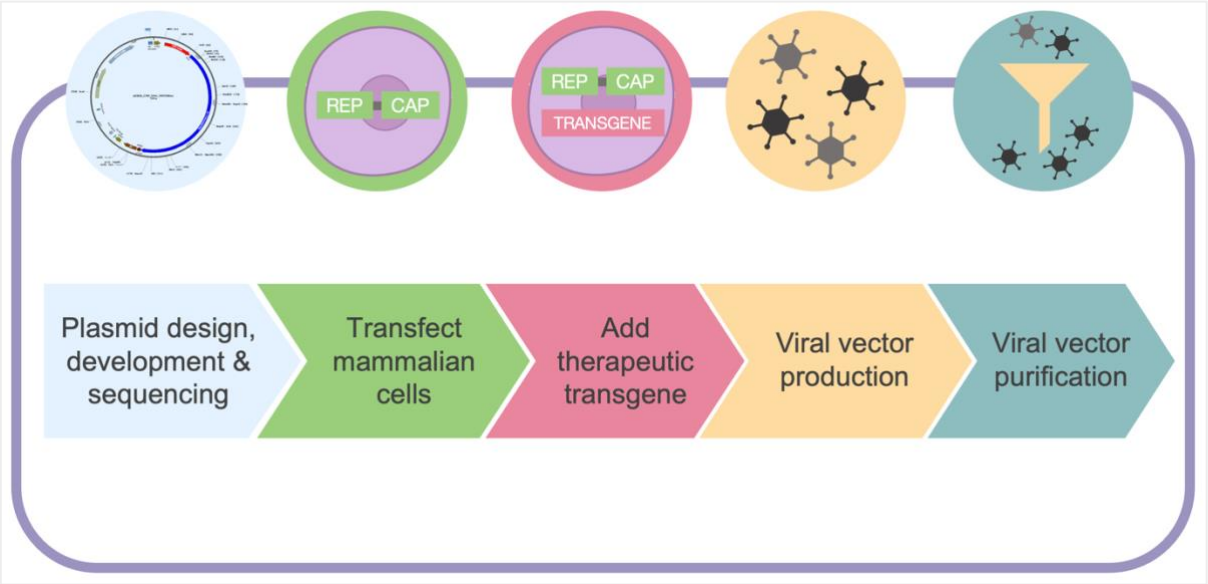

Figure 2.2: Small-sale viral vector production. The figure illustrates the viral vector manufacturing process which start with the plasmid design, development and sequencing and are followed by the transfection of *rep* and *cap* AAV genes into mammalian cells (HEK293 or HeLa). Subsequently, the therapeutic transgene is added to the cells and the viral vector is produced and purified.

2.5. AAV transduction of organotypic cultures

Prior the transduction of AAVs with the reporter genes *in vivo*, some *in vitro* experiments were performed to assess whether the constructs had a toxic effect on auditory hair cells. Therefore, I tested AAV8 and AAV9-based vectors expressing green fluorescent protein (GFP) under the control of the CMV promoter.

For this work, P4 pups were culled by cervical dislocation and submerged in 80% ethanol for a few minutes to sterilise and kill any bacteria. Pups were transferred into large petri dishes with sterile Hank's solution made with 5 mL Hepes Buffer (Sigma, H0887) and 500 mL HBSS (Gibeco, 14025100), which were kept under a laminar air flow cabinet. After sequential washes in Hank's solution, the cochleae were dissected

out and cultured on collagen (Corning, MA, USA) for 24 h (P4 + 1 day *in vitro*) in DMEM-F12 media (Sigma, D8062) supplemented with 5% foetal bovine serum (FBS, Gibeco, FB-1001H/500) and 5 µg/mL Ampicillin (Sigma, A9518). Cultures were initially prepared in these experiments by Prof. Walter Marcotti and subsequently by me. Organotypic cultures were kept in an incubator at 37°C and 5% CO_2. After 24h, the cochleae were incubated for another 48h with AAV8-GFP or AAV9-GFP titrated in F12 medium with Ampicillin. This was followed by the removal of the media and vectors and the addition of F12 medium supplemented with Ampicillin. At P4 + 8 days *in vitro*, the cultures were fixed in 4 % paraformaldehyde (PFA, Agar Scientific, AGR1026), washed in phosphate buffered saline (PBS, Oxoid, Dulbecco A, BR0014G), permeabilised in 1 × PBS + 0.5% Triton X-1000 (Sigma, T9284) and then labelled with Texas Red-X Phalloidin (1:300, **Table 11**). Subsequently, the samples were washed in 1×PBS and mounted on slides using Vectashield (VectorLabs).

2.6. Auditory brainstem response

ABRs were used to measure the electrical activity from the hair cells to the central auditor pathway, allowing to assess the hearing ability of mice (**Figure 2.3**). For example, the absence of the wave I within the ABR recordings would illustrate the dysfunction of the IHCs or damage of the type I SGN fibres (**Figure 2.3**).

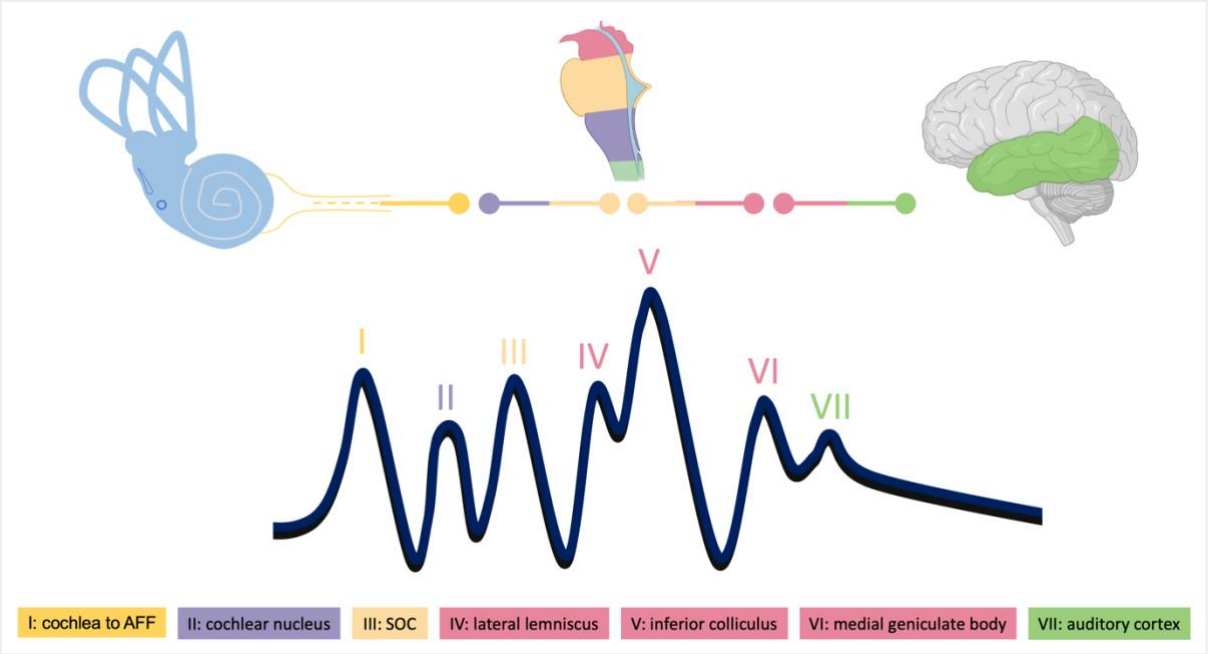

Figure 2.3: Auditory brainstem response trace. Figure to illustrate the ABR traces recorded from electrodes that are placed subdermally. ABRs are used to stimulate HCs along the cochlea by producing tone bursts that result in synchronized neural discharges. The potentials are generated by the fibre tracts and nuclei of the auditory pathway – starting from the cochlea and ending in the auditory cortex. Wave I of the ABR reflects the activity of the hair cells and the spiral ganglion (AFF), wave II illustrates that the sound information reached the cochlear nucleus, waves III is produced by the superior olivary complex (SOC) and waves IV, V, VI are generated by the lateral lemniscus, inferior colliculus and the medial geniculate body. Lastly, the seventh wave shows the response in the auditory cortex.

After reaching full anaesthesia (see Ethical statement above), mice were placed onto a heated mat set at 37℃ and were placed inside a sound-proof chamber (MAC-3 Acoustic Chamber, IAC Acoustic UK). ABRs were recorded by placing three subdermal electrodes as follows: one behind the pinna of each ear, which are the reference and ground electrodes, and a third active electrode beneath the skin in between the two pinna (**Figure 2.4**). Sound stimulation was delivered to both ears through a loudspeaker (MF-1 multi-field speaker, Tucker-Davis Technologies, USA) that was positioned at either 5 cm away from the pinna when recordings were carried out up to 120 dB SPL or 10 cm away from the pinna when the recordings were carried out up to 95 dB SPL. The speaker was calibrated using white noise and through the use of a low-noise microphone probe system (ER10B+, Etymotic, USA). The

microphone was positioned at either 5cm or 10 cm from the speaker, to mimic the position and hearing stimulation of the mouse. The recordings were collected using software developed by the group of Prof. Steel at King's College, London (Ingham et al., 2011). The software drove the Tucker Davis Technologies (TDT) system for presenting stimuli and recording (RZ6 processor and RA4PA amplifier). Sound stimulation started at 3 kHz and were up to 42 kHz and also included the broadband white noise (click). The click provided an estimation of the magnitude of hearing loss. The amplitude started at 0 dB SPL and was up to 95 dB SPL or 120 dB SPL in 5 dB increments. Each stimulation consisted of a 5 ms pulse with a 1 ms on/off ramp time, and these pulses were presented at 42.6 / second, and each reading produced was representative of 256 repetitions.

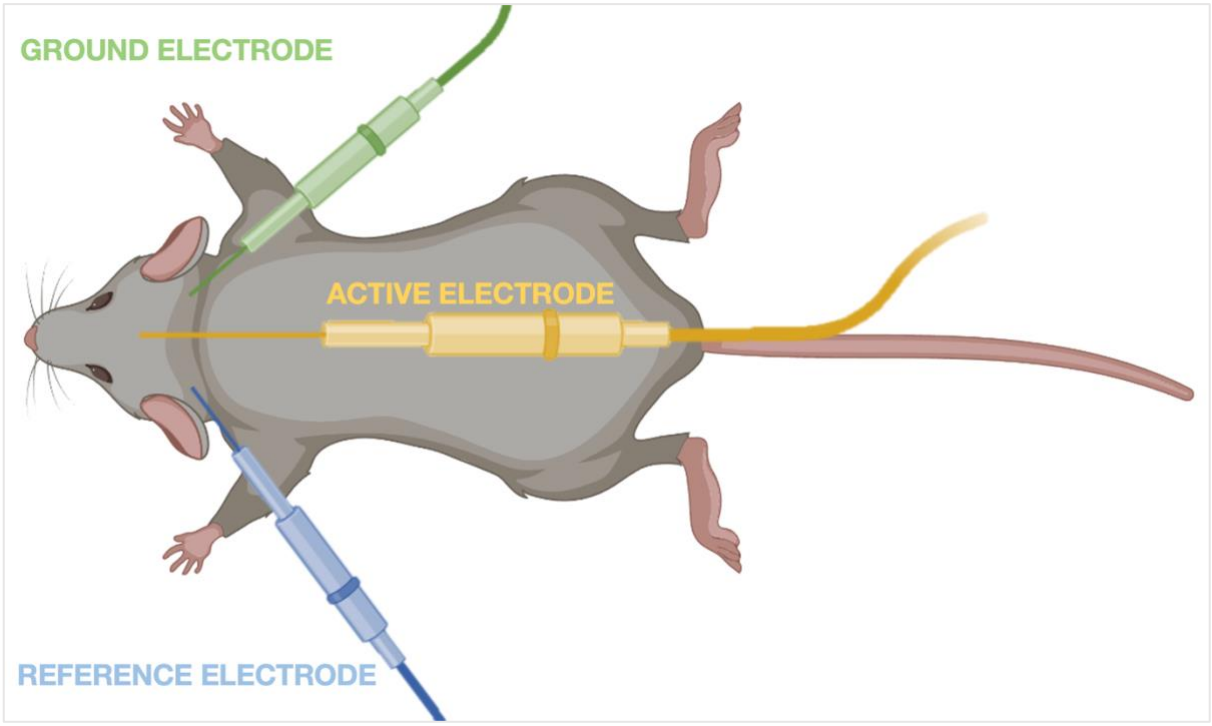

Figure 2.4: Auditory brainstem response placement of the electrodes. Figure showing how the ground, active and reference electrodes are placed under the skin. Image created using bioRender.com - https://www.biorender.com.

The hearing threshold was recorded when the first ABR waveform feature was detected and was visible. The ABR thresholds were also evaluated by Prof. Marcotti. After the procedure, the animals were either culled with Dolethal (200 mg/ml; Vetoquinol) or schedule 1 (cervical dislocation) and the cochleae were processed for scanning electron microscopy (SEM) or immunostaining.

2.7. Scanning electron microscopy

Scanning electron microscopy (SEM) was used to assess the hair cell bundle morphology. Cochleae samples were fixed for 2 hours in 2.5% glutaraldehyde that was made in 0.1M sodium cacodylate / 2mM calcium chloride. After fixation samples were washed in sodium cacodylate and were kept in 0.25% glutaraldehyde made in 0.1M sodium cacodylate / 2mM calcium chloride until further processing. Subsequently, samples were dissected and then incubated for 1h in osmium (1% osmium tetroxide in 0.1M sodium cacodylate 2 2mM calcium chloride). Following this, samples were washed three times in buffer and stored overnight in 70% ethanol and then rehydrated next day. For osmium impregnation, cochleae were incubated in thiocarbohydrazide for 20 minutes and then the samples were washed in distilled water. Afterwards, samples were placed in 1% osmium tetradoxide made in 0.1M sodium cacodylate / 2mM calcium chloride for 2 hours. Samples were then washed six times in distilled water and stored overnight in water and placed in 70% ethanol overnight. Next day, the 70% ethanol was removed, and the samples were incubated for 10 minutes in 80%, 90% and 100% ethanol. Samples underwent critical point drying using a Leica EM CPD300 dryer and following this the dissected cochleae were imaged at 10 kV on the electron microscope (Tescan Vega 3). All SEM post-fixation procedures were carried out by Dr Anna Underhill or Dr Adam Carlton.

2.8. Immunolabelling and confocal microscopy

For the dissection of the cochlea, mice or gerbils were culled by cervical dislocation and the cochlea was extracted from the temporal bones. The cochlea was perfused with 200 μL of 4 % PFA by creating small holes in the apical region of the sample. The cochlea was then placed in Eppendorf tubes containing 1 mL of 4 % PFA. The samples were fixed for 1 hour at room temperature (RT) on a shaker. After this, the tissues were placed in 0.1M EDTA for approximately 1 week (depending on the age). The EDTA was changed every 12 hours and the samples were stored at 4℃. After EDTA treatment, the cochleae were micro-dissected in 1 x PBS, washed three times in 1 x PBS (10 minutes per wash) and permeabilised in 1 x PBS + 0.5% Triton X-1000 (Sigma Aldrich, T9284) for 15 minutes. To block the non-specific binding (if applicable for the experiment), the samples were incubated in 5 horse serum (Sigma Aldrich, H0146) for 1 hour at RT. Subsequently, the following primary antibodies were used: Myosin VIIa, SK2 and / or BK (**Table 11**). The primary antibodies were diluted in 1 % horse serum and were added to the samples and were consequently incubated overnight at 37℃. Next day, the dissected tissue was washed three times with 1 x PBS, once with 1 x PBS + 0.5% Triton X-1000 and then the samples were incubated for 1h at 37℃ with the following secondary antibodies: Alexa Fluor 405, Alexa Fluor 488 or Alexa Fluor 647 (Invitrogen, **Table 11**). After this, the samples were washed three times in 1 x PBS (10 minutes per wash) and the organs of Corti were mounted on slides using Vectashield (VectorLabs) mounting medium.

Table 11. Primary and secondary antibodies used for immunofluorescence.

Primary antibody	Concentration	Manufacturer Provider	Secondary antibody	Concentration	Manufacturer Provider
Myosin VIIa (Rabbit IgG)	1:400	Proteus BioScience Catalogue # PTS-25-6790-C050	Alexa 647 goat anti-rabbit IgG	1:1000	Invitrogen Catalogue # A21245
SK2 (Rabbit IgG)	1:50	Merck Sigma Catalogue # P0483	Alexa 488 goat anti-rabbit IgG		Invitrogen Catalogue # A11034
SV2 (Mouse IgG1)	1:500	DSHB Catalogue # SV2-c	Alexa 405 goat anti-mouse IgG		Invitrogen Catalogue # A48255
BK (Mouse IgG1)	1:100	Antibodies Incorporated Catalogue # 75-408			
Texas Red-X Phalloidin	1:300	Invitrogen Catalogue # T7471			
Alexa Fluor 488 Phalloidin		Invitrogen Catalogue # A12379			

2.9. Statistical tests

Statistical comparisons of means and variance were made by caring-out Student's t-test and one-way or two-way ANOVA followed by the appropriate post-hoc tests (Tukey's or Dunnett's post-test). $p < 0.05$ was selected as the threshold for statistical significance. Mean values are presented in text and figures as mean $\pm$ SD. Statistical analyses were performed using GraphPad Prism 8 (GraphPad Prism Software, Inc., San Diego, CA, USA).

Chapter 3: Results – *In vitro* testing of AAV vector serotypes

OUTLINE

In the present result chapter the following information related to the project will be addressed:

- synopsis to the role of organotypic cochlear cultures in understanding transduction efficiency of different AAV serotypes
- results
- discussion.

3.1. Introduction

Different AAV serotypes have now been widely used to transduce a variety of tissues (see **Table 8**, Chapter 2), however at the beginning of this project the literature on this topic was limited. Therefore, the initial aim was to test the required titration, the possible toxicity and infection efficiency of different AAV serotypes expressing fluorescent reporters. These tests were done in *ex vivo* organotypic cochlear cultures, since such a system is believed to represent an ideal tool for testing efficacy and safety approaches prior to *in vivo* application.

Of the several available AAV serotypes, AAV8 and AAV9 have been reported to be effective in transducing cochlear hair cells in both neonatal and aged murine models (Landegger et al., 2017; Chen et al., 2018; Yoshimura et al., 2018; Isgrig et al., 2019; György et al., 2019). I have therefore tested AAV8, AAV9 and double-stranded AAV9 (hereafter referred as ds-AAV9) vectors that expressed the green fluorescent protein (GFP) under the control of the cytomegalovirus (CMV) promoter. The AAV8-GFP vector used for the expression studies was ordered from Addgene (see **Table 9**, Chapter 2), while the AAV9-GFP and ds-AAV9-GFP were provided by Prof. Azzouz's group (my co-supervisor at the University of Sheffield) (see **Table 9**, Chapter 2).

One relevant consideration for the current chapter relates to the type of vector genome. As mentioned in Chapter 1, vector genomes are usually single-stranded but there are also vector genomes that have a dimeric genome with two complementary DNA sequences (ds-AAV). The single-stranded AAV genomes have two ITRs, the elements required for replication and packaging of the genome into the capsid, which are very similar to the wild-type AAVs. The self-complementary AAV genomes (ds-AAV) have a deletion in one of the ITR sites, which leads to the formation of two DNA sequences that are complementary and that have the modified ITR in the middle. At the 5' and 3' ends of ds-AAV are the wild-type ITRs. Because the ds-AAV is already formed of two DNA strands, the rate-limiting step of the single-stranded AAV to undergo polymerase synthesis is avoided. Hence, the ds-AAV provides a faster way in which the transgene can be expressed in the target cell. In fact, recent studies have showed that there is an enhanced transduction efficiency in the cochlear hair cells when transduced with ds-AAV1 (Maguire and Corey, 2020). Nevertheless, one of the main limitations when using ds-AAV is that the size of the transgene cassette is halved, meaning that the vector capacity is approximately 2.3 kb instead of 4.7 kb. This highlights that such a system cannot be used for large genes such as *MYO7A* where dual constructs are required. Nonetheless, in the current project the *ex vivo* testing of ds-AAV9-GFP was used as a tool for the identification of the transduction efficiency of AAV9 as the infection is faster and does not require maintenance of cultures for extensive periods.

Previous *in vivo* and *ex vivo* studies used research-grade AAV preparation titrations in the range of 10^{10} to 1 x 10^{13} vector genomes (vg) / mL, which led to the transduction of more than 30% of the IHCs and a lower percentage of OHCs (for references see **Table 3**, **Chapter 1**, Rankovic et al., 2021).

Therefore, based on the previously published literature, we aimed to test the transduction efficiency upon infection with AAV-GFP at a titration of 10^{11} vg / mL and to assess if this concentration would be toxic and would impair the hair cell morphology.

3.2. Results

The transduction efficiency of different serotypes was first assessed by evaluating the exogenous expression profile of AAV8-GFP in dissected cochleae from P7 C57BL/6N wild-type mice. For these experiments the explants were fixed after 24h incubation with AAV8-GFP. However, the explanted cochleae did not present any GFP expression (data not shown), suggesting that either the age of the mice or the incubation period with the AAV carrying the reporter gene did not allow for the efficient transduction of the cells. Hence, in the subsequent experiments we used younger cochlear cultures (P4) since they are known to maintain their *ex vivo* viability for longer periods. Cochleae from P4 pups were dissected and incubated for 24h in DMEM-F12 media supplemented with 5 % FBS. The cultured cochleae were then incubated for 48h with different AAVs (AAV8-GFP, AAV9-GFP or ds-AAV9-GFP: 5×10^{11} vg/mL), which was then followed 120h incubation with DMEM-F12 media containing 5 μg/mL ampicillin to reduce potential bacterial infection. This protocol allowed more time for the AAV-GFP to be transcribed, translated and expressed in the target cells (**Figure 3.1A**). The samples were then fixed, stained with Texas Red-X Phalloidin and mounted on slides. Transduction efficiency in the hair cells was manually quantified across the entire cochlea explant in the apical, medium and basal turns.

For the explants incubated with AAV8-GFP, the transduction of IHCs and OHCs could not assessed since the surrounding non-sensory cells proliferated extensively and invaded the entire sensory epithelium (**Figure 3.1B**). However, the set of cochlear

cultures used for the AAV9-GFP and ds-AAV9-GFP experiments retained a normal structure that allowed the quantification of transduction efficiency in both IHCs and OHCs (**Figure 3.1B**). The results showed that for AAV9-GFP the best transduction efficiency was present in the basal region of the cochlea with approximately 60% of the IHCs and 50% of OHCs expressing GFP (**Figure 3.1C**). On the other hand, for ds-AAV9-GFP, most of the IHCs and OHCs were transduced in the middle cochlear region, with approximately 60% of the IHCs and 90% of the OHCs being GFP-positive (**Figure 3.1C**). Interestingly, ds-AAV9-GFP mainly infected OHCs (**Figure 3.1C**). When assessing the overall transduction efficiency throughout the cochlea, the highest percentage of GFP-positive cells was detected for ds-AAV9-GFP, where approximately 40% of the IHCs and 80% of the OHCs were successfully transduced by the viral vector (**Figure 3.1D**). Nonetheless, it is worth noting that similar IHC transduction efficiency and number of GFP positive cells were detected when explants were incubated with AAV9-GFP (**Figure 3.1D**). The use of AAVs did not affect the stereociliary hair bundles morphology of the hair cells (**Figure 3.1B**).

These findings show that (1) AAV9 and ds-AAV9 transduce both IHCs and OHCs with great efficiency *in vitro*; (2) even intermediate titrations of 10^{11} vg/ mL are efficient at infecting hair cells *in vitro* and (3) AAV vector serotypes are not toxic and do not impair the morphology of the hair cells.

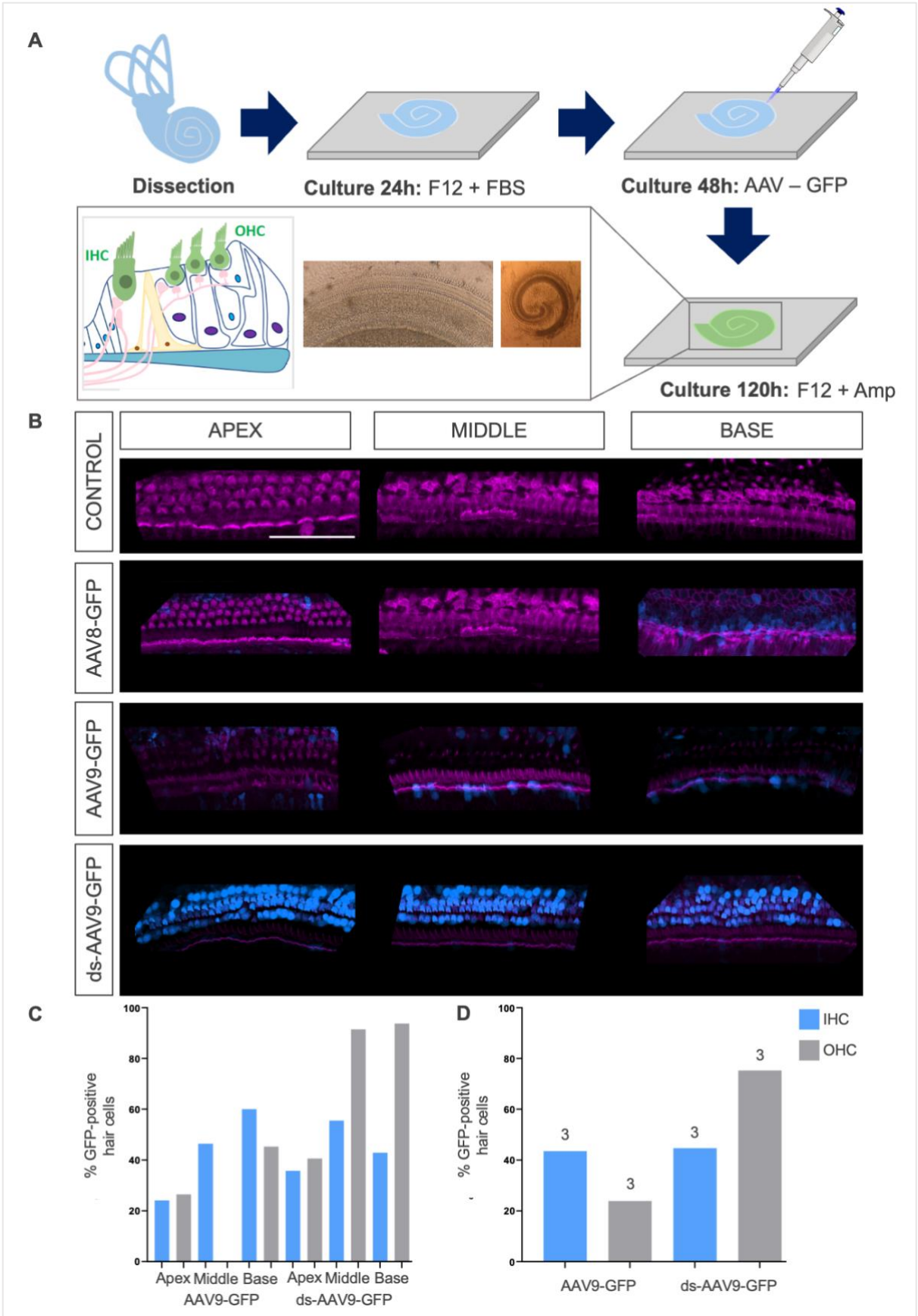

Figure 3.1: *In vitro* expression of different AAV serotypes carrying the green fluorescent reporters (GFP) in cochlear explant cultures. (A) Images depicting the experimental outline. Cochlea were dissected at P4 and cultured for 24h in F12 medium with FBS. The

following day vectors were added at a titration of 5×10^{11} vg/ mL and were incubated for an additional 48h. Subsequently, organotypic cultures were incubated for an additional 5 days to allow transduction of the viral constructs. Afterwards, samples were fixed, stained, and visualised at the confocal microscope. **(B)** Z-stack images of cochlear hair cells from organotypic cultures without (control) or with AAV-GFP. Hair cells were labelled with Texas Red-X Phalloidin (magenta), and the cells transduced with AAV-GFP are depicted in blue. Scale bar: 25 μm. **(C)** Graph illustrating the percentage of transduced IHCs (blue) and OHCs (grey) in the apex, middle and basal region of the cochlea with AAV9-GFP and ds-AAV9-GFP. ds-AAV9-GFP shows the highest transduction efficiency in the OHCs that are localised in the middle (92%) and basal (93%) coils of the cochlea. *n=1* cochlear explant. **(D)** Graph showing overall transduction efficiency in the IHCs (blue) and OHCs (grey). Approximately 45% of the IHCs and 20% of the OHCs were transduced by AAV9-GFP. For ds-AAV9-GFP, approximately 45% of the IHCs and 80% of the OHCs were transduced. *n=3* cochlear explants. Statistical tests were not carried out due to the small sample size.

FINDINGS SUMMARY

- 10^{11} vg/ mL are enough for transducing hair cells *in vitro*.
- ds-AAV9-GFP had the best transduction efficiency.
- ds-AAV9-GFP mainly infected OHCs.
- Approximately 40% of the IHCs throughout the cochlea were infected by AAV9-GFP and ds-AAV9-GFP.
- AAV8, AAV9 and ds-AAV9 are not toxic and do not impair hair cell morphology and hair cell death was not observed in explant cochlear cultures.

3.3. Discussion

Even though organotypic cochlear cultures are considered to be a valuable tool to understand hearing function, the assessment and transduction efficiency of AAV8 and AAV9 vector serotypes was variable. Nonetheless, transduction efficiency assessments of the AAV preparations seemed to show that IHCs and OHCs are successfully infected in *ex vivo* preparations by 10^{11} genome copies of viral construct and illustrated that ds-AAV9-GFP was the most efficient. Similar results showing that ds-AAV provides a higher transduction efficiency than conventional single-stranded AAVs were previously reported using ds-AAV1 *in vivo* (Maguire and Corey, 2020).

The results also showed that AAV-GFP transduction efficiency changed along the cochlea (apex, middle, base), with the basal region having the highest transduction efficiency. This could be due to basal cells having a more efficient internalization process compared to more apical hair cells. Although unlikely, it could have also been due to possible differences caused by some technical issues, such has the dissection technique potential compromising the viability and functionality of the cells in the apical or middle coils.

Previous experiments showed that organotypic cochlear culture from P4 C57BL/6 mice incubated with AAV8-GFP and AAV9-GFP (10^{10} genome containing particles) had no IHCs or OHCs transduced (Landegger et al., 2017). However, the same study reported different results for *in vivo* experiments, with higher transduction efficiencies recorded for the same serotypes that were tested *ex vivo* (Landegger et al., 2017). Results from the current study and published literature suggest that (1) a titration of at least 10^{11} vg/ mL is required for the *ex vivo* transduction of auditory hair cells and that (2) *ex vivo vitro* systems do not necessarily provide a faithful representation of the *in vivo* scenario. The differences in transduction efficiency between *ex vivo* and *in vivo* conditions could be attributed to experimental artifacts that relate to the culture conditions, variations in tissue processing, application of shear forces during the dissection leading to stretching and compression of the tissue, changes in temperature and pH. In addition, the *ex vivo* experiments are most likely influenced by the presence of a microenvironment that is deprived from an immune response and signalling factors or molecules that have the potential to influence viral uptake and intracellular trafficking of AAVs to the nucleus.

In regard to AAV8's lack of transduction *in vitro* – these could have been caused by this serotype's effect on cellular behaviour which is unlikely since literature does not report this. In addition to this, the proliferation that was observed in the AAV8 sample could represent an artifact of the environment, experimental conditions or dissection technique. Considering this, if such experiments would be relevant, further experimentation that would delineate the effects of AAV8 compared to other serotypes would be necessary.

In conclusion, the results show that *in vitro* both AAV9 and ds-AAV9 with GFP reporter, at a titration of 10^{11} vg/ mL, can transduce approximately 40% of the IHCs and 20-70% of the OHCs depending on the AAV vector genome. However, based on the current results and published work, it is expected that the transduction efficiency data from ex vivo work may not necessarily be relevant and replicable to *in vivo* studies. As such, the subsequent chapter 4 will present the development of the *in vivo* surgery and the transduction efficiency of AAV8 and AAV9 with GFP or mCherry reporters upon injections in living pups and adult mice.

Chapter 4: Results – Gene delivery through round window membrane inoculation

OUTLINE

In the present chapter, the following information related to the project will be addressed:

- introduction to gene delivery approaches to the inner ear
- establishment of the surgery technique in neonatal and adult murine models as well as gerbils
- assessment of transduction efficiency in neonatal and adult mice exposed to AAV8-GFP and AAV9-GFP
- discussion.

4.1. Introduction

Current approaches for inner ear gene therapy can be carried out only through surgical techniques, which allow for targeted delivery of genes to the inner ear. The most common techniques used *in vivo* in murine models are (1) intratympanic injections and (2) cochleostomy. Intratympanic injections involve the application of the therapeutic construct to the middle ear through the tympanic membrane, which then diffuses to the inner ear. The intratympanic injections are relatively non-invasive but do not provide a targeted delivery to the cochlear structures with precise localisation. On the other hand, cochleostomies are more invasive and involve making a small incision in the bone of the cochlea and in the round window membrane (RWM) or oval window. This allows the delivery the viral construct directly into the *scala tympani* or *scala media*, which allow the direct targeting of the inner ear hair cells with the viral constructs carrying genes of interest. In order to study, prevent, ameliorate or cure specific hearing or balance disorders, one or a combination of the techniques listed above may be used.

Currently, research shows that cochleostomy is preferred over intratympanic injection because this approach allows (1) a targeted delivery to a specific cell population, (2) enhanced efficiency through higher transduction, (3) reduced viral vector titration and (4) allowance of administration of a larger construct volume which could promote the widespread gene transduction. By contrast, one major disadvantage of cochleostomy is the invasive nature of the procedure, which carries the risk of damaging the delicate structures of the inner ear.

The transduction efficiency of gene-based therapy also largely depends on the AAV serotype used. The serotypes selected for this project were AAV8 and AAV9, as previous studies showed that both are able to transduce IHCs with high efficiency. AAV8 and AAV9 are also safe to use because they show minimal immune responses and have long-term gene expression. AAV8 has been shown to have superior efficiency in transducing IHCs from adult mice compared to other serotypes (Chien et al., 2015). On the other hand, AAV9 seems to be more efficient in transducing IHCs in neonatal mice (Chen et al., 2019). Furthermore, a synthetic engineered capsid variant of AAV9, called PHP.eB, has been shown to be highly efficient in transducing both IHCs and OHCs, and it has been deemed suitable for human therapeutic approaches (Oestreicher et al., 2021; Marcovich et al., 2022; van Beelen et al., 2022; Reynaud-Dulaurier and Decressac, 2020). The present project was performed using the AAV9 serotype PHP.eB and it is referred throughout the thesis as AAV9.

The results in the previous chapter, and those from the published literature (see **Table 3, Chapter 1**), show that AAV transduction efficiency of the hair cells will depend not only on the surgical technique, but also on the mouse strain, serotype, promoter,

volume and titration of the construct as well as the timing of the therapeutic approach. Therefore, the initial aim of the project was to (1) establish the *in vivo* surgical approach to be used in neonatal and adult mice as well as in neonatal gerbils and (2) determine the transduction efficiency of AAV8-GFP and AAV9-GFP in neonatal and adult animals upon administration of the viral construct. These experiments were carried out with the overall aim to achieve optimal transduction efficiency when injecting AAV-MYO7A in neonatal and adult mice.

4.2. Establishing the *in vivo* surgery technique in neonatal and adult mice and in neonatal gerbils

Although multiple surgical approaches have been developed for the virally-mediated gene delivery, the injection through the RWM allows rapid and direct delivery of AAVs to the inner ear. This approach has been implemented by multiple laboratories focused on inner ear gene therapy because the RWM is easily accessible, it is located in the proximity to the hair cells and incisions in the RWM allow the preservation of the cochlear wall. To do this, neonatal (P0 - P5) or adult (P15 – P30) mice were moved to a dedicated sterile room and were anaesthetized with gaseous Isoflurane. After the induction of anaesthesia, the animals were placed on heat pads that assisted in keeping the appropriate body temperature, and their eyes were covered with ophthalmic gel to keep the eyes moist. When animals lost their withdrawal response to toe pinch, they were administered subcutaneously Metacam analgesic, and the surgical area was sterilised with povidone-iodine (**Figure 4.1**). In adult mice, the fur in the surgical area was trimmed prior the application of povidone-iodine. Subsequently, scissors were used to make a post-auricular incision of the right ear and fat and muscle tissue were retracted and separated in order to expose the facial nerve, bulla and cochlear bone.

In adult mice (depicted as “A” in **Figure 4.1**), access to the RWM was gained by perforating the bulla with a 25 G needle and fine forceps. In pups (depicted as “P” in **Figure 4.1**), a small incision was made with a borosilicate glass pipette under the facial nerve and on the right-hand side of the bulla (for the right ear). In both cases, the RWM was then punctured with a borosilicate glass pipette to let perilymphatic fluid to exit the inner ear and allow for the injection of the AAV into the inner ear. Afterwards, 1 μL or 2 μL of AAV8-GFP, AAV9-GFP (PHP.eB serotype used throughout experiments presented in Chapter 4) or PBS (used as control) were placed into a new borosilicate glass pipette and then injected through the RWM. In adults, the RWM was sealed with muscle and one small drop of tissue adhesive glue was added on top to prevent the construct from leaking out. At the end of the procedure, the incision in the bulla was covered with adipose tissue, and fat and muscle tissues were placed back in their original positions. The incision in the skin was closed with tissue adhesive and the surgical site was disinfected again with povidone-iodine. Post-surgery animals were placed in cages positioned on heated mats until fully recovery. When mice regained consciousness and were able to move, they were taken back to their original cage. Breeding males were removed from the cages before moving back the animals that underwent surgery with their mother. For pain management, oral Metacam was given to animals 24 hours after surgery. Animals were monitored for five days after surgery for abnormal weight loss, signs of distress, infection, or pain. About one month after surgery animals had their ABR tested, after which they were killed by schedule 1 and their cochleae dissected out for immunostaining or SEM.

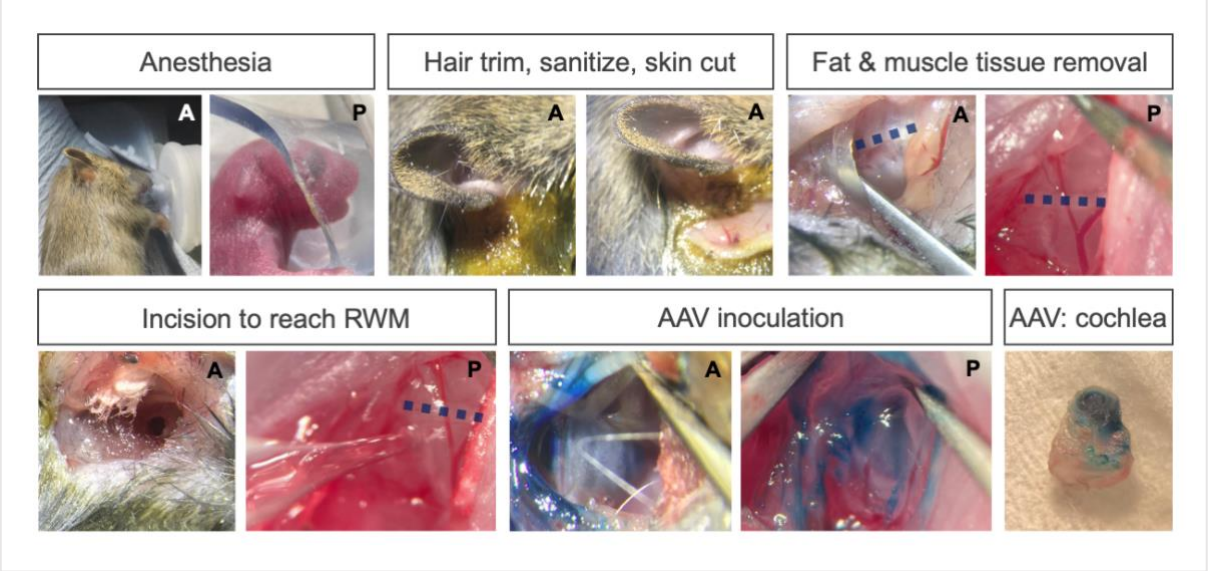

Figure 4.1: *In vivo* surgery technique for neonatal and adult murine models and neonatal gerbils. Example of images illustrating the sequential steps involved in the surgical procedure for the delivery of AAV construct to the inner ear. Adults (A) and pups (P) were anesthetized with Isoflurane and the surgical area was prepared, including hair trimming and sterilization with povidone-iodine. Afterwards, a small skin incision was made to expose the target area and fat and muscle layers were carefully pulled apart and retracted to reach the facial nerve (dashed dark blue line), bulla and cochlear bone. An incision in the bulla was made to reach the RWM and once the RWM was reached the membrane was penetrated with a glass pipette to allow the perilymph to exit the inner ear. For the purpose of this figure, blue dye was injected to illustrate that through the RWM route the construct reaches the inner ear.

For the neonatal gerbils, the surgical procedure was done at P1 as previous described for the mice (**Figure 4.2A**), and 3 μL of AAV8-GFP were injected through the RWM. One-month post-surgery, the cochleae were dissected out and were immunostained with Texas Red-X Phalloidin and after mounting them on slides were imaged to assess AAV8-GFP expression. Since these experiments were conducted with the sole purpose to demonstrate their feasibility of the procedure in gerbils, the transduction efficiency was not calculated. However, it was noted that AAV8-GFP at a titration of 1.2×10^{12} vg/mL successfully transduced most of the IHCs and some OHCs in all cochlear coils – apex, middle, base (**Figure 4.2B**).

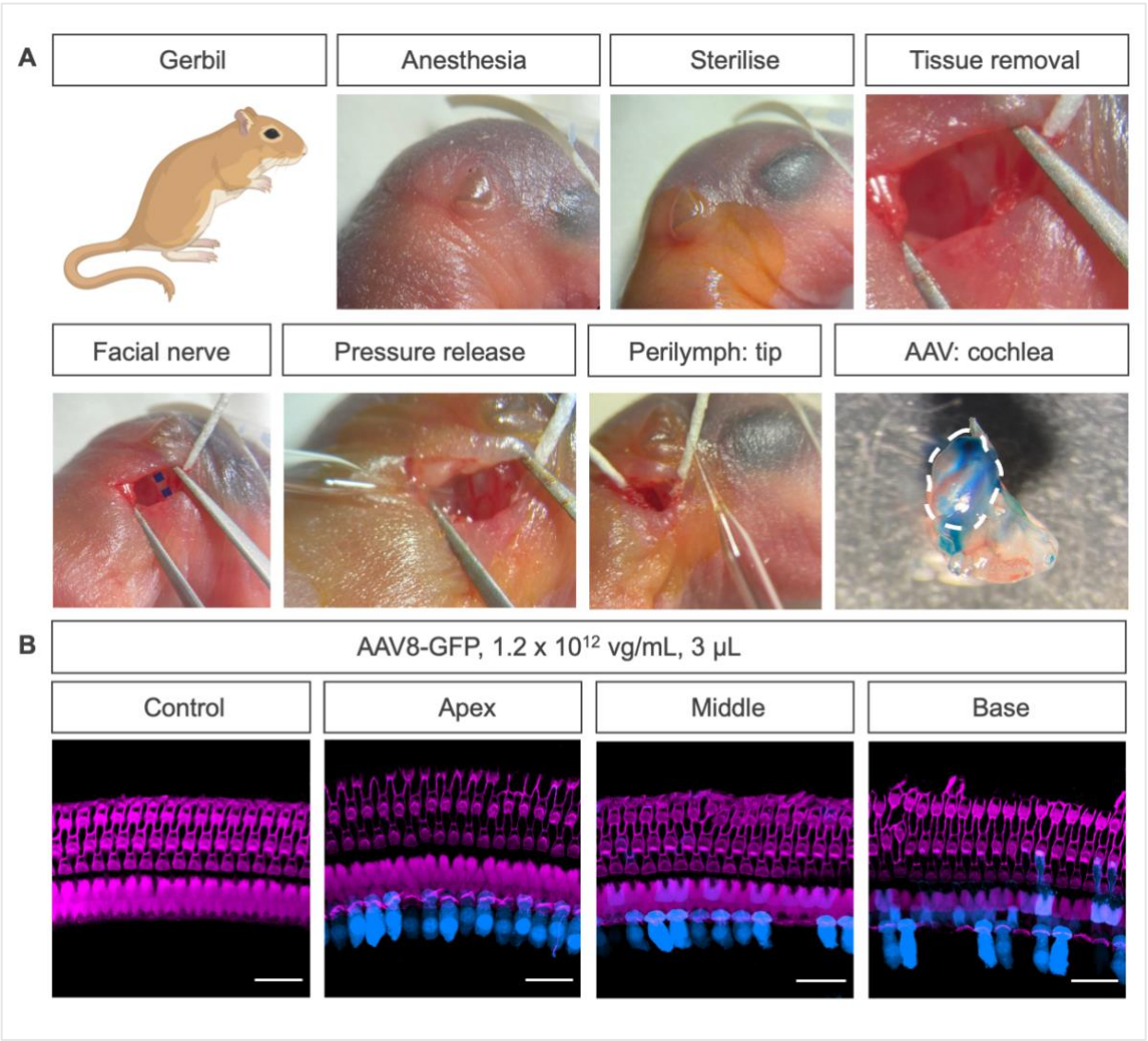

Figure 4.2: In vivo surgery technique for neonatal gerbils. (A) Images to illustrate the step-by-step surgical procedure for inner ear surgery done in P1 gerbils. Gerbils were anesthetized and the surgical area was sterilised to maintain the aseptic conditions. A small incision was made, adipose tissue was removed until reaching the facial nerve level (dark blue dashed line) and intracochlear pressure was released by penetrating the RWM with a borosilicate glass pipette – in the figure the perilymph liquid can be seen in the tip of the pipette. The white dashed line in the last image shows the blue dye (equivalent of AAV construct) present in the cochlea. **(B)** Confocal z-stack images of cochlear hair cells in control (non-injected gerbils) and gerbils that had surgery at P1 with AAV8-GFP (3 µL, 1.2 x 10^{12} vg/mL). The cochlea one month post-surgery had the hair cells labelled with Texas Red-X Phalloidin (magenta), and the cells transduced with AAV8-GFP are visible in blue (GFP expression). It can be seen that mainly the IHCs express GFP when injected with the AAV8-GFP construct. Scale bar: 25 µm.

4.3. AAV8-GFP and AAV9-GFP transduction efficiency in neonatal mice

The transduction efficiency of different volumes of the viral vectors was determined by injecting neonatal mice between P0 – P5. Animals were transduced with AAV8-GFP (1.2 x 10^{12} vg/mL) or AAV9-GFP (6.1 x 10^{12} vg/mL) at volumes of 1 µL or 2 µL. Constructs were delivered through the RWM, as described in previous section. About

4 weeks post-surgery, mice were sacrificed, and the cochleae were collected and immunostained with Texas Red-X Phalloidin (**Figure 4.3A**). Samples were assessed for GFP expression in z-stack images taken from the apical, middle and basal regions of the cochlea. Z-steps were of 0.7 μm and the zoom for the image was selected to 1.3-1.6 to allow between 10 – 15 IHCs in the field of view. Positive transduced cells for AAV were defined based on the detection of the GFP reporter expression that the virus carried. The criteria for a cell being considered positive included the presence of fluorescence within the cell body. The exact threshold for considering a cell positive varied depending on the amount of AAV construct, the experiment and the intensity of the signal. Pups injected with 1 μL of AAV8-GFP, showed about 50% of their IHCs and 10% of the OHCs infected in the apical, middle and basal regions of the cochlea (**Figure 4.3B**). On the other hand, pups injected with the double volume of construct (2 μL) had about 70% of the IHCs transduced in the apical region. However, the transduction efficiency decreased towards the basal region, with 33% and 40% IHCs transduced in the middle and basal coils, respectively (**Figure 4.3B**). For the OHCs, the transduction efficiency remined constant with less than 10% of the cells transduced throughout the cochlea (**Figure 4.3B**). Merged data showed that throughout the cochlea AAV8-GFP at a volume of 1 μL transduced about 40% of the IHCs and about 7% of the OHCs, while a volume of 2 μL transduced about 69% of the IHCs and about 3% of OHCs (**Figure 4.3C**). Statistical tests showed that transduction efficiency between the two volumes tested was significantly different for the IHCs ($p = 0.0012$, two-way ANOVA, **Figure 4.3C**).

To assess whether the surgery had an impact on hearing function, mice were tested *in vivo* for ABR thresholds prior to culling them for immunostaining. Statistical analysis of ABR thresholds showed no significant differences between non-injected controls

and mice injected with 1 μL or 2 μL of AAV8-GFP (*p=0.3518:* two-way ANOVA; post-hoc results are mentioned in the figure legend). Interestingly, the control non-injected mice had higher thresholds recorded at higher frequencies compared to the injected mice. This could have been caused by the fact that the ABR recordings include data from my training period when I was learning to place the ABR electrodes appropriately.

The above results demonstrated that irrespective of the volume injected hearing function is not affected and that a larger volume of AAV8-GFP construct transduced a higher number of cochlear IHCs.

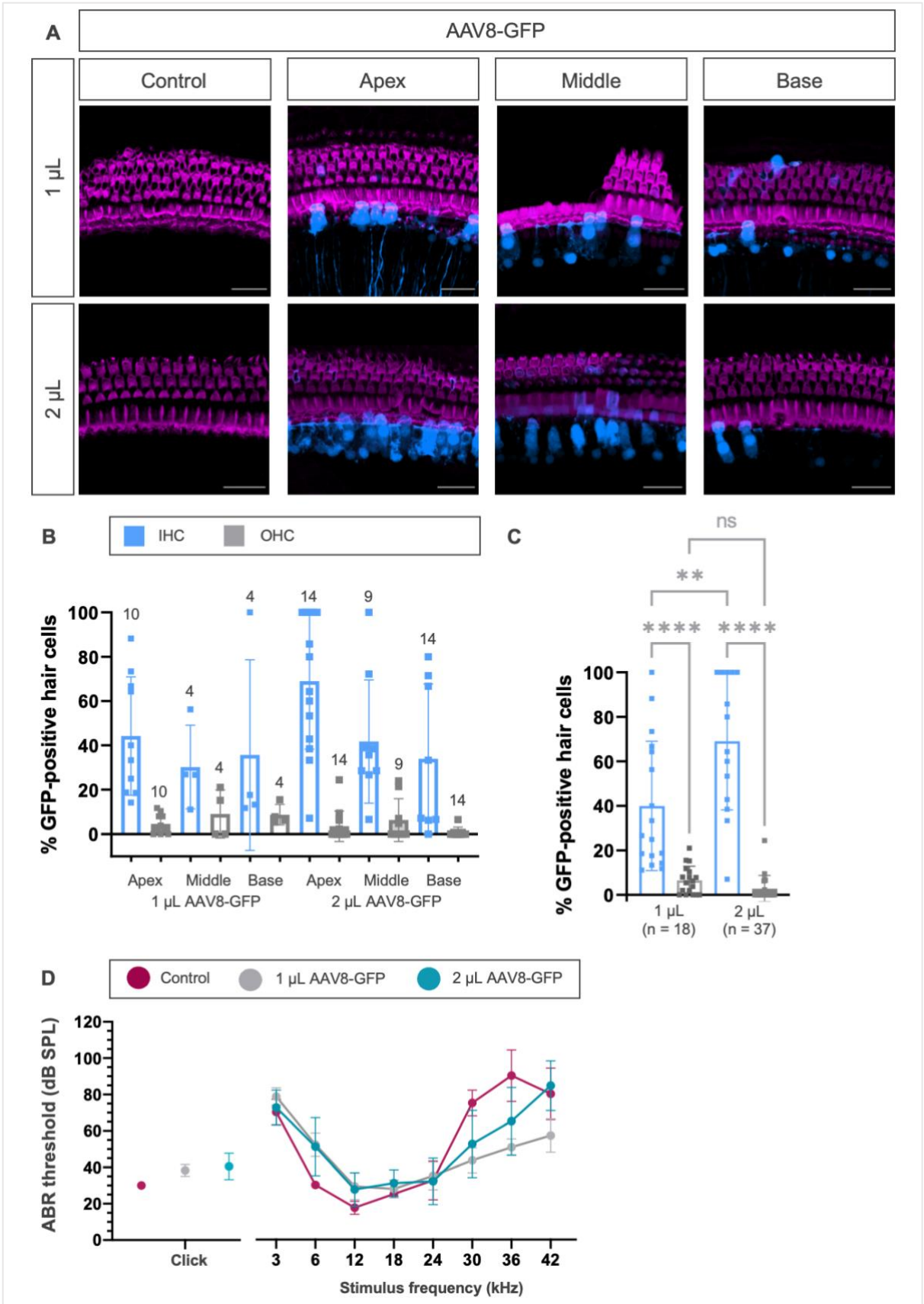

Figure 4.3: Analysis of hair cell AAV8-GFP transduction after neonatal *in vivo* surgeries. **(A)** Representative z-stack images from C57BL/6N mice injected with 1 µL or 2 µL of AAV8-GFP (titration: 1.2 x 10^{12} vg/mL) at P1-P5. The cochlea of post-surgery mice (P31 – P40) was immunostained with Texas Red-X Phalloidin (magenta) and assessed for GFP expression

(blue). More IHCs express GFP when injected with 2 μL of construct. Scale bar: 25 μm. **(B)** Percentage of transduced cells in the apical, middle and basal regions of the cochlea after injection with 1 μL or 2 μL of AAV8-GFP. Number of mice used for the different conditions is listed above the data. Statistical tests were not carried out for this dataset as the main interest was in the IHCs located in the apical region of the cochlea. **(C)** Graph showing the percentage of IHCs and OHCs transduced throughout the cochlea upon injection with 1 μL or 2 μL of AAV8-GFP. The number of mice injected with 1 μL or 2 μL of AAV8-GFP is listed underneath the graph. **(D)** Average ABR thresholds for click (left) and 3 – 42 kHz pure tone stimuli (right). Data is recorded from control mice (magenta), mice injected with 1 μL (grey) and 2 μL (green) of AAV8-GFP. The collected data includes recordings captured during the initial phase of learning the surgical technique and form the subsequent period after the procedure was carried out with more confidence. Post-test from the two-way ANOVA showed that between control and mice injected with 1 μL or 2 μL of AAV8-GFP there were no statistical significances detected (*p=0.4938* and *p=0.9301*). The number of mice tested for each condition is: 2 for controls; 7 injected with 1 μL; 10 injected with 2 μL. Data in this figure is represented as mean ± SD.

Neonatal mice were also injected with AAV9-GFP. Similar to AAV8-GFP (**Figure 4.3**), surgeries were carried out via the RWM in murine models between P0 – P5. After about 30 days post-surgery, mice were tested for ABR thresholds in vivo prior being culled to assess the transduction efficiency based on GFP expression in the hair cell body using immunostaining (**Figure 4.4A**). In pups injected with 1 μL of AAV9-GFP, the transduction efficiency in the IHCs of the apical and middle cochlear coils was about 30% and almost 5% in the basal region, while that for the OHCs the transduction was about 50% in the apical coil, 20% in the middle region and about 4% in the base (**Figure 4.4B**). When pups were injected with 2 μL of AAV9-GFP, almost 60% of the IHCs were expressing GFP in the apical and basal cochlear region, and approximately 30% of the IHCs in the middle coil (**Figure 4.4B**). For the OHCs, the percentage of infected cells did not go above 20% in any of the cochlear coils (**Figure 4.4B**). When assessing the overall transduction efficiency throughout the cochlea, a single volume of AAV9-GFP led to about 26% of the IHCs and 31% of the OHCs being GFP positive. The double dose of AAV9-GFP transduced 53% of the IHCs and 13% of the OHCs (**Figure 4.4C**). The percentage of transduced cells (IHCs and OHCs) throughout the

cochlea was significantly different between the two concentrations tested (*p = 0.0005*, two-way ANOVA). The multiple comparison test showed that there were no significant differences in IHCs transduction efficiency recorded between the two volumes of viral construct administered (*p=0.0558*). To further evaluate whether the procedure caused any hearing impairment, ABR recordings were performed in control and mice injected with 1 μL and 2 μL. The statistical analysis conducted on the tone and click stimuli recorded from injected and non-injected mice revealed no significant differences (*p=0.2691*, two-way ANOVA result, **Figure 4.4D**). Therefore, the results suggest that AAV9-GFP is effective at transducing primarily cochlear IHCs and that the procedure and the volume of viral construct tested in neonatal mice do not impair hearing function.

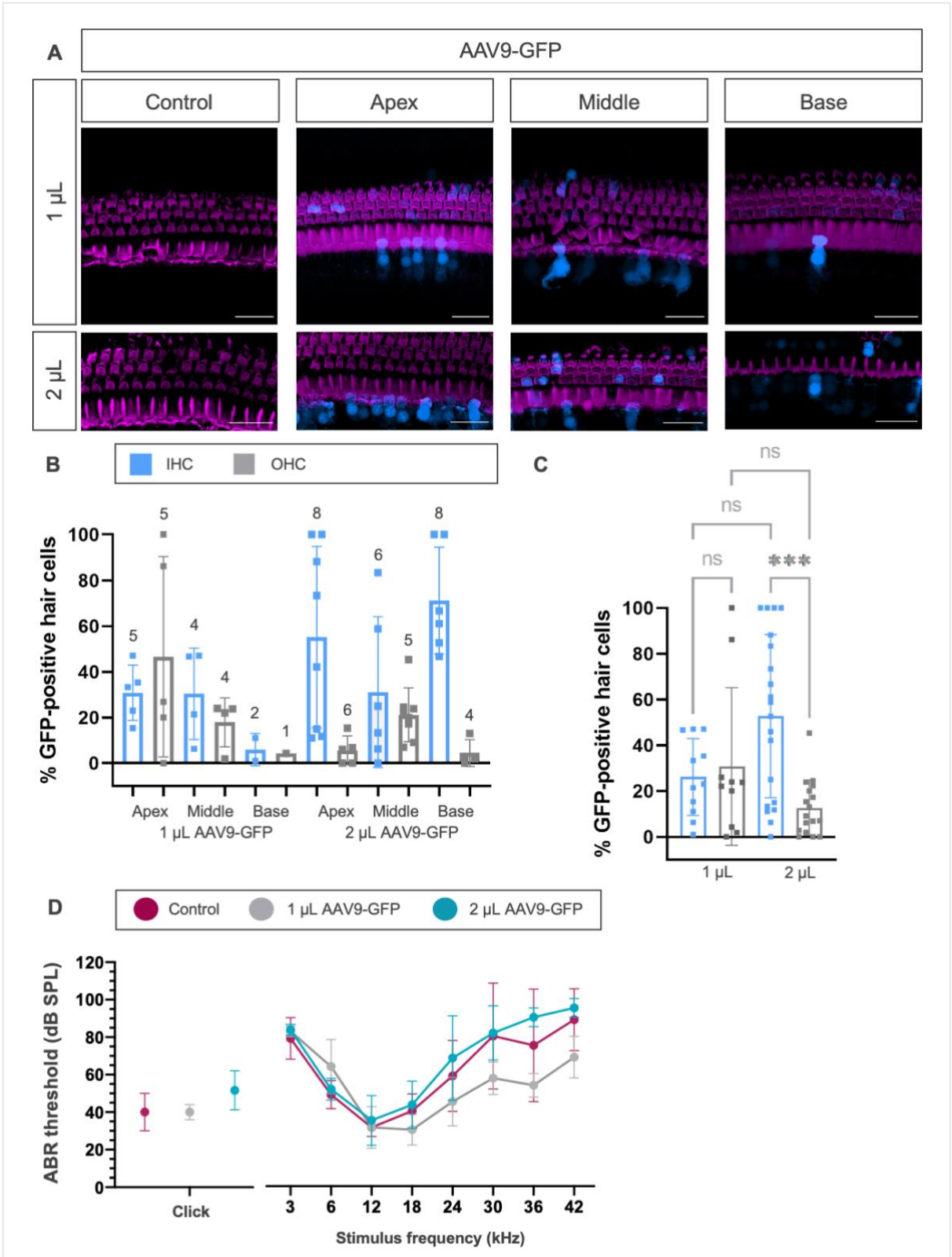

Figure 4.4: Neonatal murine models injected with AAV9-GFP. (A) Representative z-stack images from control mice and those injected with 1 µL or 2 µL of AAV9-GFP (titration: 6.1 x 10^{12} vg/mL) at P1-P3. The cochlea of post-surgery mice (P31 – P40) was immunostained with Texas Red-X Phalloidin (magenta) and assessed for GFP expression (blue). More IHCs express GFP when cochleae were injected with 2 µL of construct. Scale bar: 25 µm. **(B)** Percentage of transduced cells in the apical, middle and basal regions of the cochlea after injection with 1 µL or 2 µL of AAV9-GFP. Number of mice used for the different conditions is

listed above the data. Statistical tests were not carried out for this dataset as the main interest was in the IHCs located in the apical region of the cochlea. **(C)** Graph showing the percentage of IHCs and OHCs transduced throughout the cochlea upon injection with 1 μL or 2 μL of AAV9-GFP. Number of mice injected with 1 μL AAV9-GFP: 11 for IHCs and 10 for OHCs Mice injected with 2 μL AAV9-GFP: 20 for IHCs and n = 17 for OHCs. **(D)** Average ABR thresholds for click (left) and 3 – 42 kHz pure tone stimuli (right). Data is recorded from control mice (magenta), mice injected with 1 μL (grey) and 2 μL (green) of AAV9-GFP. Recorded data includes recordings from both initial learning phase and from when the procedure was executed with more confidence. The examined data did not reveal any statistical significance. The number of mice tested for each condition is: 4 for controls; 4 injected with 1 μL; 3 injected with 2 μL. Data in this figure is represented as mean ± SD.

4.4. AAV8-GFP and AAV9-GFP efficiently transduce IHCs in adult mice

Published literature suggests that AAV8 and AAV9 robustly and efficiently transduce cochlear hair cells, especially IHCs, in adult murine models (Tao et al., 2018). To investigate the transduction profile of these serotypes in our experimental settings, C57BL/6N adult mice (P15 – P30) were injected through the RWM with 1 μL or 2 μL of viral construct containing GFP. One-month post-surgery, the mice had their ABR tests done and afterwards the cochleae were harvested to quantify the transduction efficiency by assessing GFP expression in the apical, middle and basal region of the cochlea. AAV8-GFP infection with 1μL of construct showed that approximately 30% of the IHCs and OHCs were transduced in the apical region, but it was lower in the middle and basal cochlear coils (middle: 10% IHCs and 49 % OHCs; base: 9% IHCs and 2% OHCs, **Figure 4.5B**). Upon injection with the double amount of volume, the transduction of IHCs throughout the cochlea largely increased (apex: 80%, middle: 84%, base: 32%) compared to 1 μL, while there were no OHCs transduced (**Figure 4.5B**). Assessment of the overall transduction throughout the cochlea showed that there were significant differences in transduction efficiency between IHCs and OHCs exposed to the two viral vector volumes ($p < 0.0001$, two-way ANOVA - **Figure 4.5C**). Auditory function through ABR measurements were carried out one-month post-procedure (P44 onwards) in control, control injected (PBS injected) and mice injected

with 1 or 2 μL of AAV8-GFP. It was observed that increased thresholds were recorded in the mice injected with 2 μL at higher thresholds (**Figure 4.5D**). The overall two-ANOVA showed no statistical significance recorded between controls and injected mice (*p=0.1385*, **Figure 4.5D**). The post-hoc test showed no significant differences between the control and mice injected with 1 μL of AAV8-GFP (*p=0.9841*) or mice injected with 2 μL of AAV8-GFP (*p = 0.0716*).

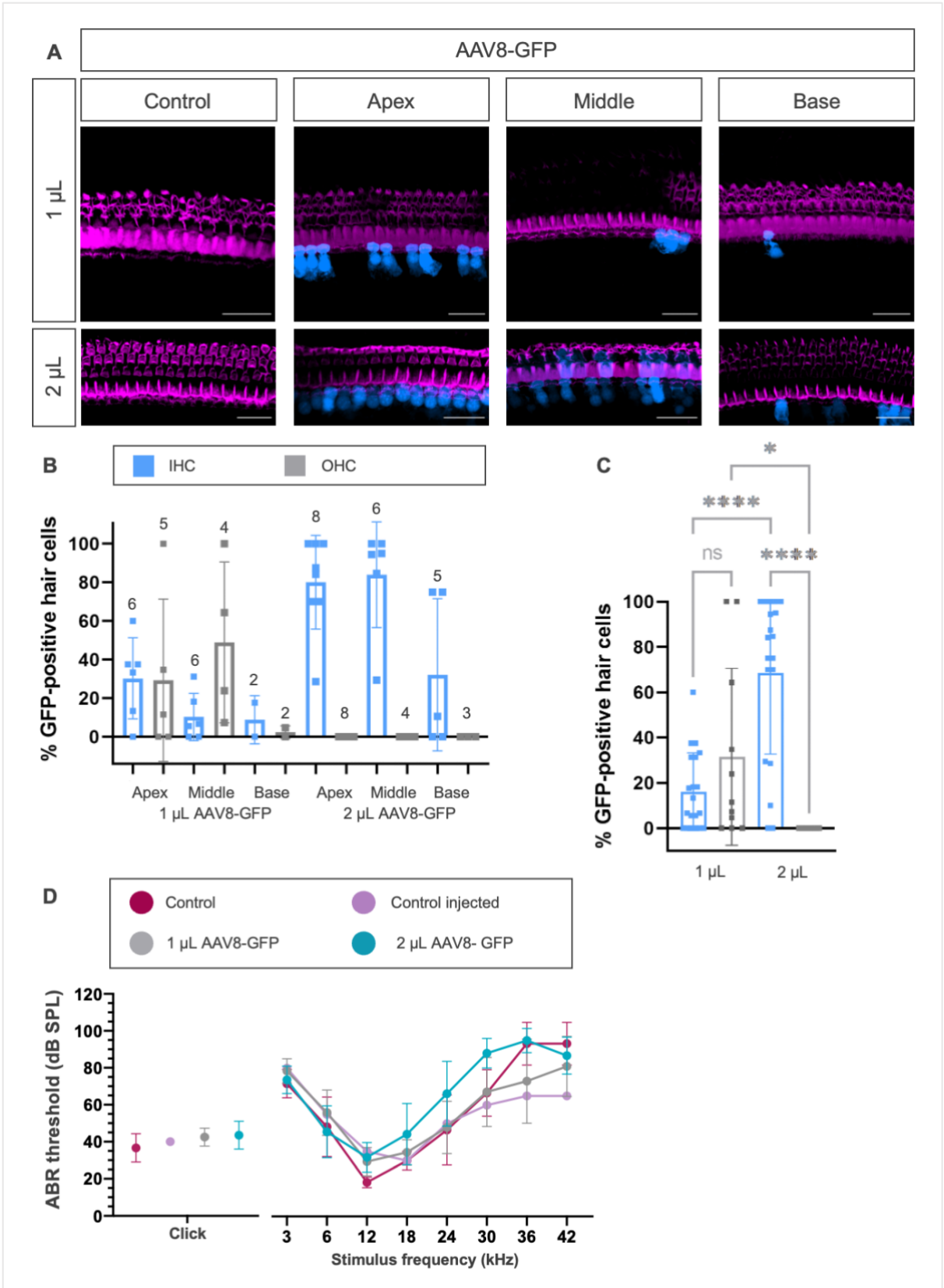

Figure 4.5: Comparison of two volumes of AAV8 at equivalent titres upon adult murine surgery. (A) Z-stack images from control mice and those injected with 1 µL or 2 µL of AAV8-GFP (titration: 1.2 x 10^{12} vg/mL) or with 2 µL of 1 x PBS (control injected). Injections were carried out at P15-P25, and the cochlea was immunostained with Texas Red-X Pahlloidin (magenta) and assessed for GFP expression (blue) at P45 – P55. More IHCs express GFP

when injected with 2 μL of construct and this was valid for the apex, middle and basal coils. Magnification: 60x. Scale bar: 25 μm. **(B)** Graph showing the percentage of transduced cells in the apical, middle and basal regions of the cochlea after injection with 1 μL or 2 μL of AAV8-GFP. Number of mice used for the different conditions is listed above the data. Statistical tests were not carried out for this dataset as the main interest was in the IHCs located in the apical region of the cochlea. **(C)** Graph showing the percentage of IHCs and OHCs transduced throughout the cochlea upon injection with 1 μL or 2 μL of AAV8-GFP. Significant differences in transduction efficiency were recorded between the cells of interest (IHCs) upon administration of 1 or 2 μL AAV8-GFP ($p < 0.0001$). Number of mice injected with 1 μL of AAV8-GFP: 20 for IHCs and 11 for OHCs; mice injected with 2 μL of AAV8-GFP: 19 for IHCs and 15 for OHCs. **(D)** Average ABR thresholds for click (left) and 3 – 42 kHz pure tone stimuli (right). Data is recorded from control mice (magenta), control injected (pink), mice injected with 1 μL (grey) and 2 μL (green) of AAV8-GFP. Recorded data presents with variation as it includes recordings from both initial learning phase and from when the procedure was carried out with more confidence. The examined data did not reveal any statistical significance – p=0.1385, two-way ANOVA followed by post-hoc test (control vs control injected: p=0.5675; control vs 1 μL AAV8-GFP: p=0.9841; control vs 2 μL AAV8-GFP: p=0.0716). The number of mice tested for each condition is: 3 for controls; 1 for controls injected with 1 x PBS; 10 for mice injected with 1 μL and 8 for mice injected with 2 μL. Data is represented as mean ± SD, two-way ANOVA followed by post-hoc test.

An additional objective of the study was to investigate the efficiency of AAV9-GFP transduction in adult mice. As 2 μL of viral construct transduced a higher number of hair cells, we evaluated the percentage of GPF-positive cells upon injection in adult murine models only with this volume of AAV9-GFP (6.1×10^{12} vg/mL). One-month post-surgery, approximately 78% of IHCs and 44% of OHCs were transduced in the apical coil of the cochlea (**Figure 4.6A** and **Figure 4.6B**). In the middle and basal coils, around 45% and 72% of IHCs were transduced, respectively, but no OHCs (**Figure 4.6B**). The overall transduction efficiency assessment carried out throughout the cochlea showed that there were about 64% of IHCs and 16% of OHCs transduced (**Figure 4.6C**). The ABR assessment showed that there were no statistically significant differences between mice that did not have surgery (control), mice that were injected with 2 μL 1 x PBS (control injected) and the animals that undergone the procedure with 2 μL of AAV9-GFP (*p=0.1040*, two-way ANOVA, **Figure 4.6D**). Furthermore, all the injected animals, in all the experiments presented in the current chapter did not show any vestibular defects that could be detected through visible balance deficits.

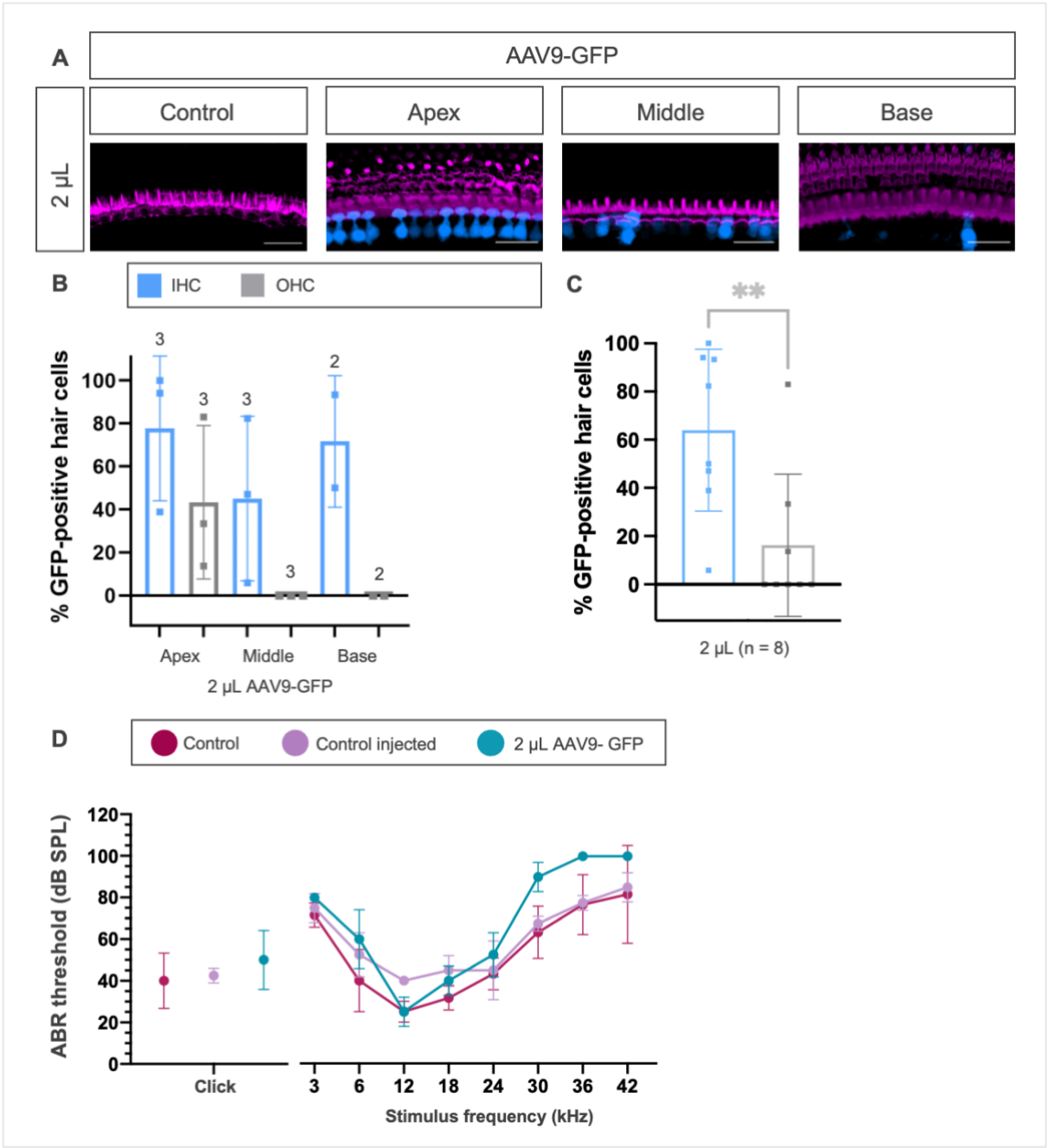

Figure 4.6: AAV9-GFP transduction in adult murine models upon injection through RWM. (A) Representative z-stack images from control and injected mice with 2 µL of AAV9-GFP (titration: 6.1 x 10^{12} vg/mL) or with 2 µL of 1 x PBS. Surgeries were carried out at P15-P25 and the cochlea of post-surgery mice (P45 – P55) was immunostained with Texas Red-X Phalloidin (magenta) and assessed for GFP expression (blue). Scale bar: 25 µm. **(B)** Percentage of transduced cells in the three cochlear coils after injection with 2 µL of AAV9-GFP. Number of mice used for the different conditions is listed above the data. Statistical tests were not carried out for this dataset as the main interest was in the IHCs located in the apical region of the cochlea. **(C)** Graph showing the percentage of His and OHCs transduced throughout the cochlea upon injection with 2 µL of AAV9-GFP. The number of mice injected is 8. **(D)** Average ABR thresholds for click (left) and 3 – 42 kHz pure tone stimuli (right). Data is recorded from control mice (magenta), control injected with 2 µL of 1 x PBS (pink) and 2 µL of AAV9-GFP (green). Two-way ANOVA did not reveal any statistical significance (*p=0.1040*). Post-test showed no significant differences between control and control injected (*p=0.0131*) and significant differences between control and mice injected with 2 µL of AAV9-GFP

(*p=0.0031*). The number of mice tested for each condition is: 3 for controls; 2 for control injected; 2 for injected with 2 μL. Data in this figure is represented as mean ± SD.

FINDINGS SUMMARY

- Surgeries carried out in neonatal and adult mice through the RWM allowed for constructs to reach the cochlear hair cells.
- The surgical approach used in the mouse can be implemented in neonatal gerbil.
- AAV8-GFP and AAV9-GFP successfully transduced some of the IHCs and a limited number of OHCs localised in the apical, middle and basal regions of the cochlea when administered in neonatal gerbils and mice.
- Statistical tests showed that hearing function is not affected, but at higher frequencies / the site of injection the thresholds are increased – most likely due to how I carried out the surgical procedure.
- AAV8 and AAV9 viral vectors (of similar titrations) successfully transduced the IHCs, which are the cells of interest for the current project with the following efficiency:

Pups (P0 – P5)				
	AAV8-GFP (1.2 x 10^{12} vg/mL)		**AAV9-GFP (6.1 x 10^{12} vg/mL)**	
	IHCs	OHCs	IHCs	OHCs
1 μL	39.94%	6.51%	23.07%	30.81%
2 μL	68.93%	2.80%	52.72%	12.66%
Adult (P15 – P30)				
	AAV8-GFP (1.2 x 10^{12} vg/mL)		**AAV9-GFP (6.1 x 10^{12} vg/mL)**	
	IHCs	OHCs	IHCs	IHCs
1 μL	16.12%	31.49%	-	-
2 μL	68.61%	0%	63.95%	16.25%

4.5. Discussion

The present chapter described the surgery approach and the transduction efficiency of both AAV8 and AAV9 vector serotypes using wild-type neonatal and adult mice and neonatal gerbils. The injections were tolerated well by both mice and gerbils and animals did not present any vestibular defects (disequilibrium). In addition, AAV8-GFP and AAV9-GFP efficiently transduced IHCs and a limited number of OHCs with no off-target expression when the surgeries were carried out in both pups and adults. Higher IHC transduction was noted in previous studies and it is proposed that the molecular differences between IHCs and OHCs could lead to these differences. It is possible that IHCs have a higher density of AAV receptors that facilitate the entry into these cells (Gu et al., 2019). Compared to AAV8, the AAV9 serotype seemed to transduce more efficiently OHCs, although the infection capacity was limited to 30%. This limited transduction efficiency in the OHCs was previously described in a study in which adult mice were injected with AAV9-GFP at P30 (Chen et al., 2019). However, the same group reported a much higher transduction efficiency (69%) in the apical OHCs when the surgery through the RWM was carried out at P9, implying that the transduction efficiency is age dependent (Chen et al., 2019). However, our data did not show considerable differences in transduction efficiency between neonatal and adult mice. Instead, we found differences in transductions efficiency along the cochlea, with the highest hair cell transduction in the apical cochlear turn, which has also been previously suggested (Chen et al., 2019; Ivanchenko et al., 2020; Omichi et al., 2020; Andres-Mateos et al., 2022).

The few differences in the ABR thresholds recorded between control (PBS injected) and AAV-GFP injected mice was likely to be caused by the surgery procedure, including mechanical trauma. The observed increased thresholds at higher

frequencies may be attributed, in part, to combining experimental data from early procedural learning stages, as well as subsequent investigations where the error rate associated with the surgical intervention was lower. Research carried out in non-human primates after RWM injection with PBS showed that ABR thresholds are not altered by more than 5 dB at any stimulus frequency (Dai et al., 2017). Yet, other studies done in adult guinea pigs showed that when the surgery was performed through the round or oval window there was a 10 – 20 dB shift in the ABR recordings (Wang et al., 2022). Furthermore, in a study in which RWM injection was carried out at P1, P9 and P30 showed that the ABRs were least affected when the procedure was done at P1 (Chen et al., 2019). Overall, these results highlight that surgeries through the RWM represent effective delivery methods for exogenous genes to the hair cells (Akil et al., 2012; Askew et al., 2015; Gyorgy et al., 2019).

While the current results provide insights into IHC and OHC transduction upon AAV8 and AAV9 viral infection, there are certain limitations that should be considered. The sample size for some of the experiments listed above was small, which made some of the statistical tests less accurate. In addition to this, the project carried out in Chapters 5 and 6 will make use of the dual vector AAV-MYO7A, while the AAV-GFP constructs tested were single viral vectors. This suggests that the AAV-GFP experiments may not display the actual transduction efficiency expected when using the dual AAV construct. Published literature suggests that dual AAV constructs have a lower transduction efficiency compared to single constructs, as both capsids would need to reach the IHCs and recombine in the nucleus (Trapani et al., 2014; Dyka et al., 2014; Maguire and Corey, 2020). This points out that the dual-AAV-MYO7A construct may have lower transduction efficiencies.

Future studies could assess different AAV serotypes, including Anc80L65 which is a synthetic vector which presents with high transduction efficiency (Landegger et al., 2017), and could investigate different cell-type specific promoters that could drive a higher expression in the IHCs and OHCs. Most of the current research is carried out using the CMV or CBA promoters as they have strong, stable and ubiquitous expression and have an enhance region. Moreover, different surgery techniques could be implemented or combined to enhance the effectiveness of transduction. For example, studies showed that combining RWM injections with canal fenestration delivery considerably increases the number of infected hair cells (Omichi et al., 2020). In addition to this, more work is required to establish the reason behind the graded apical-to-basal GFP expression, as well as determine why longer coding sequences that are packaged in AAVs have an impact on transduction efficiency. For example, a study that assessed packaged vector genomes ranging from 4.7 – 8.7 kb showed that the transduction efficiency was lower when the vector genomes were higher than 5 kb (Wu et al., 2010).

Overall, these results show that AAV8 and AAV9 capsid-mediated transduction in the neonatal and adult mice upon RWM surgery application is effective, safe and illustrates that these serotypes can be used for gene therapy approaches. The data presented in this chapter provided the base-line approach used to carried out the work with dual-AAV-MYO7A in the *Shaker-1* and *Myosin VIIa*$^{fl/fl}$ *x Myosin15-CRE*$^{+/-}$ mouse lines, which is presented in the subsequent two chapters.

Chapter 5: Results – *In vivo* gene-based therapy in Usher Syndrome Type I mouse model of congenital hearing loss

OUTLINE

In the present chapter the following information will be addressed:

- introduction to congenital hearing loss, Usher Syndrome Type 1B, the *Shaker-1* mouse and gene therapy approaches that have been already implemented for Usher Syndrome
- results
- discussion.

5.1. Introduction

Usher syndrome is the most common form of syndromic hearing loss and is responsible for about 50% of the deaf-blindness cases in humans (National Institute of Health, https://www.nidcd.nih.gov/health/usher-syndrome). Due to the advances in genetic testing, we now have a greater understanding of the genes leading to Usher syndrome. An extensive genetic study has reported that among 172 patients diagnosed with Usher syndrome, the most common mutation was in located in the *MYO7A* gene, which accounted for 53.2% of the families tested (Le Quesne Stabej et al., 2012). Furthermore, research carried out in 1995 suggested that the subtype 1B, which is caused by *MYO7A* mutations, accounted in approximately 75% of the cases of patients diagnosed with Usher syndrome (Weil et al., 1995). More recent literature reported that type 1 represents the most severe form of Usher syndrome, and that it is responsible for 25-44% of all cases (Géléoc and El-Amraoui, 2022). These studies also suggested that targeting *MYO7A* through gene therapy would be of relevance for determining whether this technique could be used to treat Usher syndrome type 1B.

One of the models that replicates some the symptoms observed in Usher Syndrome Type 1B in patients, excluding the retinal degeneration, is the *Shaker-1* mouse (Self

et al., 1998; Mathur and Yang, 2015). The *Shaker-1* mice progressively lose their hearing and have severe vestibular dysfunction identifiable through balance, circling behaviours and head tossing.

The *Shaker-1* missense mutation (R502P) is characterised by a single nucleotide change at position 502 in the motor domain of the protein, with an arginine (R) replaced by proline (P), leading to a different amino acid being encoded (Gibson et al., 1995). Due to this modification, the structure and function of the protein are altered, but the expression levels of Myosin VIIa mRNA and protein are unchanged compared to wild-type animals (Hasson and Walsh, 1997; Nisenbaum et al., 2023). This mutation in *MYO7A* has been shown to cause morphological defects in the hair cells, including the absence of one or two rows of stereocilia, gross hair bundle disorganisation starting from the second postnatal week, and loss of the hair cells at older ages (Self et al., 1998). In terms of physiological changes, cochlear microphonic studies at P20 have demonstrated that sound stimulation was able to produce some degree of changes in their receptor potentials (Self et al., 1998). The cochlear microphonic is an electrical potential generated by the OHCs of the cochlea in response to acoustic stimulation. This potential mirrors the frequency and phases of the sound wave and it helps in assessing the OHCs function, On the other hand, the same study showed that the compound action potential (summation of action potentials from multiple auditory nerve fibres) was altered, suggesting that the IHCs were not able to transduce sound information (Self et al., 1998). These behavioural, morphological and physiological changes in the *Shaker-1* mutant mice highlight the key role of Myosin VIIa in the maintenance of the hair cell stereociliary bundles and their function. In addition to this, the *Shaker-1* mouse seems to provide researchers with an ideal mouse model to

better understand the cellular and molecular manifestations associated with the Usher Syndrome type 1B and for testing potential therapeutic approaches.

Gene therapy approaches for Usher syndrome are still in progress, but there are already studies in phase 1 and 2 clinical trials that aim to target the visual dysfunction (NCT02065011).

MYO7A is a large gene, and it cannot be packaged into a single AVV vector. Therefore, one of the first studies performed aimed to assess whether *MYO7A* could be split between two AAV vectors and would then recombine *in* vivo (Dyka et al., 2014). Using the dual AAV vector, Myosin VIIa was shown to be present in retinal sensory cells both under an *ex vivo* preparation and *in vivo*, indicating that *MYO7A* cloned in AAV vector pairs can recombine and form the full-length protein (Dyka et al., 2014). Later on, the same group showed that the application of the dual construct containing the human *MYO7A* improved retinal defects in the Usher syndrome type 1B mouse model (Ferla et al., 2023). In addition to Myosin VIIa, other studies have also showed some degree of hair cell and hearing function recovery by transducing the exogenous gene affecting other USHER Syndromes when mutated. One study focused on the administration of *USH1C* (Harmonin) to the inner ear. Harmonin is involved in the development of the hair cell bundle and plays key roles in the process of sensory transduction (Pan et al., 2017). Administration of Anc80L65-USH1C at P1 in *Ush1c c.216G>A* knock-in mutant mice showed that one month after surgery the animals showed normal bundle morphology and had partial restoration of hair cell function, especially at lower frequencies (Pan et al., 2017). In Usher syndrome type 3, which is caused by mutations in the *CLRN1* gene, knockout mice exhibit hair cells with

disrupted hair bundles and show profound hearing loss already at P21-P22 (Geng et al., 2017). The administration at P1-P3 of AAV2-CLRN1 or AAV8-CLRN1 in *CLRN1* knockout mice led to the preservation of the hair cell bundle morphology and showed that hearing function could be preserved through adulthood (Geng et al., 2017). Subsequent work in *CLRN1* knockout mice, the injection of the AAV9-PHP.B vector serotype at P1 resulted in an increased hearing sensitivity of up to 50 dB, although this was primarily occurring in the low-frequency region of the cochlea (György et al., 2019). A more recent study has performed gene therapy on a mouse model for Usher Syndrome type 1F, which is caused by the mutation in the tip link protein *PCDH15* (Ivanchenko et al., 2023). In this study, the authors have used a single AAV, in which *PCDH15* was engineered to fit into a single AAV vector by deleting 3-5 of the 11 cadherin repeats (Ivanchenko et al., 2023). Despite the partial protein, AAV9-PHP.B-mini-PCDH15 injected through the RWM into the cochlea of P1 mice was able to rescue stereocilia tip links, mechanotransduction and hearing function (Ivanchenko et al., 2023). This approach was possible because the molecular structure, function and interactome of *PCDH15* are well known and it could be determined which one of its three alternative spliced C-termini of *PCDH15* are needed for its function (Ivanchenko et al., 2023). It was determined that only the PCDH15-CD2 splice form is required for its function, while the extracellular cadherin repeats could be removed to allow *PCDH15* to be packaged into a single AAV (Ivanchenko et al., 2023). Although eight versions of mini-PCDH15 were designed and tested, only three versions were short enough to be packed into the viral vector (Ivanchenko et al., 2023). The successful design and characterization of function of the mini-PCDH15 represent an interesting and promising approach to address different forms of hereditary hearing loss,

especially for genes that are too large to fit in a single AAV capsid (Ivanchenko et al., 2023).

Overall, these studies have illustrated that gene therapy could be effective in mitigating sensory deficits associated with genetic mutations. However, additional research and optimization are needed to better understand the effect, safety, efficacy, best time of administration, dosage, engineering techniques and delivery methods that could be employed for better results and for providing patients with a therapeutic benefit (Amariutei et al., 2023).

Since at the start of this project there was no published work on gene therapy on Usher syndrome type 1B, the initial aim was to test whether the dual-AAV-MYO7A vector delivered to the cochlea of *Shaker-1* mice could aid in any restoration of hearing function.

5.2. Results

The presence of Myosin VIIa in the hair cells of *Shaker-1* was assessed by performing immunostaining experiments from adult heterozygous controls (HET, *Shaker-1*$^{+/-}$) and homozygous (HOM, *Shaker-1*$^{-/-}$) mice. The result show that Myosin VIIa was present in both HET and HOM mice (**Figure 5.1**), indicating that the point mutation in the gene present in *Shaker-1* mice does not affect the generation and localization of Myosin VIIa in the hair cells.

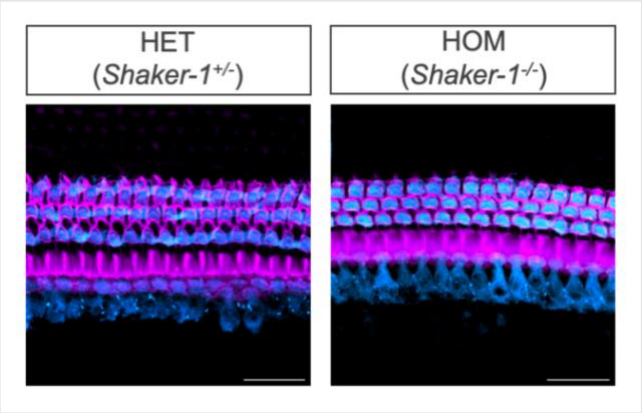

Figure 5.1: Myosin VIIa expression in Usher Syndrome Type I model. Confocal images showing phalloidin (magenta) and Myosin VIIa (blue) in the IHCs and OHCs of HET (*Shaker-1*$^{+/-}$) and HOM (*Shaker-1*$^{-/-}$) mice at P26 – P37 (n=3 mice for each condition). Myosin VIIa expression can be seen in both the control and the mutant mice that are affected by the point mutation. Magnification: 60x. Scale bar: 25 μm.

To identify whether the dual-AAV8-MYO7A at a titration of 3.87×10^{12} vg/mL upon RWM inoculation was able to rescue the morphological and functional phenotypes observed in HOM mice, the viral construct was injected in the cochlea at P0-P1. Since Myosin VIIa expression was still present in the HOM mice (**Figure 5.1**), transduction efficiency for the dual-AAV8-*MYO7A* could not be assessed. However, it was possible to assess the hair bundle morphology using SEM in P26 – P37 old mice (**Figure 5.2A**). To score a bundle as "normal" or "abnormal" we defined the criteria based on the typical structure of hair bundles in the cochlea. The hair bundles were classified as normal if they presented the typical "staircase" structure with rows of stereocilia arranged in ascending order of height. The criteria used included (1) the presence of the three rows of stereocilia, (2) the absence of extra rows and (3) the presence of the tallest row of stereocilia. A bundle would then be classified as "abnormal" from a morphological perspective if it (1) presented with the loss of the shortest third row of stereocilia, (2) had disorganised rows or (3) had missing or fused stereocilia. While the IHC bundles from HET mice showed the classical staircase structure with three rows of stereocilia, HOM mice exhibited very disorganised bundles with the loss of the shortest third row, and often the second row of stereocilia (**Figure 5.2A**). The tallest row of stereocilia seemed to be normal in the HOM mice. However, the HOM mice

that were inoculated with the dual-AAV8-MYO7A appeared to have recovered at least part of the staircase structure (**Figure 5.1A**, white arrow). Nonetheless, injected HOM mice still had several IHCs with abnormal bundles. The number of IHCs that showed near-normal hair bundles was significantly increased in HOM injected compared to HOM mice ($p = 0.0021$, one-way ANOVA, **Figure 5.2B**). However, it is worth noting that this analysis was inherently subjective and additional examination or automated methods of assessment may be needed to minimize bias.

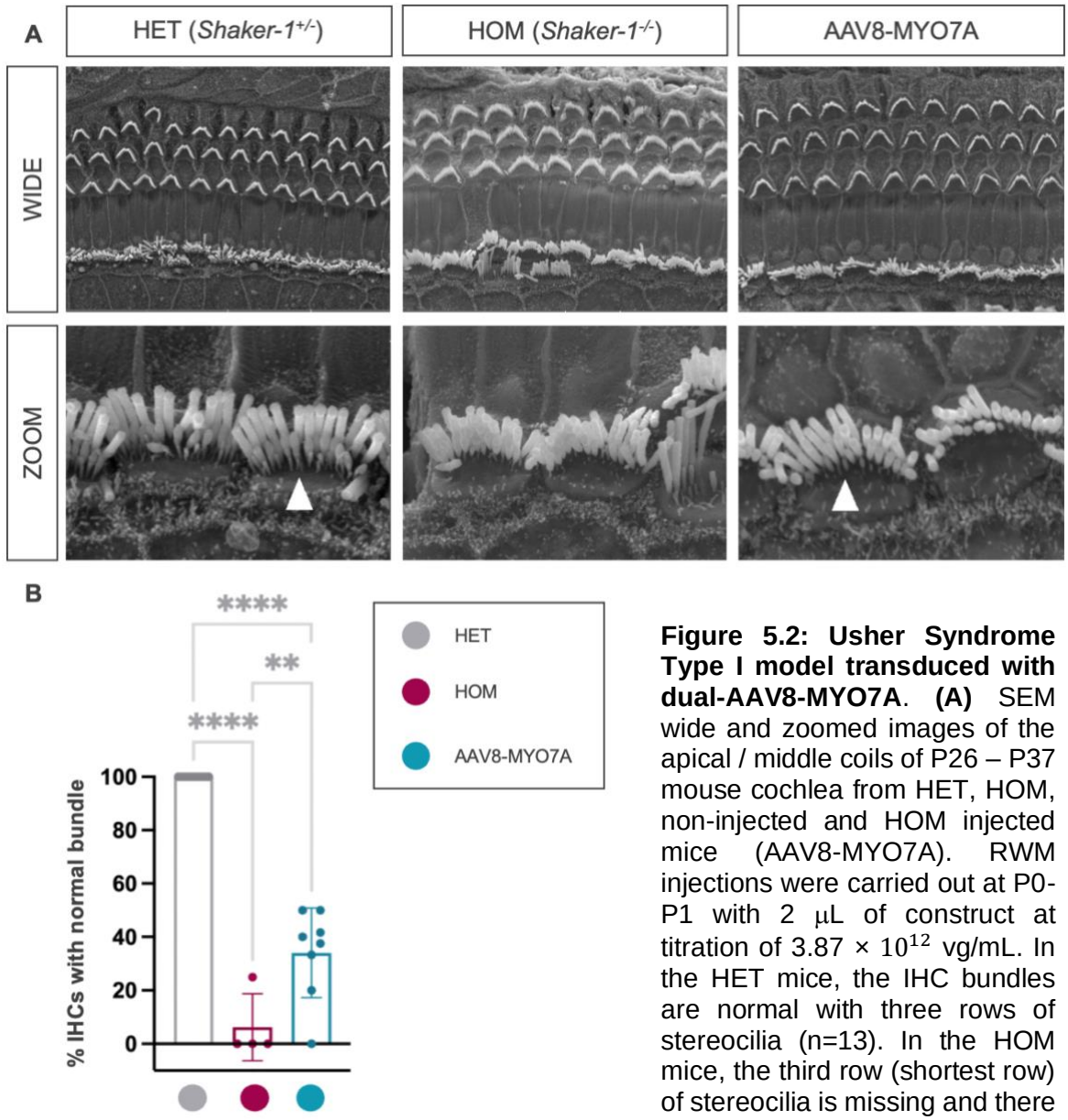

Figure 5.2: Usher Syndrome Type I model transduced with dual-AAV8-MYO7A. **(A)** SEM wide and zoomed images of the apical / middle coils of P26 – P37 mouse cochlea from HET, HOM, non-injected and HOM injected mice (AAV8-MYO7A). RWM injections were carried out at P0-P1 with 2 μL of construct at titration of 3.87×10^{12} vg/mL. In the HET mice, the IHC bundles are normal with three rows of stereocilia (n=13). In the HOM mice, the third row (shortest row) of stereocilia is missing and there are cells in which the second row is also retracted (n=3). In the mice injected with dual-AAV8-MYO7A the third row of IHC stereocilia was present in some cells (white arrow, n=17). **(C)** Graph showing the percentage of IHCs that showed normal stereocilia bundles one-month after the injection with AAV8-MYO7A. In the control samples (n=10) all IHCs had normal bundles (100%), in the mutant (HOM, n=4) there were 6.25% IHCs with normal bundles and in the injected mice (n=8) approximately 34% of the IHCs had three rows of stereocilia. Significant differences in the percentage of cells with normal bundles were recorded between the mutant and mutant injected mice (*p = 0.0021*, one-way ANOVA followed by Dunnett's multiple comparisons test). Data is represented as mean ± SD.

To investigate whether the partial recovery in the shape of the IHC bundle in the HOM injected mice led to some degree of hearing recovery, ABRs were recorded in P26 – P37 mice. These recordings were carried out prior to sample fixation for SEM analysis. ABR thresholds were significant decreased in the HOM injected compared to HOM non-injected (**Figure 5.3**, $p<0.0001$, two-way ANOVA). At frequencies between 6 – 24 kHz, auditory thresholds reached as low as 75 dB (**Figure 5.3**). However, only partial rescue was observed at higher frequencies (**Figure 5.3**). These data suggest that dual-AAV8-MYO7A injections in neonatal *Shaker-1* HOM mice result in a small, but significant morphological and functional restoration. These results also underly the need for improvements of the current approach.

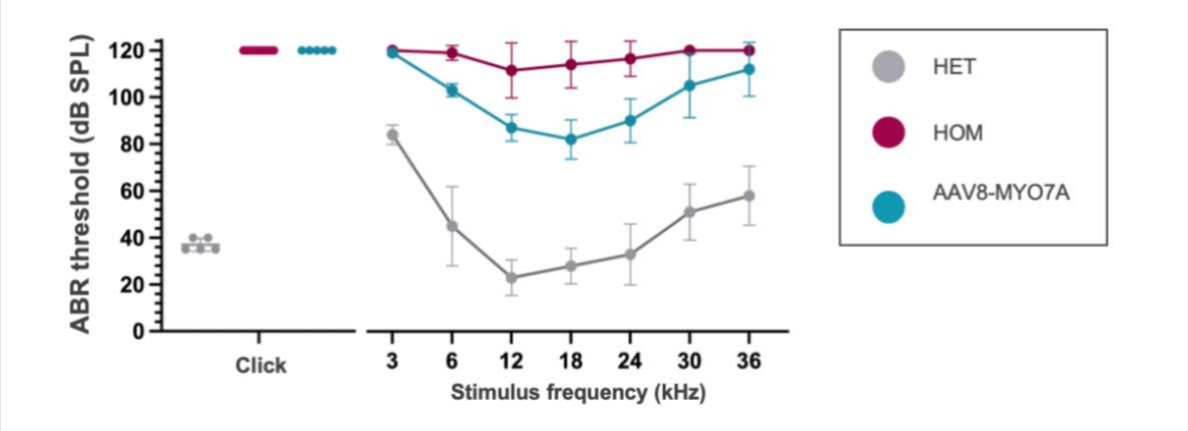

Figure 5.3: ABR thresholds from Usher Syndrome Type I model transduced with dual-AAV8-MYO7A. Average ABR thresholds for click and pure tones between 3 and 36 kHz stimuli. Data is recorded from control (HET, grey), mutant (HOM, magenta) and mutant injected mice upon injection with AAV8-MYO7A (cyan). The examined data revealed significant differences between mutant and mutant injected mice at all frequencies between 6 to 30 kHz (6 kHz: $p = 0.0014$; 12 – 24 kHz: $p<0.0001$; 30 kHz: $p=0.0028$; Dunnett's multiple comparison test from two-way ANOVA). The number of mice tested for each condition is: control = 5; mutant = 10; mutant injected = 5. Data is represented as mean ± SD.

FINDINGS SUMMARY

- Myosin VIIa is present in the *Shaker-1* mutant mice, highlighting that the point mutation affects Myosin VIIa's function but not its expression.
- Mice injected with dual-AAV8-MYO7A have some IHCs that showed near-normal stereociliary bundles.
- Mice inoculated with dual-AAV8-MYO7A recovered some of the hearing function.

5.3. Discussion

About 60% of all the genetic disorders in humans are caused by point mutations, which in most cases lead to loss-of-function of the targeted gene as also seen in Usher syndrome type 1 (Rees et al., 2018). In the present project we aimed to assess whether gene augmentation with normal copies of *MYO7A* could reinstate hearing function in *Shaker-1* mice. The injection of dual-AAV8-MYO7A in the cochlea of neonatal *Shaker-1* mice lead to an improved structure of the hair bundles in the IHCs and an improvement of ABR thresholds by up to 30 dB.

SEM data previously obtained by another PhD student in the lab (Dr Anna Underhill) showed that the IHCs bundles appear to be normal until the beginning of the second postnatal week, and then starts to be disorganised (unpublished data), which is in agreement with previous published work (Self et al., 1998). At P29 – P32 the IHCs from *Shaker-1*$^{-/-}$ mice have already lost their third and second row of stereocilia (**Figure 5.1B**). The transduction of AAV8-MYO7A in P0-P1 *Shaker-1*$^{-/-}$ mice was able to partially restore the staircase structure of some of the IHC hair bundles at (about 34% of the IHCs) in P26 – P37 HOM mice.

The partial recovery of the IHC stereocilia bundle in HOM injected mice appears to correlate with the observed improvement in auditory function. In the mutant non-injected mice, the ABR thresholds were highly elevated, with the lower values being 100 dB or above. On the other hand, in the injected HOM mice the ABR thresholds were as lower as 75 dB, demonstrating some degree of recovery especially at frequencies between 12-24 kHz. The reason for this partial functional recovery may relate to (1) the low transduction efficiency that could be caused by the titration or the AAV vector serotype used, (2) the level of IHC maturation or damage accumulated and (3) the absence of OHC transduction:

(1) The current study has several limitations that warrant consideration. First of all, only one vector (AAV8) was assessed in the present work and only one administration route was implemented (through the RWM). Although some of the experiments were carried out using the AAV9 serotype, the data could not be incorporated into the current report as the mice were still under recovery at the time this report was written.

Secondly, research showed that in the vestibular system administration of AAV-ATOH1 vectors at a higher titration (1×10^{13} vg/ mL) lead to an increase in the therapeutic benefit and enhance hair cell bundle regeneration (Guo et al., 2021). This suggests that by increasing ten times the titration of the construct used in the present experiment (3.87×10^{12} vg/ mL) could have improved the recovery of the phenotype.

Other ways in which the effect of the surgery effect could be improved is by using single vectors, which are known to have higher transduction efficiencies as the construct would not have to recombine *in vivo*. Considering that *Shaker-1* mice have a point mutation in *MYO7A*, single viral constructs could be

designed to deliver allele-specific corrections, a method that has recently been used to recover hearing function in a mouse carrying a mutation in *MYO6* (Xiao et al., 2022).

In addition to this, future work could assess whether non-viral technologies that have higher packaging capacities and higher transduction rate could aid in maximising hearing restoration. This may be of relevance also because the recent literature suggests that there are issues surrounding oncogenicity that may arise upon viral vector administration (Sheridan, 2023).

(2) Considering that in mice Myosin VIIa start to be expressed in the otic placode from about E9 (Sahly et al., 1997), it is possible that the window of therapeutic intervention is limited to embryonic stages. In line with these findings, compelling evidence indicates that the AAV gene therapy approach is significantly enhanced and more effective when performed *in utero* (Hu et al., 2020) or at least prior to any damage to the hair cells has occurred (György et al., 2017; Yoshimura et al., 2019). This has also been suggested by a recent study trying to rescue the hearing dysfunctions caused by the absence of Eps8 at the hair cell stereociliary bundle (Jeng et al., 2022). In this study the injection of Anc80L65-EPS8 at P1, but not at P19-P20, led to the partial rescue the morphological or functional defects present in the hair cells of *Eps8*$^{-/-}$ mice (Jeng et al., 2022). The failure of hearing recovery in the adult emphasizes that accumulated cellular and / or genetic damage may reach a threshold when reparative interventions are rendered ineffective. These publications emphasize that gene therapy approaches may be useful as prevention techniques and not necessarily as therapeutic approaches.

Therefore, additional experiments could assess whether surgery at earlier time points could aid to a better functional recovery. Addressing this would allow to determine if such an approach suffices in treating hearing loss in humans or if it necessitates to be added in combination with other treatments or replacement with alternative techniques. For example, it may be worth considering whether hearing could be restored after IHC degeneration through the application of AAVs together with signalling molecules that could induce the transdifferentiation of supporting cells into HCs, thus inducing development prior the AAV-based gene therapy. Nevertheless, research showed that transdifferentiation of supporting cells into fully functional hair cells is not yet achievable (Wang et al., 2023), highlighting that translation to humans may need additional testing and further refinement.

Since patients diagnosed with Usher syndrome type 1B are born deaf, there may be a limited, if any, therapeutic window of intervention.

Whether the injection of dual-AAV-MYO7A into the mature auditory system represents a viable approach remains to be identified.

Added to the limitations listed above, the present work mainly assessed the hair cell morphology and ABR thresholds. Hence, future work could analyse the biophysical properties of the mechanoelectrical transducer current to better assess the level of recovery in the IHCs from *Shaker-1* mice. In addition to this, RNAscope could potentially be used to detect gene expression and confirm the delivery of AAV into the IHCs (Du et al., 2023). Moreover, behavioural tests could also be employed once inner ear transduction efficiency is increased, as the *Shaker-1* present vestibular defects such as circling and abnormal head shaking and tossing.

In conclusion, the present data showed that dual-AAV8-MYO7A was able restore, at least in part, the morphological feature of the hair bundle structure in some of the IHCs and reduced the ABR thresholds by approximately 20 – 30 dB for frequencies between 6 – 30 kHz.

Chapter 6: Results – *In vivo* gene-based therapy in a mouse model that replicates some of the age-related hearing loss phenotypes

OUTLINE

In the present chapter the following information related to the project will be addressed:

- introduction to age-related hearing loss and associated phenotypes, the *Myosin VIIa*$^{fl/fl}$ *x Myosin15-CRE*$^{+/-}$ mouse model and gene therapy approaches implemented in adult mice
- results
- discussion.

6.1. Introduction

Age-related hearing loss (ARHL) represents the most common chronic disease and affects 65% of the adults aged 60 and above (Tang et al., 2023). The main characteristics of the disease include progressive auditory sensitivity decline, speech comprehension decline and inability to localise sound. Currently, the gold standard for ARHL treatment encompasses hearing aids and cochlear implants, which are beneficial but are not curative (Delmaghani and El-Amraoui, 2020). One approach for addressing ARHL could be through the use of antioxidant therapies, growth factors or through the implementation of gene therapy approaches that could act as preventive, decelerative or potentially curative options.

In order to develop any therapeutic intervention, it is important to have an understanding of the molecular and physiological changes that occur to the cochlea while ageing. It is known that the aged cochlea presents with various changes that include the degeneration of SGNs, a reduction in the density of HCs and changes in the stria vascularis, decrease in endocochlear potential, as well as alterations in the synaptic connections between the sensory cells and adjacent neurons. For example

research in aged C57BL mice showed that the auditory system of one year old mice underwent a process of efferent re-innervation, which led to a higher number of functional LOC efferent fibres making directly synapses with the IHCs (see also Chapter 1; Marcotti et al., 2004a; Lauer et al., 2012; Zachary and Fuchs, 2015). Therefore, in the context of ARHL, one aspect of the aging cochlea is the process of efferent re-wiring on the IHCs. This synaptic configuration mirrors the pre-hearing stages of development, and it has been suggested that the cochlea attempts to re-enact growth and repair (see Chapter 1 and **Figures 1.4** and **1.12**). However, for this to work the different cell types and neurons within the adult and aged cochlea need to be able to repair themselves following genetic-based dysfunctions. Therefore, the current project aimed at testing this hypothesis using a conditional knockout mouse (*Myosin VIIa*$^{fl/fl}$ *x Myosin15-CRE*$^{+/-}$) in which the IHCs, similar to aged mice, become re-innervation by the efferent fibres. The aim was to assess whether replacing the mutated *MYO7A* gene with an exogenous functional one would lead to normal innervation patterns that are supported or reinstated following gene correction.

In the *Myosin VIIa*$^{fl/fl}$ *x Myosin15-CRE*$^{+/-}$ mouse, Myosin15 drives the CRE enzyme which then deletes the MYO7A gene that is flanked by the LoxP (fl) sites (Caberlotto et al., 2011; Corns et al., 2018). Because Myosin15 is normally expressed in the hair cells from about P3-P4, but the functional consequence of removing Myosin VIIa is not visible until the hearing onset the IHC develop normally and the mice have normal hearing until about P15 (Corns et al., 2018). However, Myosin VIIa is no longer detected in the IHCs by P15-P20, and soon after the IHCs begin to be re-innervated by the efferent neurons and mice become deaf (unpublished work, Prof Walter Marcotti). To identify whether the direct, targeted gene therapy delivery to the inner ear of the *Myosin VIIa*$^{fl/fl}$ *x Myosin15-CRE*$^{+/-}$ mice could promote the reformation of

normal mature innervation onto the IHCs and restore their function, we injected AAV-MYO7A in the adult cochlea.

Currently, there are very few studies that show efficient gene transfer in the murine adult cochlea. For example, one of the most recent publications showed that administration of AAV2-hTMPRSS3 through the RWM with canal fenestration in *TMPRSS3* knockin mutant mice of 18.5 months helped restore hearing by promoting hair cell survival (Du et al., 2023). The *TMPRSS3* knockin mutant mice present with late onset of progressive hearing loss, which is caused by the loss of the hair cells. In addition to this, another study showed that AAV1-VGLUT3 injection at P10-P12 in *VGLUT3* knockout mice, which are profoundly deaf, led to the expression of the transgene into the IHCs and to the restoration of ABR thresholds two weeks after injection (Akil et al., 2012). VGLUT3 is first expressed in the cochlea around E19 (Seal et al., 2008) and it is essential for packaging glutamate into synaptic vesicles within the IHCs, thus playing a key role in the activation of the postsynaptic afferent neurons (Akil et al., 2012). Interestingly, the same study showed that the injections carried out in P12-P13 mice were less efficient than when performed at P1-P3, suggesting that AAV-based gene delivery may be less successful when carried out in the adult murine models (Akil et al., 2012). Nonetheless, the same group later administered dual-AAV2-OTOF at P10, P17 and P30 in *Otof*$^{-/-}$ mice, in which the hair cells lack the Ca^{2+} sensor for exocytosis otoferlin (Akil et al., 2019). In this study it was shown that the injection of the dual-AAV2-OTOF into the cochlea of mice at all three ages produced similar hearing function recovery (Akil et al., 2019). This may suggest that the results do not only depend on the age at which the therapeutic approach is administered but also on the targeted gene.

6.2. Results

3 μL of dual-AAV-MYO7A were administered between P13-P16 in *Myosin VIIa*$^{fl/fl}$ *x Myosin15-CRE*$^{+/-}$ mice. To test whether 3 μL of construct would impair hearing function, different mice were injected with 3 μL of 1 x PBS. One-month after surgery, mice had their ABRs recorded, and cochleae were then fixed and immunostained for Myosin VIIa (**Figure 6.1A**). I have mainly assessed the transduction efficiency of dual-AAV8-MYO7A (1.2 x 10^{12} vg/mL), but a few mice were also assessed with dual-AAV9-MYO7A (6.8 x 10^{12} vg/mL; n=3 mice) – from herein these are referred as dual-AAV-MYO7A.

The results show that, as expected, Myosin VIIa expression was detected in the controls but not is knockout mice. In knockout mice injected with AAV, some of the IHCs were able to re-express Myosin VIIa, the proportion of which changed along the cochlea (**Figure 6.1A**): apical coil 27%; middle coil 23% and basal coil 10% (**Figure 6.1B**). Throughout the cochlea, there were no OHCs transduced. Merged data from all cochlear coils showed that Myosin VIIa was expressed in 100% of the control hair cells, 0% of the cells in the knockout and approximately 18% of the IHCs in injected mice (**Figure 6.1C**). Statistical test carried out between the control and injected mice showed that the Myosin VIIa expression was significantly different between the two conditions (*p<0.0001*; one-way ANOVA).

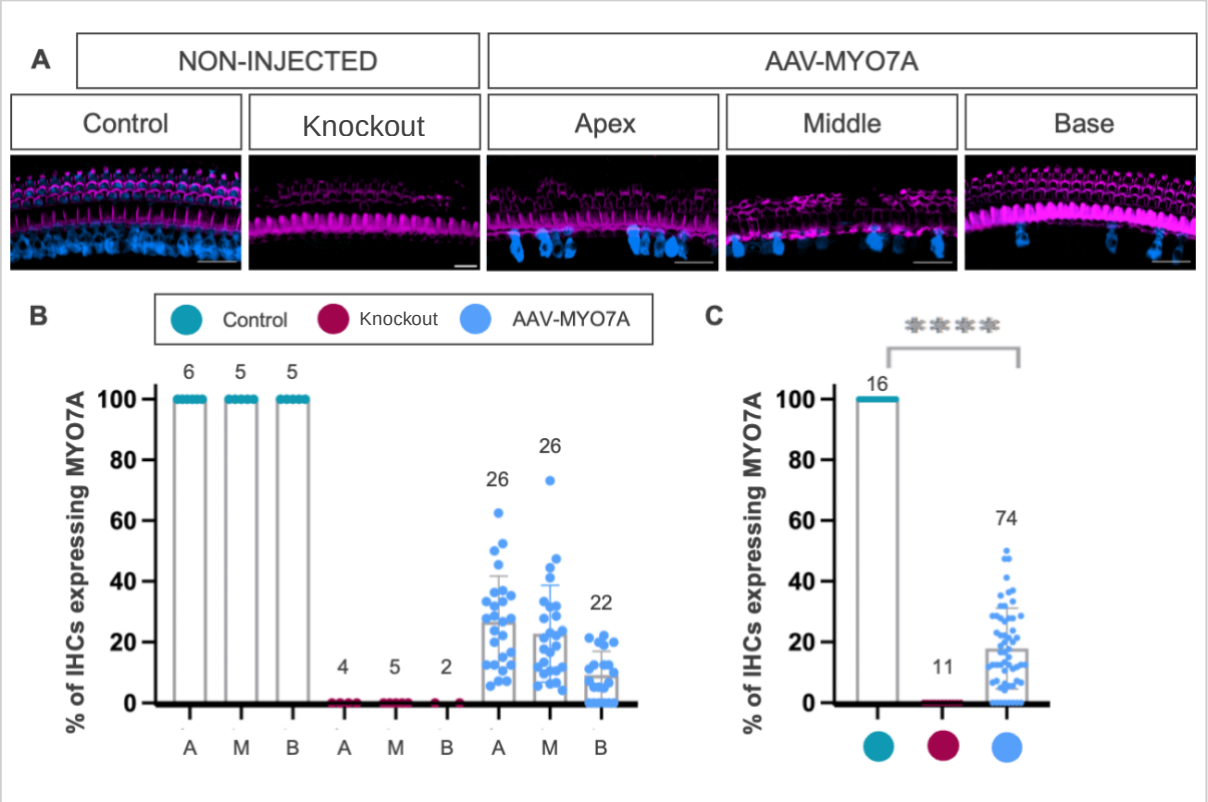

Figure 6.1: *Myosin VIIa$^{fl/fl}$ x Myosin15-CRE$^{+/-}$* mice transduced with dual-AAV-MYO7A. **(A)** Confocal z-stack images (projections done at 0.7 μm steps and using 1.4 – 1.6 zoom) showing phalloidin (magenta) and Myosin VIIa expression (blue) in the IHCs and OHCs of control, knockout and knockout injected mice with 3 μL of dual-AAV8-MYO7A (1.2 x 10^{12} vg/mL) or dual-AAV9-MYO7A (6.8 x 10^{12} vg/mL); (n=6 control mice, n=4 knockout mice, n=26 injected mice). Surgeries were carried out between P13 – P16 and the analysis was carried out between P45 – P52. Myosin VIIa expression can be seen in the control and the knockout mice that were transduced with dual-AAV-MYO7A, but it is absent in the knockout non-injected mice. Magnification: 60x. Scale bar: 25 μm. **(B)** Graph showing the percentage of Myosin VIIa expressing cells one-month post-surgery at P45 – P52. Data was collected from controls (green), knockout (magenta) and knockout injected mice (blue). The number of cochleae/mice per condition is listed above the graph. Data is represented as mean ± SD. **(C)** Overall transduction efficiency with dual-AAV-MYO7A throughout the cochlea in control mice (green), knockout (magenta) and knockout injected (blue). The result of the one-way ANOVA statistical tests showed that there are significant differences recorded (*p<0.0001*) and the multiple comparison test showed that there were significant differences between the number of cells expressing Myosin VIIa in the control and knockout injected mice were noted (*p<0.0001*, one-way ANOVA followed by Tukey post-test). The number of samples tested is listed above the graph. Data is represented as mean ± SD.

To investigate whether the gene therapy procedure aided in the restoration of hearing function, ABRs were recorded between P45 – P52. Statistical analysis carried out between control, control injected, knockout and knockout injected mice showed that

there were significant differences in ABR thresholds (*p<0.001*, two-way ANOVA, **Figure 6.2B**). Further statistics that included Dunnett's multiple comparison test showed that the ABR thresholds were significantly decreased in knockout injected mice compared to knockout non-injected mice (*p* values reported in the figure legend, **Figure 6.2B**), with a small, but significant hearing recovery at certain frequencies.

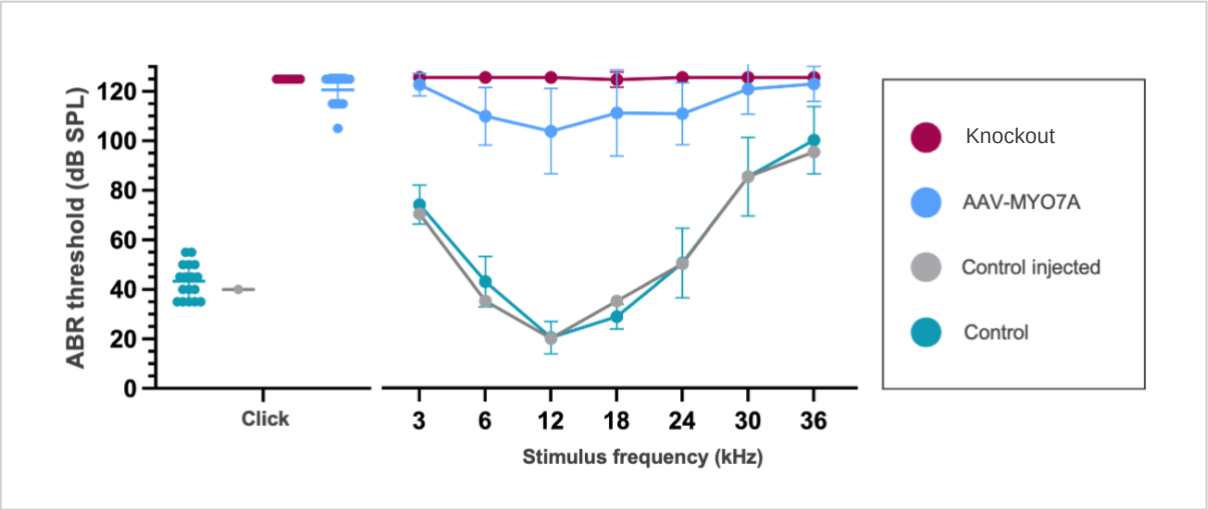

Figure 6.2: *Myosin VIIa$^{fl/fl}$ x Myosin15-CRE$^{+/-}$* model ABR thresholds in knockout mice and animals transduced with dual-AAV-MYO7A. Mean ABR thresholds for clicks and stimuli from 3 to 42 kHz recorded from controls (green), control injected (grey), knockout injected (blue) and knockout non-injected (magenta) mice. Mice were injected with 3 μL of dual-AAV8-MYO7A (1.2 x 10^{12} vg/mL) or dual-AAV9-MYO7A (6.8 x 10^{12} vg/mL) or 3 μL of 1 x PBS between P13 – P16 and ABRs were recorded between P45 – P52.Two-way ANOVA statistical tests followed by Dunnett's multiple comparison test showed that significant differences were detected between knockout and knockout injected mice at 6 kHz (*p=0.0003*), 12 kHz (*p<0.0001*), 18 kHz (*p= 0.0027*), 24 kHz (*p= 0.0009*). The number of mice tested for each condition is: control=16; control injected=1; knockout injected=11; knockout =15. Data is represented as mean ± SD.

To assess whether the transduced IHCs regained their mature, functional characteristics, the cochleae of controls, knockout and injected mice were stained for the large conductance Ca^{2+} activated K^+ current (BK). The reason for staining the samples with BK antibody is because (1) BK contributes to the normal functional maturation of the IHCs (Marcotti et al., 2006) and because (2) previous results show that BK channels are down-regulated in the IHCs from the *Myosin VIIa$^{fl/fl}$ x Myosin15-*

CRE$^{+/-}$ mice (Corns et al., 2018) and aged mice (Jeng et al., 2021). Even though the presence of BK channels can suggest functional capacity, the expression will not direcly measure the hair cell performance and physiological response. Additional experiments such as electrophysiological recordings would be needed to assess the IHCs' response to stimuli. The current results provide an indication of functional characteristics but they do not equate a definitive functional assay. BK expression is normally present in the neck region of the IHCs, and the confocal images showed that in the control BK was present in all the IHCs (**Figure 6.3A**). BK channels were mainly absent in the knockout mice, but some very small puncta could still be seen in some IHCs, possibly due to some staining background (**Figure 6.3A**). In the knockout injected mice, BK puncta reappeared in the neck region of the IHCs (**Figure 6.3A**). Further analysis showed approximately 98% of the IHCs in the control, 27% in the knockout (although very small: see above comments) and 44% in the injected mice expressed BK channels throughout the cochlea (**Figure 6.3B**, the data was pulled together for the apical, middle and basal regions). However, there was no statistical significance recorded between the knockout and injected mice ($p=0.22$, t-test).

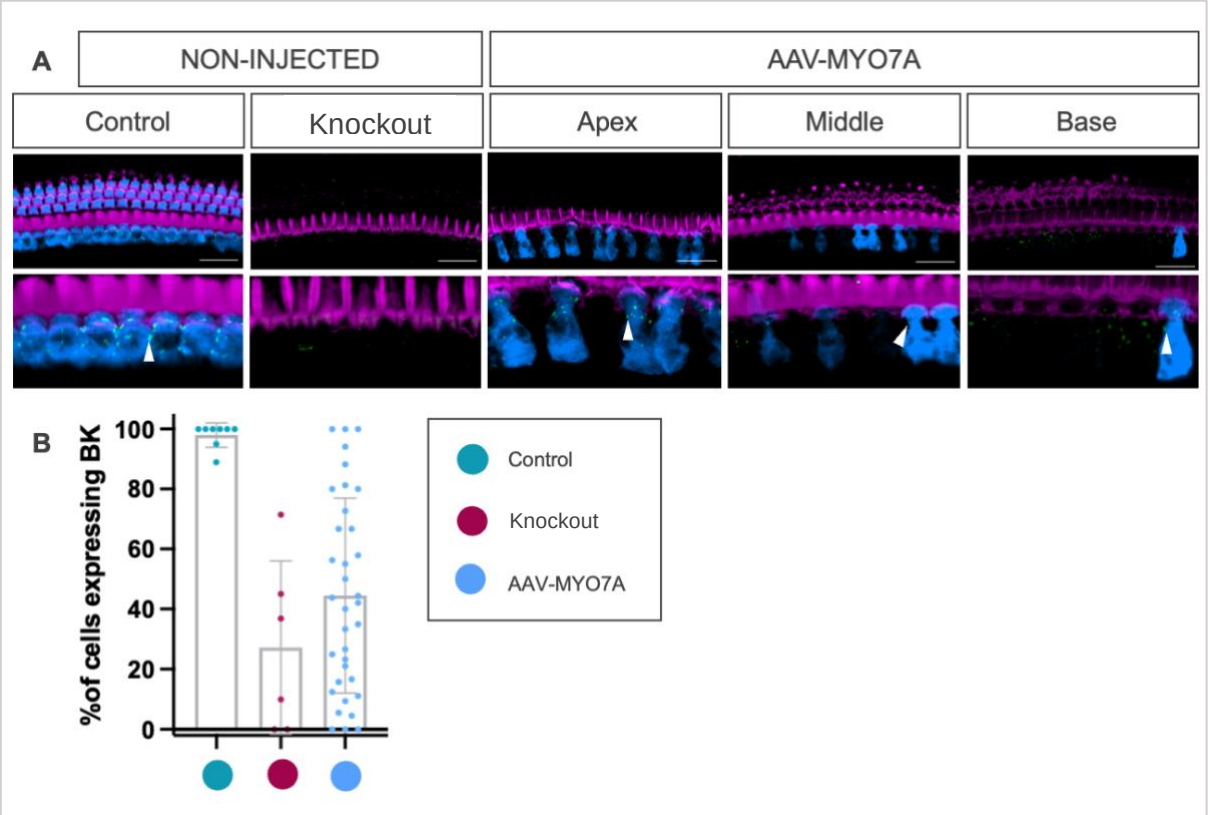

Figure 6.3: Transduced cells from *Myosin VIIa$^{fl/fl}$ x Myosin15-CRE$^{+/-}$* re-express BK at P45 – P52. (A) Confocal z-stack images showing phalloidin (magenta), Myosin VIIa (blue) and BK (green) in the hair cells of control, knockout and knockout injected between P45 – P52 (n=5 control mice, n=4 knockout mice, n=11 injected mice). Magnification: 60x. Scale bar: 25 μm. **(B)** Graph showing the percentage of cells that express BK in control (green), knockout mice (magenta) and knockout injected mice (blue). The injected mice had BK puncta present in the transduced cells (white arrows) and the puncta was in some cases present in cells that were not transduced by the dual-AAV-MYO7A. No significant differences were recorded between the knockout and knockout injected mice in the percentage of cells expressing BK (*p=0.*022, unpaired t-test). The number of samples assessed for each condition is: control=8; knockout =6; AAV-MYO7A injected=35. Data is represented as mean ± SD.

To assess whether the mature efferent innervation pattern was also re-established in the IHCs transduced with AAV-Myo7a, control, knockout and knockout injected samples were stained for the small conductance Ca^{2+}-activated potassium channel (SK2). SK2 labelling expression in the IHCs knockout mice would indicate the presence of the axosomatic efferent innervation (LOC) onto the IHCs, while its absence in the knockout injected, similar to control mice, would show that the IHCs returned to a mature-like state upon dual-AAV-MYO7A gene therapy (Jeng et al., 2020). However, all experiment conducted from the different mouse models, showed

that SK2 puncta were not localised in the basal region of the cells, but instead they were present in their neck region (**Figure 6.4)**, and overlapping with Phalloidin Texas-Red staining. Therefore, after three experimental repeats with a similar artefactual distribution of the SK2 puncta, no conclusions could be drawn on whether the transduced IHCs switch from being innervated directly by efferent fibres to losing the axosomatic efferent connection on the sensory cells.

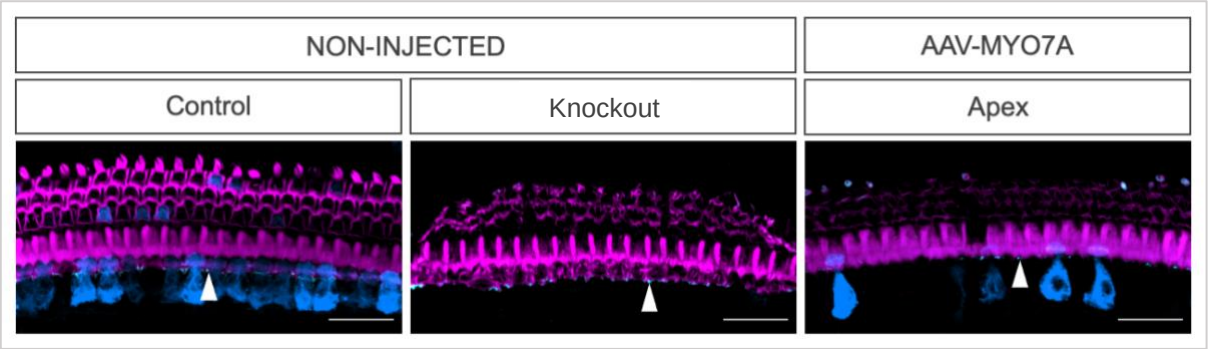

Figure 6.4: SK2 expression in controls and *Myosin VIIa$^{fl/fl}$ x Myosin15-CRE$^{+/-}$* knockout and knockout injected mice. Confocal z-stack images showing phalloidin (magenta), Myosin VIIa (blue) and SK2 (cyan, white arrows) in the IHCs of control, knockout and knockout injected mice between P45 – P52 (n=3 control mice, n=2 knockout mice, n=6 injected mice). The SK2 expression is present in the neck region of the cell instead of being present in the basal pole. Magnification: 60x. Scale bar: 25 μm.

The data presented in the current chapter suggests that application of dual-AAV-*MYO7A* in adult *Myosin VIIa$^{fl/fl}$ x Myosin15-CRE$^{+/-}$* mice is able to revert the expression of the BK channels and partially rescue the hearing function.

FINDINGS SUMMARY

- Mice injected with dual-AAV-MYO7A had approximately 18% of the IHCs transduced and none of the OHCs.
- Dual-AAV-MYO7A delivery improved the hearing thresholds of the injected mice, with some mice showing thresholds as low as 80 dB.
- IHCs from injected mice re-express BK channels similar to control mice.

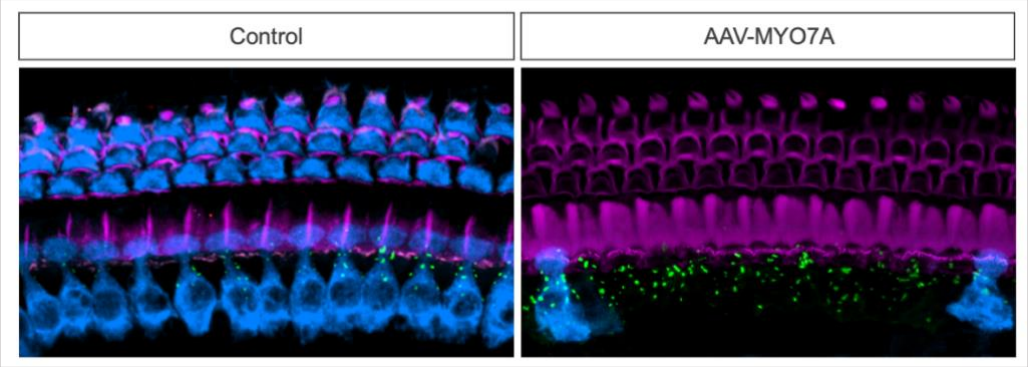

- The data obtained from the *Myosin VIIa*$^{fl/fl}$ *x Myosin15-CRE*$^{+/-}$ mice highlights that the adult IHCs retain the ability to re-express mature-like proteins even after being reverted to a pre-hearing phenotype that is also observed in the aged cochlea. This suggests that gene-based therapy could potentially be used to target late onset progressive hearing loss.

6.3. Discussion

Age-related hearing loss is a progressive condition that affects many people as they get older. According to the United Nations' *World Population Ageing Report*, it is expected that the global population of individuals aged 65 and over to increase from 703 million in 2019 to 1.5 billion by 2050 (https://www.un.org/en/development/desa/population/publications/pdf/ageing/WorldPopulationAgeing2019-Report.pdf). Hence, an increased number of individuals will likely suffer from hearing loss and gene therapy represents a promising strategy to

enhance the functionality of the auditory system. Preclinical studies carried out in mammals have shown that the delivery of specific genes in the cochlea could improve hearing. In the current work we aimed to assess whether gene therapy with dual-AAV-MYO7A could assist in reinstating hearing function and re-establishing the mature IHC configuration in *Myosin VIIa*$^{fl/fl}$ *x Myosin15-CRE*$^{+/-}$ adult mice, which mimic some of the changes observed in early onset ARHL mice. The results showed that inoculation of the viral construct could reinstate hearing function with improvements in ABR thresholds by up to 40 dB and aided in the recovery of the IHC maturation markers BK. In this discussion section the (1) transduction efficiency, (2) hearing recovery and (3) BK and SK2 expression will be assessed in relation to already published literature.

Transduction

Previous work in the lab has showed that the cells of the *Myosin VIIa*$^{fl/fl}$ *x Myosin15-CRE*$^{+/-}$ mice stop expressing Myosin VIIa a few days before P20 (unpublished work Prof. Walter Marcotti). Hence, by carrying out the surgeries at P13 – P16 it was expected that exogenous Myosin VIIa would be re-expressed from about P20 onwards, as it takes more than 7 days for genes delivered using AAVs to be expressed and even a longer period (2-4 weeks post-injection) for the expression to reach peak and stable levels (Zincarelli et al., 2008). In our results we observed that one-month post-surgery the IHCs expressed Myosin VIIa upon viral injection with dual-AAV-MYO7A. However, only 18% of the IHCs express the protein suggesting that the surgery technique or the serotypes used may lead to low infection rates. In line with this, recent research assessed three different gene delivery methods carried out through the posterior semicircular canal, RWM and RWM+posterior semicircular canal injection (Zhao et al., 2022). The results of the study showed that in the adult mice the

posterior semicircular canal injection with single AAV vectors leads to higher transduction rates compared to the other methods (Zhao et al., 2022a). In addition to this, previous work showed that injections carried out with AAV8, AAV9 and Anc80L65 serotypes, administered through the oval window in the adult guinea pig, had the highest IHC transduction rate of 71-90% only with the latter AAV (Wang et al., 2022). Therefore, such studies suggest that implementing an alternative route of administration and changing the vector serotype may help increasing the transduction efficiency. Irrespective of that, it is important to note that the literature assessing transduction efficiency of different AAV serotypes used single viral constructs and dual vectors usually present lower transduction rates.

Hearing recovery

As presented in the introduction section of this chapter, a small number of studies showed that AAV gene therapy approaches were successful when administered to the adult cochlea. Reports suggest that such methods are not implemented because of the age-related decline in viral tropism (Marcovich et al., 2022). However, research using either genes or microRNAs carried in AAV vectors showed that such approaches could aid in preventing or restoring hearing function. For example, RNAi-mediated gene silencing administered with AAV could slow progression of hearing loss, improve IHC survival and prevent the degeneration of the bundle in adult *Beethoven* mouse mutants (Yoshimura et al., 2019). In addition to this, a recent report suggests that AAV8-VGLUT3 administration in the cochleae of 5, 8 or 20 weeks old knockout mice helped in restoring hearing function (Zhao et al., 2022). In line with these findings, our work also showed that dual-AAV-MYO7A injection in *Myosin VIIa*$^{fl/fl}$ *x Myosin15-CRE*$^{+/-}$ mice improved hearing function. The limited hearing recovery observed in the present

experiments is also caused by the lack of transduction of the OHCs. Previous work also observed that upon cochlear inoculation via the RWM in adults fail to transduce OHCs (Chen et al., 2019). In addition to this, the adult surgical procedure may have partially affected the hearing recovery as well. Based on data reported by us in Chapter 4, and based on previously published work, some cochlear damage it is likely to be expected from the RWM surgery, which has a direct impact on hearing function. For example, Chen and colleagues reported significantly higher ABR thresholds in the injected ears of adult mice compared to contralateral non-injected ears (Chen et al., 2019). In addition to this, other groups showed a 10 dB ABR threshold shifts when surgery was carried out through the oval window (Wang et al., 2022). Therefore, it is likely that the following changes could assist in further improving the functionality upon dual-AAV-MYO7A administration: (1) designing the AAV-MYO7A construct in such a way that a single vector containing only the *MYO7A* coding sequences required for function are delivered to the cochlea and (2) developing a less invasive inoculation technique that prevents the additional loss of hearing.

BK expression

Immunolabelling data revealed there was more BK channel expression was observed in the apical coil of the cochlea, and this may be caused by the higher transduction efficiency in the apex, or it may relate to the time needed for enhancing and stabilising the protein expression in the middle and basal regions. We noted that BK expression was present in some IHCs of knockout injected mice with no clear Myosin VIIa expression, although low level of the protein could be present but not detectable by immunostaining. However, to support this statement additional molecular analysis such as Western blotting could be carried out. The BK expression that is present in

the IHCs from knockout injected mice may suggest that the IHCs are re-acquiring a mature and functional phenotype. For example, it is known that during development BK starts to be expressed at P12 onwards, a period that overlaps with the establishment of IHC function (Hafidi et al., 2005). In addition to this, previous research carried on the *Myosin VIIa*$^{fl/fl}$ *x Myosin15-CRE*$^{+/-}$ knockout mice showed that there was a gradual loss of the adult-type K^+ current (I_{Kf}) that is detected by the BK antibody and that the IHCs exhibited immature profiles (Corns et al., 2018). These studies highlight that BK is needed for and could be used in the present study as a marker for hair cell function and maturation.

Considering that the injected mice showed some degree of hearing recovery together with BK expression, it is likely that the transduced cells are able to switch back to a mature phenotype and, possibly re-establish the correct efferent innervation pattern. However, the experiments performed during this project were inconclusive on whether the efferent post-synaptic SK2 channels are not expressed in the IHCs from the AAV injected mice. This was probably due to some technical issue in the immunostaining procedure, which unfortunately I was not able to address within the timeframe of this PhD project. This was mainly due to the fact that even IHCs from control mice showed mislocalised SK2 puncta, possible due to the use of EDTA. EDTA is normally used to decalcify the bony cochlea of adult mice and it has been shown to alter the tissue structure and disrupt or lead to the loss of protein epitopes (Krenacs et al., 2010). Therefore, to analyse SK2 expression the decalcification process could be avoided, or immunogold transmission electron microscopy could be carried out to assess whether the LOC efferent contacts the afferent neuron instead of the IHCs upon dual-AAV-MYO7A transduction. However, data obtained post-PhD thesis submission by Andrew O'Connor indicated that SK2 is absent in injected mice and it is present in knockout

mice that are non-injected. Therefore, the latest findings suggest that the absence of SK2 puncta in treated mice leads to reversal of the pre-hearing-like innervation aligning more closely with the mature innervation pattern of normal IHCs.

In conclusion, the present results demonstrate that dual-AAV-MYO7A gene therapy in a model of early-onset progressive hearing loss yielded partial hearing recovery, highlighting the inherent plasticity of the aged cochlea. The published literature and current work indicate that the auditory system can be manipulated and modified with the purpose of restoring or improving hearing. While the current findings are promising, they also underscore the complexity of the system and the challenges that need to be faced to acquire complete functional recovery. The BK markers present in the images may not be solely due to the AAV-MYO7A injections considering that the values of BK puncta are similar in injected and knockout mice. The partial effectiveness of this approach suggests that optimization of the AAV vector, the implementation and testing of different surgery techniques, the adjustment of the treatment timing and dosage to increase the effect are needed. In addition to this, future work could also assess whether gene therapy could be integrated alongside other therapeutic modalities such as pharmacotherapy. The present work suggests that with continued research, the effectiveness of gene therapy for hearing loss could be further enhanced and in time provide a viable treatment for patients suffering worldwide of ARHL.

Chapter 7: Conclusions and future work

The initial work of this project focused on establishing and refining the technique for delivering gene therapy to the inner ear through the RWM. The procedure proved to be effective for direct AAV delivery in both neonatal and adult mice, as well as neonatal gerbils. Key findings included the successful transduction of IHCs using AAV8 and AAV9 serotypes, with AAV9-PHP.eB showing particularly enhanced uptake in the hair cells. It was noted that transduction efficiency varied with viral volumes and shower that higher volumes generally lead to increased IHC transduction without impacting hearing function as confirmed by the ABR tests. In addition to this, the AAV9 serotype was shown to be more effective in transducing OHCs, however only with limited capacity.

Overall, the first findings of this project demonstrated that RWM surgery is a viable approach for delivering genes to the cochlear hair cells and highlighted that the transduction success of the AAV8 and AAV9 serotypes in IHC transduction is influenced by the surgical technique, the serotype and the promoters, as well as the timing of the intervention. Nevertheless, there were limitations in the present work that related to the small sample size and the unknown efficiency of dual-vector constructs compared to single-vectors that were tested.

Therefore, future studies may explore different AAV serotypes, promoters and surgical techniques that may enhance transduction efficiency, addressing the graded transduction seen across the cochlea and understand the effects of longer coding sequences on transduction efficiency. The baseline work carried in this project had the aim of assisting in testing dual-AAV constructs that targeted MYO7A for gene therapy approaches in mouse models of hearing loss.

Myosin VIIa is an unconventional motor protein that in is expressed in the sensory hair cells of the inner ear. Myosin VIIa has a key role in the development and maintenance of the stereociliary hair bundles projecting from the top of the hair cells. By being a key component of the stereocilia, Myosin VIIa plays key roles in the mechanoelectrical transduction of sound into an electrical signal and is aiding the transport of molecule along their actin filaments (Hasson et al., 1995; Self et al., 1998). Mutations in the *MYO7A* gene cause the most debilitating form of Usher Syndrome (Usher Syndrome 1B: Sun et al., 2011; Blanco-Kelly et al., 2015), which is associated with bilateral hearing loss, reduced vestibular function and retinal degeneration. Because of the key role that *MYO7A* has in a common form of hearing loss in humans, it represents an ideal target for gene therapy. In recent years, gene therapy has been highlighted as a promising method for treating hearing loss. Therefore, the current project aimed at investigating whether hearing function could be restored using gene-based therapy in (1) *MYO7A* mutant mice that represent a model for Usher syndrome type 1 (*Shaker-1*) and in (2) the *MYO7A* conditional knockout mouse model that exhibits phenotypes identified during progressive hearing loss or ARHL (*Myosin VIIa*$^{fl/fl}$ *x Myosin15-CRE*$^{+/-}$).

***Shaker-1*: Cochlear gene therapy for Usher syndrome type 1**

The results in the *Shaker-1* model showed that dual-AAV8-MYO7A injection to P0-P1 pups via the RWM led to up to 45 dB improvement in hearing function and in the morphological structure of the stereociliary bundles. Although the recovery was limited the results are promising. However, the translation of these findings to clinical application requires further investigation and refinement. For example, early delivery of the of the AAVs *in utero,* which is prior the appearance of major morphological

defects in the hair cells due to the mutation in *MYO7A*, could provide significant improvements in the recovery of hearing function. Furthermore, to enhance IHC and OHC transduction more efficient AAV capsids such as AAV9 or the next generation AAVs such as Anc80L65 could be investigated. However, the use of artificial vectors would require additional safety testing as synthetic vectors could present with issues in a clinical setting. As such, these approaches would need to be validated in larger animal models *in vivo* and potentially *in vitro* in human tissue. The use of hair cell specific promoters could also provide a large improvement in the transduction efficiency of the AAVs. Alternatively, instead of using dual-AAV-MYO7A gene addition in a model that has a point mutation, several other strategies such as CRISPR-Cas9 could be implemented to correct the point mutation. AAV vectors could be used to deliver the CRISPR system to the hair cells. Using this approach, guide RNA could be used to direct the Cas9 protein to the specific *MYO7A* location on the DNA and create a cut; the guide RNA directs the Cas9 to the right location and then the Cas9 enzyme acts as “scissors” that cuts the DNA. The DNA template would carry the correct sequence and the hair cell repair machinery could use the template to repair the cut and replace the mutated *MYO7A* sequence with the correct one. Such approaches have been implemented in mouse models of acquired sensorineural hearing loss caused by ototoxic drugs or in models of autosomal dominant hearing loss (Gu et al., 2021; Cui et al., 2022).

Myosin VIIa$^{fl/fl}$ x Myosin15-CRE$^{+/-}$: Cochlear gene therapy for a model of progressive hearing loss

The delivery of the dual-AAV-MYO7A to the inner ear of the *Myosin VIIa$^{fl/fl}$ x Myosin15-CRE$^{+/-}$* knockout mouse, which recapitulates some of the changes occurring in the

cochlea of aged mice (e.g. efferent re-innervation on the IHCs and downregulation of BK channels), led to the transduction of Myosin VIIa in the IHCs. Once expressed in the IHCs, Myosin VIIa helped to restore some of the physiological and morphological characteristics of mature IHCs (BK channel expression), which led to the improvement of the hearing function up to 40 dB. The limited restoration may be due to several factors including the time window of the intervention (P13-P15), the AAV serotype and its promoter, the dual AAV vector that does not efficiently recombine *in vivo*, the administration route. To address some of these issues, the injections could be carried out at an earlier time point before the onset of hearing function (<P12), as the cochlear changes due to the mutation could have been easier to revert. Moreover, previous studies indicated that high transduction efficiency and significant auditory recovery can be achieved when using the CB6 promoter with the WPRE element (Marcovich et al., 2022) – therefore, replacing the CMV promoter may further improve hearing rescue. In addition to this, it could be also assessed whether only the *MYO7A* domains that are required for the protein function could be delivered to the inner ear, since by reducing the size of the construct it could be possible that a single AAV is required, thus avoiding the rate limiting step of dual *in vivo* recombination.

For both mouse models the functional recovery appeared to be frequency-dependent – with the best recovery being located at frequencies between 6 – 24 kHz. Similar to others, we observed that the very high frequency (42 kHz) remained largely unaffected by the gene delivery (Pan et al., 2017). To improve the efficiency of AAV transduction, and thus IHC recovery, in the high-frequency region of the cochlea, future work could look into the delivery of the viral vectors through different routes.

The reasoning for having a slightly better recovery in the *MYO7A* point mutation mouse model (*Shaker-1*) compared to the conditional knockout *MYO7A* model (*Myosin VIIa$^{fl/fl}$ x Myosin15-CRE$^{+/-}$*) could be attributed to the time of the intervention and the fact that neonatal procedures are less challenging to carry-out compared to adult.

Building on the existing knowledge, additional research could shed some light on the specific molecular mechanism through which Myosin VIIa carries its functions, supports the organization and maintenance of the hair bundle and is involved in mechanotransduction. These results would contribute to our broader understanding of hearing and would assist in identifying whether co-expression of other genes, proteins or small molecules would be needed to maximise the current observed therapeutical effects.

Overall, the present findings demonstrated that dual-AAV-MYO7A gene replacement therapy represents a viable strategy for the restoration of morphological and physiological deafness phenotypes. We show that dual-AAV-MYO7A vectors can promote the partial hearing recovery in *MYO7A* murine models of congenital and progressive hearing loss. In addition to this, it was observed that the mature auditory system maintains its plasticity and has the ability to recover its function. Hence, such technology holds the potential not just to treat but to cure hereditary hearing loss. Therefore, after further refining, such approaches have the potential to reach a clinical setting and significantly improve the hearing for numerous individuals.

References

Ahmed, H., Shubina-Oleinik, O. and Holt, J.R. (2017) 'Emerging gene therapies for genetic hearing loss', *Journal of the Association for Research in Otolaryngology*, 18(5), pp. 649–670. doi:10.1007/s10162-017-0634-8.

Akil, O. *et al.* (2012) 'Restoration of hearing in the VGLUT3 knockout mouse using virally mediated gene therapy', *Neuron*, 75(2), pp. 283–293. doi:10.1016/j.neuron.2012.05.019.

Akil, O. *et al.* (2019) 'Dual AAV-mediated gene therapy restores hearing in a DFNB9 mouse model', *Proceedings of the National Academy of Sciences*, 116(10), pp. 4496–4501. doi:10.1073/pnas.1817537116.

Al-Moyed, H., Cepeda, A. P., Jung, S., Moser, T., Kügler, S., & Reisinger, E. (2019). A dual-AAV approach restores fast exocytosis and partially rescues auditory function in deaf otoferlin knock-out mice. *EMBO molecular medicine*, *11*(1), e9396. doi:10.15252/emmm.201809396.

Al-Moyed, H. *et al.* (2018) 'A dual-aav approach restores fast exocytosis and partially rescues auditory function in deaf otoferlin knock-Out Mice', *EMBO Molecular Medicine*, 11(1). doi:10.15252/emmm.201809396.

Amariutei, A.E. *et al.* (2023) 'Recent advances and future challenges in gene therapy for hearing loss', *Royal Society Open Science*, 10(6). doi:10.1098/rsos.230644.

Andres-Mateos, E. *et al.* (2022) 'Choice of vector and surgical approach enables efficient cochlear gene transfer in nonhuman primate', *Nature Communications*, 13(1). doi:10.1038/s41467-022-28969-3.

Anson, D.S. (2004) 'The use of retroviral vectors for gene therapy-what are the risks? A review of retroviral pathogenesis and its relevance to retroviral vector-mediated gene delivery ', *Genetic Vaccines and Therapy*, 2(1), p. 9. doi:10.1186/1479-0556-2-9.

Anthwal, N. and Thompson, H. (2015) 'The development of the mammalian outer and middle ear', *Journal of Anatomy*, 228(2), pp. 217–232. doi:10.1111/joa.12344.

Askew, C. *et al.* (2015) ‘Tmc gene therapy restores auditory function in deaf mice’, *Science Translational Medicine*, 7(295). doi:10.1126/scitranslmed.aab1996.

Bankoti, K. *et al.* (2021) ‘Advances and challenges in adeno-associated viral inner-ear gene therapy for sensorineural hearing loss’, *Molecular Therapy – Methods and Clinical Development*, 21, pp. 209–236. doi:10.1016/j.omtm.2021.03.005.

Barclay, M., Ryan, A.F. and Housley, G.D. (2011) ‘Type I vs type II spiral ganglion neurons exhibit differential survival and neuritogenesis during cochlear development’, *Neural Development*, 6(1). doi:10.1186/1749-8104-6-33.

Bardhan, T. *et al.* (2019) ‘GATA3 is required for the functional maturation of inner hair cells and their innervation in the mouse cochlea’, *The Journal of Physiology*, 597(13), pp. 3389–3406. doi:10.1113/jp277997.

Belova, L., Lavrov, A. and Smirnikhina, S. (2022) ‘Organoid transduction using recombinant adeno-associated viral vectors: Challenges and opportunities’, *BioEssays*, 44(9), p. 2200055. doi:10.1002/bies.202200055.

Berry, G.E. and Asokan, A. (2016) ‘Cellular transduction mechanisms of adeno-associated viral vectors’, *Current Opinion in Virology*, 21, pp. 54–60. doi:10.1016/j.coviro.2016.08.001.

Blanco-Kelly, F. *et al.* (2015) ‘Clinical aspects of usher syndrome and the ush2a gene in a cohort of 433 patients’, *JAMA Ophthalmology*, 133(2), p. 157. doi:10.1001/jamaophthalmol.2014.4498.

Brown, P.G. and Ruben, R.J. (1969) ‘The endocochlear potential in the shaker-1 (SH-1/SH-1) mouse’, *Acta Oto-Laryngologica*, 68(1–6), pp. 14–20. doi:10.3109/00016486909121538.

Caberlotto, E. *et al.* (2011) ‘Usher type 1G protein sans is a critical component of the tip-link complex, a structure controlling actin polymerization in stereocilia’, *Proceedings of the National Academy of Sciences*, 108(14), pp. 5825–5830. doi:10.1073/pnas.1017114108.

Castiglione, A. and Möller, C. (2022) ‘Usher syndrome’, *Audiology Research*, 12(1), pp. 42–65. doi:10.3390/audiolres12010005.

Chen, B., *et al.* (2019) The study of AAV9 expression in cochleae of mice at different ages. Zhonghua Er Bi Yan Hou Tou Jing Wai Ke Za Zhi. 2019 Oct 7;54(10):769-775. Chinese. doi: 10.3760/cma.j.issn.1673-0860.2019.10.012.

Chen, H. *et al.* (2018) ‘Aav-mediated NT-3 overexpression protects cochleae against noise-induced synaptopathy’, *Gene Therapy*, 25(4), pp. 251–259. doi:10.1038/s41434-018-0012-0.

Cheng, Y.-F. (2017) ‘ATOH1 regulation in the cochlea: More than just transcription’, *Journal of Zhejiang University-SCIENCE B*, 20(2), pp. 146–155. doi:10.1631/jzus.b1600438.

Chessum, L. *et al.* (2018) ‘Helios is a key transcriptional regulator of outer hair cell maturation’, *Nature*, 563(7733), pp. 696–700. doi:10.1038/s41586-018-0728-4.

Chien, W.W. *et al.* (2015) ‘Gene therapy for sensorineural hearing loss’, *Ear & Hearing*, 36(1), pp. 1–7. doi:10.1097/aud.0000000000000088.

Choudhury, S.R. *et al.* (2016) ‘Widespread central nervous system gene transfer and silencing after systemic delivery of novel aav-as vector’, *Molecular Therapy*, 24(4), pp. 726–735. doi:10.1038/mt.2015.231.

Clause, A. *et al.* (2014) ‘The precise temporal pattern of prehearing spontaneous activity is necessary for tonotopic map refinement’, *Neuron*, 82(4), pp. 822–835. doi:10.1016/j.neuron.2014.04.001.

Clause, A., Lauer, A.M. and Kandler, K. (2017) ‘Mice lacking the alpha9 subunit of the nicotinic acetylcholine receptor exhibit deficits in frequency difference limens and sound localization’, *Frontiers in Cellular Neuroscience*, 11. doi:10.3389/fncel.2017.00167.

Coate, T.M. and Kelley, M.W. (2013) ‘Making connections in the inner ear: Recent insights into the development of spiral ganglion neurons and their connectivity with

sensory hair cells', *Seminars in Cell & Developmental Biology*, 24(5), pp. 460–469. doi:10.1016/j.semcdb.2013.04.003.

Coffin, A.B. *et al.* (2010) 'Chemical screening for hair cell loss and protection in the zebrafish lateral line', *Zebrafish*, 7(1), pp. 3–11. doi:10.1089/zeb.2009.0639.

Colella, P. *et al.* (2013) 'MYOSIN VIIA deficiency results in reduced retinal activity which is improved by gene therapy', *PLoS ONE*, 8(8). doi:10.1371/journal.pone.0072027.

Colella, P., Ronzitti, G. and Mingozzi, F. (2018) 'Emerging issues in AAV-mediated in vivo gene therapy', *Molecular Therapy - Methods & Clinical Development*, 8, pp. 87–104. doi:10.1016/j.omtm.2017.11.007.

Corns, L.F. *et al.* (2018) 'Mechanotransduction is required for establishing and maintaining mature inner hair cells and regulating efferent innervation', *Nature Communications*, 9(1). doi:10.1038/s41467-018-06307-w.

Cui, C. *et al.* (2022) 'Precise detection of CRISPR-Cas9 editing in hair cells in the treatment of autosomal dominant hearing loss', *Molecular Therapy - Nucleic Acids*, 29, pp. 400–412. doi:10.1016/j.omtn.2022.07.016.

Dai, C. *et al.* (2017) 'Rhesus cochlear and vestibular functions are preserved after inner ear injection of saline volume sufficient for gene therapy delivery', *Journal of the Association for Research in Otolaryngology*, 18(4), pp. 601–617. doi:10.1007/s10162-017-0628-6.

Deafness and hearing loss (who.int) (accessed on 25 February 2023).

Delmaghani, S. and El-Amraoui, A. (2020) 'Inner ear gene therapies take off: Current promises and future challenges', *Journal of Clinical Medicine*, 9(7), p. 2309. doi:10.3390/jcm9072309.

Deol, M.S. (1956) 'The Anatomy and Development of the Mutants Pirouette, shaker-1 and Waltzer in the mouse', *Proceedings of the Royal Society of London. Series B - Biological Sciences*, 145(919), pp. 206–213. doi:10.1098/rspb.1956.0028.

Du, W. *et al.* (2023) ‘Rescue of auditory function by a single administration of AAV-TMPRSS3 gene therapy in aged mice of human recessive deafness DFNB8’, *Molecular Therapy* [Preprint]. doi:10.1016/j.ymthe.2023.05.005.

Duan, D. *et al.* (2003) ‘Trans-splicing vectors expand the packaging limits of adeno-associated virus for gene therapy applications’, *Viral Vectors for Gene Therapy*, pp. 287–308. doi:10.1385/1-59259-304-6:287.

Dudek, A.M. *et al.* (2020) ‘GPR108 is a highly conserved AAV entry factor’, *Molecular Therapy*, 28(2), pp. 367–381. doi:10.1016/j.ymthe.2019.11.005.

Durrbach, A. *et al.* (1996) ‘Brush border myosin-I truncated in the motor domain impairs the distribution and the function of endocytic compartments in an hepatoma cell line.’, *Proceedings of the National Academy of Sciences*, 93(14), pp. 7053–7058. doi:10.1073/pnas.93.14.7053.

Duvall, A.J., Sutherland, C.R. and Rhodes, V.T. (1969) ‘XXX ultrastructural changes in the cochlear duct following mechanical disruption of the organ of corti’, *Annals of Otology, Rhinology & Laryngology*, 78(2), pp. 342–357. doi:10.1177/000348946907800213.

Dyka, F.M. *et al.* (2014) ‘Dual adeno-associated virus vectors result in efficient in vitro and in vivo expression of an oversized gene, Myo7a’, *Human Gene Therapy Methods*, 25(2), pp. 166–177. doi:10.1089/hgtb.2013.212.

Earley, L.F. *et al.* (2020) ‘Adeno-associated virus serotype-specific inverted terminal repeat sequence role in vector transgene expression’, *Human Gene Therapy*, 31(3–4), pp. 151–162. doi:10.1089/hum.2019.274.

Eckrich, T. *et al.* (2012) ‘Development and function of the voltage-gated sodium current in immature mammalian cochlear inner hair cells’, *PLoS ONE*, 7(9). doi:10.1371/journal.pone.0045732.

Ehret, G. (1983) ‘Development of hearing and response behavior to sound stimuli: Behavioral studies11research in this chapter was supported by the Deutsche

Forschungsgemeinschaft (eh 53/1–5 and Ma 374/2.4).', *Development of Auditory and Vestibular Systems*, pp. 211–237. doi:10.1016/b978-0-12-594450-2.50012-5.

Felix, R.A., Gourévitch, B. and Portfors, C.V. (2018) 'Subcortical pathways: Towards a better understanding of auditory disorders', *Hearing Research*, 362, pp. 48–60. doi:10.1016/j.heares.2018.01.008.

Ferla, R. *et al.* (2023) 'Efficacy, pharmacokinetics, and safety in the mouse and primate retina of dual AAV vectors for Usher syndrome type 1B', *Molecular Therapy - Methods & Clinical Development*, 28, pp. 396–411. doi:10.1016/j.omtm.2023.02.002.

Fettiplace, R. (2017) 'Hair cell transduction, tuning, and synaptic transmission in the mammalian cochlea', *Comprehensive Physiology*, pp. 1197–1227. doi:10.1002/cphy.c160049.

Frank, M.M. and Goodrich, L.V. (2018) 'Talking back: Development of the Olivocochlear Efferent System', *WIREs Developmental Biology*, 7(6). doi:10.1002/wdev.324.

Frolenkov, G.I. *et al.* (2004) 'Genetic insights into the morphogenesis of inner ear hair cells', *Nature Reviews Genetics*, 5(7), pp. 489–498. doi:10.1038/nrg1377.

Fuchs, P.A. and Lauer, A.M. (2018) 'Efferent inhibition of the cochlea', *Cold Spring Harbor Perspectives in Medicine*, 9(5). doi:10.1101/cshperspect.a033530.

Gao, X. *et al.* (2017) 'Treatment of autosomal dominant hearing loss by in vivo delivery of genome editing agents', *Nature*, 553(7687), pp. 217–221. doi:10.1038/nature25164.

Géléoc, G.G.S. and El-Amraoui, A. (2020) 'Disease mechanisms and gene therapy for Usher syndrome', *Hearing Research*, 394, p. 107932. doi:10.1016/j.heares.2020.107932.

Geng, R. *et al.* (2017) 'Modeling and preventing progressive hearing loss in Usher Syndrome III', *Scientific Reports*, 7(1). doi:10.1038/s41598-017-13620-9.

Ghosh, A. *et al.* (2008) 'A hybrid vector system expands adeno-associated viral vector packaging capacity in a transgene-independent manner', *Molecular Therapy*, 16(1), pp. 124–130. doi:10.1038/sj.mt.6300322.

Ghosh, A., Yue, Y., & Duan, D. (2011). Efficient transgene reconstitution with hybrid dual AAV vectors carrying the minimized bridging sequences. *Human gene therapy*, *22*(1), 77–83. doi:10.1089/hum.2010.122.

Gibson, F. *et al.* (1995) 'A type VII myosin encoded by the mouse deafness gene shaker-1', *Nature*, 374(6517), pp. 62–64. doi:10.1038/374062a0.

Govindan, B., Bowser, R. and Novick, P. (1995) 'The role of MYO2, a yeast class V myosin, in vesicular transport.', *Journal of Cell Biology*, 128(6), pp. 1055–1068. doi:10.1083/jcb.128.6.1055.

Grati, M. and Kachar, B. (2011) 'Myosin VIIA and sans localization at stereocilia upper tip-link density implicates these Usher syndrome proteins in mechanotransduction', *Proceedings of the National Academy of Sciences*, 108(28), pp. 11476–11481. doi:10.1073/pnas.1104161108.

Grieger, J.C. and Samulski, R.J. (2005) 'Packaging capacity of adeno-associated virus serotypes: Impact of larger genomes on infectivity and Postentry Steps', *Journal of Virology*, 79(15), pp. 9933–9944. doi:10.1128/jvi.79.15.9933-9944.2005.

Gu, X. *et al.* (2019) 'Transduction of adeno-associated virus vectors targeting hair cells and supporting cells in the neonatal mouse cochlea', *Frontiers in Cellular Neuroscience*, 13. doi:10.3389/fncel.2019.00008.

Gu, X. *et al.* (2021) 'Prevention of acquired sensorineural hearing loss in mice by in vivo HTRA2 gene editing', *Genome Biology*, 22(1). doi:10.1186/s13059-021-02311-4.

Guo, J.-Y. *et al.* (2021) 'AAV8-mediated atoh1 overexpression induces dose-dependent regeneration of vestibular hair cells in adult mice', *Neuroscience Letters*, 747, p. 135679. doi:10.1016/j.neulet.2021.135679.

György, B. *et al.* (2019) 'Gene transfer with AAV9-PHP.B rescues hearing in a mouse model of Usher Syndrome 3a and transduces hair cells in a non-human primate', *Molecular Therapy - Methods & Clinical Development*, 13, pp. 1–13. doi:10.1016/j.omtm.2018.11.003.

Hafidi, A., Beurg, M. and Dulon, D. (2005) 'Localization and developmental expression of BK channels in mammalian cochlear hair cells', *Neuroscience*, 130(2), pp. 475–484. doi:10.1016/j.neuroscience.2004.09.038.

Han, Z. *et al.* (2022) 'AAV13 enables precise targeting of local neural populations', *International Journal of Molecular Sciences*, 23(21), p. 12806. doi:10.3390/ijms232112806.

Hartman, M.A. and Spudich, J.A. (2012) 'The myosin superfamily at a glance', *Journal of Cell Science*, 125(7), pp. 1627–1632. doi:10.1242/jcs.094300.

Hashimoto, K. *et al.* (2019) 'Protection from noise-induced cochlear synaptopathy by virally mediated overexpression of NT3', *Scientific Reports*, 9(1). doi:10.1038/s41598-019-51724-6.

Hasson, T. *et al.* (1995) 'Expression in cochlea and retina of myosin viia, the gene product defective in usher syndrome type 1B.', *Proceedings of the National Academy of Sciences*, 92(21), pp. 9815–9819. doi:10.1073/pnas.92.21.9815.

Heissler, S.M. and Manstein, D.J. (2011) 'Functional characterization of the human myosin-7a motor domain', *Cellular and Molecular Life Sciences*, 69(2), pp. 299–311. doi:10.1007/s00018-011-0749-8.

Holme, R.H. and Steel, K.P. (2002) 'Stereocilia defects in Waltzer (cdh23), shaker1 (Myo7a) and Double Waltzer/shaker1 mutant mice', *Hearing Research*, 169(1–2), pp. 13–23. doi:10.1016/s0378-5955(02)00334-9.

Holt, J.R. and Vandenberghe, L.H. (2012) 'Gene therapy for deaf mice goes viral', *Molecular Therapy*, 20(10), pp. 1836–1837. doi:10.1038/mt.2012.196.

Hu, C.-J. *et al.* (2020) ‘Efficient in utero gene transfer to the mammalian inner ears by the synthetic adeno-associated viral vector anc80l65’, *Molecular Therapy - Methods & Clinical Development*, 18, pp. 493–500. doi:10.1016/j.omtm.2020.06.019.

Hudry, E. *et al.* (2018) ‘Efficient gene transfer to the central nervous system by single-stranded ANC80L65’, *Molecular Therapy - Methods and Clinical Development*, 10, pp. 197–209. doi:10.1016/j.omtm.2018.07.006.

Hudspeth, A.J. (1989) ‘How the ear’s works work’, *Nature*, 341(6241), pp. 397–404. doi:10.1038/341397a0.

Im, G.J. (2012) ‘Role of nicotinic acetylcholine receptor on efferent inhibition in Cochlear Hair Cell’, *Korean Journal of Audiology*, 16(3), p. 108. doi:10.7874/kja.2012.16.3.108.

Ingham, P.W., Nakano, Y. and Seger, C. (2011) ‘Mechanisms and functions of hedgehog signalling across the metazoa’, *Nature Reviews Genetics*, 12(6), pp. 393–406. doi:10.1038/nrg2984.

Irving, S. *et al.* (2011) ‘Olivocochlear Efferent Control in sound localization and experience-dependent learning’, *The Journal of Neuroscience*, 31(7), pp. 2493–2501. doi:10.1523/jneurosci.2679-10.2011.

Isgrig, K. *et al.* (2019) ‘AAV2.7M8 is a powerful viral vector for inner ear gene therapy’, *Nature Communications*, 10(1). doi:10.1038/s41467-018-08243-1.

Isgrig, K. *et al.* (2022) ‘AAV8BP2 and AAV8 transduce the mammalian cochlear lateral wall and endolymphatic sac with high efficiency’, *Molecular Therapy - Methods & Clinical Development*, 26, pp. 371–383. doi:10.1016/j.omtm.2022.07.013.

Ivanchenko, M.V. *et al.* (2020) ‘Preclinical testing of AAV9-PHP.B for transgene expression in the non-human primate cochlea’, *Hearing Research*, 394, p. 107930. doi:10.1016/j.heares.2020.107930.

Ivanchenko, M.V. *et al.* (2021) ‘Aav-S: A versatile capsid variant for transduction of Mouse and primate inner ear’, *Molecular Therapy - Methods and Clinical Development*, 21, pp. 382–398. doi:10.1016/j.omtm.2021.03.019.

Ivanchenko, M.V. *et al.* (2023) ‘Mini-pcdh15 gene therapy rescues hearing in a mouse model of Usher syndrome type 1F’, *Nature Communications*, 14(1). doi:10.1038/s41467-023-38038-y.

Jacques, B.E., Dabdoub, A. and Kelley, M.W. (2012) ‘FGF signaling regulates development and transdifferentiation of hair cells and supporting cells in the basilar papilla’, *Hearing Research*, 289(1–2), pp. 27–39. doi:10.1016/j.heares.2012.04.018.

Jafari, Z., Kolb, B.E. and Mohajerani, M.H. (2019) ‘Age-related hearing loss and tinnitus, dementia risk, and auditory amplification outcomes’, *Ageing Research Reviews*, 56, p. 100963. doi:10.1016/j.arr.2019.100963.

Jeng, J. *et al.* (2019) ‘Hair cell maturation is differentially regulated along the tonotopic axis of the mammalian cochlea’, *The Journal of Physiology*, 598(1), pp. 151–170. doi:10.1113/jp279012.

Jeng, J. *et al.* (2020) ‘Biophysical and morphological changes in inner hair cells and their efferent innervation in the ageing Mouse Cochlea’, *The Journal of Physiology*, 599(1), pp. 269–287. doi:10.1113/jp280256.

Jeng, J.-Y. *et al.* (2022) ‘AAV-mediated rescue of EPS8 expression in vivo restores hair-cell function in a mouse model of recessive deafness’, *Molecular Therapy - Methods & Clinical Development*, 26, pp. 355–370. doi:10.1016/j.omtm.2022.07.012.

Johnson, S.L. *et al.* (2016) ‘Connexin-mediated signaling in nonsensory cells is crucial for the development of sensory inner hair cells in the mouse cochlea’, *The Journal of Neuroscience*, 37(2), pp. 258–268. doi:10.1523/jneurosci.2251-16.2016.

Johnson, S.L. *et al.* (2019) ‘Hair cell afferent synapses: Function and dysfunction’, *Cold Spring Harbor Perspectives in Medicine*, 9(12). doi:10.1101/cshperspect.a033175.

Kearney, G. *et al.* (2019) ‘Developmental synaptic changes at the transient olivocochlear-inner hair cell synapse’, *The Journal of Neuroscience*, pp. 2746–18. doi:10.1523/jneurosci.2746-18.2019.

Kelley, M.W. (2006) ‘Regulation of cell fate in the sensory epithelia of the inner ear’, *Nature Reviews Neuroscience*, 7(11), pp. 837–849. doi:10.1038/nrn1987.

Kiernan, A.E. (2013) ‘Notch signaling during cell fate determination in the inner ear’, *Seminars in Cell & Developmental Biology*, 24(5), pp. 470–479. doi:10.1016/j.semcdb.2013.04.002.

Klotz-Weigand, L. and Enz, R. (2022) ‘Metabotropic glutamate receptors at ribbon synapses in the retina and cochlea’, *Cells*, 11(7), p. 1097. doi:10.3390/cells11071097.

Kong, J.-H., Adelman, J.P. and Fuchs, P.A. (2008) ‘Expression of the SK2 calcium-activated potassium channel is required for cholinergic function in mouse cochlear hair cells’, *The Journal of Physiology*, 586(22), pp. 5471–5485. doi:10.1113/jphysiol.2008.160077.

Korver, A.M. *et al.* (2017) ‘Congenital hearing loss’, *Nature Reviews Disease Primers*, 3(1). doi:10.1038/nrdp.2016.94.

Krenacs, L. *et al.* (2009) ‘Heat-induced antigen retrieval for immunohistochemical reactions in routinely processed paraffin sections’, *Immunocytochemical Methods and Protocols*, pp. 103–119. doi:10.1007/978-1-59745-324-0_14.

Kros, C.J. *et al.* (2001) ‘Reduced climbing and increased slipping adaptation in cochlear hair cells of mice with Myo7a mutations’, *Nature Neuroscience*, 5(1), pp. 41–47. doi:10.1038/nn784.

Kros, C.J., Ruppersberg, J.P. and Rüsch, A. (1998) ‘Expression of a potassium current in inner hair cells during development of hearing in mice’, *Nature*, 394(6690), pp. 281–284. doi:10.1038/28401.

Kuhn, S. *et al.* (2011) ‘Mir-96 regulates the progression of differentiation in mammalian cochlear inner and outer hair cells’, *Proceedings of the National Academy of Sciences*, 108(6), pp. 2355–2360. doi:10.1073/pnas.1016646108.

Landegger, L.D. *et al.* (2017) ‘A synthetic AAV vector enables safe and efficient gene transfer to the mammalian inner ear’, *Nature Biotechnology*, 35(3), pp. 280–284. doi:10.1038/nbt.3781.

Lauer, A.M. *et al.* (2012) ‘Efferent synapses return to inner hair cells in the aging cochlea’, *Neurobiology of Aging*, 33(12), pp. 2892–2902. doi:10.1016/j.neurobiolaging.2012.02.007.

Le Quesne Stabej, P. *et al.* (2011) ‘Comprehensive sequence analysis of nine Usher syndrome genes in the UK national collaborative usher study’, *Journal of Medical Genetics*, 49(1), pp. 27–36. doi:10.1136/jmedgenet-2011-100468.

Lee, J. *et al.* (2020) ‘Efficient viral transduction in mouse inner ear hair cells with utricle injection and AAV9-PHP.B’, *Hearing Research*, 394, p. 107882. doi:10.1016/j.heares.2020.107882.

Lee, M.Y. and Park, Y.-H. (2018) ‘Potential of gene and cell therapy for inner ear hair cells’, *BioMed Research International*, 2018, pp. 1–11. doi:10.1155/2018/8137614.

Lee, Y.-S., Liu, F. and Segil, N. (2006) ‘A morphogenetic wave of p27Kip1 ranscription directs cell cycle exit during organ of Corti Development’, *Development*, 133(15), pp. 2817–2826. doi:10.1242/dev.02453.

Lefèvre, G. *et al.* (2008) ‘A core cochlear phenotype in USH1 mouse mutants implicates fibrous links of the hair bundle in its cohesion, orientation and differential growth’, *Development*, 135(8), pp. 1427–1437. doi:10.1242/dev.012922.

Li, S. *et al.* (2020) ‘Myosin-VIIA is expressed in multiple isoforms and essential for tensioning the hair cell mechanotransduction complex’, *Nature Communications*, 11(1). doi:10.1038/s41467-020-15936-z.

Lillo, C. *et al.* (2003) ‘Mouse models for Usher Syndrome 1B’, *Advances in Experimental Medicine and Biology*, pp. 143–150. doi:10.1007/978-1-4615-0067-4_18.

Lord, E.M. (1929) ‘Shaker, a new mutation of the house mouse (mus musculus)’, *The American Naturalist*, 63(688), pp. 435–442. doi:10.1086/280276.

Maass, J.C. *et al.* (2016) ‘Transcriptomic analysis of mouse cochlear supporting cell maturation reveals large-scale changes in notch responsiveness prior to the onset of hearing’, *PLOS ONE*, 11(12). doi:10.1371/journal.pone.0167286.

Maguire, C.A. and Corey, D.P. (2020) ‘Viral vectors for gene delivery to the inner ear’, *Hearing Research*, 394, p. 107927. doi:10.1016/j.heares.2020.107927.

Marcotti, W. (2012) ‘Functional Assembly of mammalian cochlear hair cells’, *Experimental Physiology*, 97(4), pp. 438–451. doi:10.1113/expphysiol.2011.059303.

Marcotti, W. and Masetto, S. (2010) ‘Hair cells’, *eLS* [Preprint]. doi:10.1002/9780470015902.a0000181.pub2.

Marcotti, W. *et al.* (2003) ‘Sodium and calcium currents shape action potentials in immature mouse inner hair cells’, *The Journal of Physiology*, 552(3), pp. 743–761. doi:10.1113/jphysiol.2003.043612.

Marcotti, W. *et al.* (2006) ‘Tmc1 is necessary for normal functional maturation and survival of inner and outer hair cells in the mouse cochlea’, *The Journal of Physiology*, 574(3), pp. 677–698. doi:10.1113/jphysiol.2005.095661.

Marcotti, W., Johnson, S.L. and Kros, C.J. (2004) ‘Effects of intracellular stores and extracellular Ca2+ on Ca2-activated k+ currents in mature mouse inner hair cells’, *The Journal of Physiology*, 557(2), pp. 613–633. doi:10.1113/jphysiol.2003.060137.

Marcotti, W., Johnson, S.L. and Kros, C.J. (2004a) ‘A transiently expressed SK current sustains and modulates action potential activity in immature mouse inner hair cells’, *The Journal of Physiology*, 560(3), pp. 691–708. doi:10.1113/jphysiol.2004.072868.

Marcovich, I. *et al.* (2022) ‘Optimized AAV vectors for TMC1 gene therapy in a humanized mouse model of DFNB7/11’, *Biomolecules*, 12(7), p. 914. doi:10.3390/biom12070914.

Mathur, P. and Yang, J. (2015) ‘Usher Syndrome: Hearing loss, retinal degeneration and associated abnormalities’, *Biochimica et Biophysica Acta (BBA) - Molecular Basis of Disease*, 1852(3), pp. 406–420. doi:10.1016/j.bbadis.2014.11.020.

McClements, M. E., & MacLaren, R. E. (2017). Adeno-associated Virus (AAV) Dual Vector Strategies for Gene Therapy Encoding Large Transgenes. *The Yale journal of biology and medicine*, *90*(4), 611–623.

McPherson, D.R. (2018) ‘Sensory hair cells: An introduction to structure and physiology’, *Integrative and Comparative Biology*, 58(2), pp. 282–300. doi:10.1093/icb/icy064.

Miller, K.A. *et al.* (2012) ‘Inner ear morphology is perturbed in two novel mouse models of recessive deafness’, *PLoS ONE*, 7(12). doi:10.1371/journal.pone.0051284.

Nance, M.E. and Duan, D. (2015) ‘Perspective on adeno-associated virus capsid modification for Duchenne muscular dystrophy gene therapy’, *Human Gene Therapy*, 26(12), pp. 786–800. doi:10.1089/hum.2015.107.

Nisenbaum, E. *et al.* (2021) ‘Review of genotype-phenotype correlations in Usher syndrome’, *Ear & Hearing*, 43(1), pp. 1–8. doi:10.1097/aud.0000000000001066.

Nouvian, R. *et al.* (2006) ‘Structure and function of the hair cell ribbon synapse’, *The Journal of Membrane Biology*, 209(2–3), pp. 153–165. doi:10.1007/s00232-005-0854-4.

Ó Maoiléidigh, D. and Ricci, A.J. (2019) ‘A bundle of mechanisms: Inner-ear hair-cell mechanotransduction’, *Trends in Neurosciences*, 42(3), pp. 221–236. doi:10.1016/j.tins.2018.12.006.

Oestreicher, D. *et al.* (2021) ‘CABP2-gene therapy restores inner hair cell calcium currents and improves hearing in a DFNB93 mouse model’, *Frontiers in Molecular Neuroscience*, 14. doi:10.3389/fnmol.2021.689415.

Ohta, S. *et al.* (2016) ‘BMP regulates regional gene expression in the dorsal otocyst through canonical and non-canonical intracellular pathways’, *Development* [Preprint]. doi:10.1242/dev.137133.

Omichi, R. *et al.* (2020) ‘Hair cell transduction efficiency of single- and dual-AAV serotypes in adult murine cochleae’, *Molecular Therapy - Methods and Clinical Development*, 17, pp. 1167–1177. doi:10.1016/j.omtm.2020.05.007.

Pan, B. *et al.* (2017) ‘Gene therapy restores auditory and vestibular function in a mouse model of Usher syndrome type 1c’, *Nature Biotechnology*, 35(3), pp. 264–272. doi:10.1038/nbt.3801.

Pan, N. *et al.* (2011) ‘Conditional deletion of ATOH1 using pax2-CRE results in viable mice without differentiated cochlear hair cells that have lost most of the organ of corti’, *Hearing Research*, 275(1–2), pp. 66–80. doi:10.1016/j.heares.2010.12.002.

Perabo, L. *et al.* (2006) ‘Heparan sulfate proteoglycan binding properties of adeno-associated virus retargeting mutants and consequences for their in vivo tropism’, *Journal of Virology*, 80(14), pp. 7265–7269. doi:10.1128/jvi.00076-06.

Petit, C. and Richardson, G.P. (2009) ‘Linking genes underlying deafness to hair-bundle development and function’, *Nature Neuroscience*, 12(6), pp. 703–710. doi:10.1038/nn.2330.

Petrs-Silva, H. *et al.* (2009) ‘High-efficiency transduction of the mouse retina by tyrosine-mutant AAV serotype vectors’, *Molecular Therapy*, 17(3), pp. 463–471. doi:10.1038/mt.2008.269.

Pietersz, K.L. *et al.* (2020) ‘Transduction patterns in the CNS following various routes of AAV-5-mediated gene delivery’, *Gene Therapy*, 28(7–8), pp. 435–446. doi:10.1038/s41434-020-0178-0.

Pillay, S. *et al.* (2016) ‘An essential receptor for adeno-associated virus infection’, *Nature*, 530(7588), pp. 108–112. doi:10.1038/nature16465.

Prosser, H.M. *et al.* (2008) ‘Mosaic complementation demonstrates a regulatory role for myosin viia in actin dynamics of stereocilia’, *Molecular and Cellular Biology*, 28(5), pp. 1702–1712. doi:10.1128/mcb.01282-07.

Pujol, R., Lavigne-Rebillard, M. and Lenoir, M. (1998) ‘Development of sensory and neural structures in the mammalian cochlea’, *Development of the Auditory System*, pp. 146–192. doi:10.1007/978-1-4612-2186-9_4.

Qiu, X. and Müller, U. (2018) ‘Mechanically gated ion channels in mammalian hair cells’, *Frontiers in Cellular Neuroscience*, 12. doi:10.3389/fncel.2018.00100.

Rankovic, V. *et al.* (2021) ‘Overloaded adeno-associated virus as a novel gene therapeutic tool for otoferlin-related deafness’, *Frontiers in Molecular Neuroscience*, 13. doi:10.3389/fnmol.2020.600051.

Raphael, Y. and Altschuler, R.A. (2003) ‘Structure and innervation of the cochlea’, *Brain Research Bulletin*, 60(5–6), pp. 397–422. doi:10.1016/s0361-9230(03)00047-9.

Rees, H.A. and Liu, D.R. (2018) ‘Base editing: Precision chemistry on the genome and transcriptome of living cells’, *Nature Reviews Genetics*, 19(12), pp. 770–788. doi:10.1038/s41576-018-0059-1.

Ren, Y., Landegger, L.D. and Stankovic, K.M. (2019) ‘Gene therapy for human sensorineural hearing loss’, *Frontiers in Cellular Neuroscience*, 13. doi:10.3389/fncel.2019.00323.

Dulaurier-Reynaud, R. and Decressac, M. (2020) ‘PHP.B/EB vectors bring new successes to gene therapy for brain diseases’, *Frontiers in Bioengineering and Biotechnology*, 8. doi:10.3389/fbioe.2020.582979.

Riccomagno, M.M. *et al.* (2002) ‘Specification of the mammalian cochlea is dependent on sonic hedgehog’, *Genes & Development*, 16(18), pp. 2365–2378. doi:10.1101/gad.1013302.

Sahly, I. *et al.* (1997) 'Expression of myosin VIIA during mouse embryogenesis', *Anatomy and Embryology*, 196(2), pp. 159–170. doi:10.1007/s004290050088.

Sai, X. and Ladher, R.K. (2015) 'Early steps in inner ear development: Induction and morphogenesis of the Otic placode', *Frontiers in Pharmacology*, 6. doi:10.3389/fphar.2015.00019.

Samaranch, L. *et al.* (2014) 'AAV9-mediated expression of a non-self protein in nonhuman primate central nervous system triggers widespread neuroinflammation driven by antigen-presenting cell transduction', *Molecular Therapy*, 22(2), pp. 329–337. doi:10.1038/mt.2013.266.

Saw, Jr., D., STEEL, K.P. and BROWN, S.D.M. (1997) 'Shaker Mice and a peek into the House of usher.', *Experimental Animals*, 46(1), pp. 1–9. doi:10.1538/expanim.46.1.

Schwander, M. *et al.* (2009) 'A novel allele of myosin viia reveals a critical function for the C-terminal FERM domain for melanosome transport in retinal pigment epithelial cells', *The Journal of Neuroscience*, 29(50), pp. 15810–15818. doi:10.1523/jneurosci.4876-09.2009.

Seal, R.P. *et al.* (2008) 'Sensorineural deafness and seizures in mice lacking vesicular glutamate transporter 3', *Neuron*, 57(2), pp. 263–275. doi:10.1016/j.neuron.2007.11.032.

Self, T. *et al.* (1998) 'Shaker-1 mutations reveal roles for myosin VIIA in both development and function of cochlear hair cells', *Development*, 125(4), pp. 557–566. doi:10.1242/dev.125.4.557.

Senften, M. *et al.* (2006) 'Physical and functional interaction between protocadherin 15 and myosin viia in mechanosensory hair cells', *The Journal of Neuroscience*, 26(7), pp. 2060–2071. doi:10.1523/jneurosci.4251-05.2006.

Sheridan, C. (2023) 'Why gene therapies must go virus-free', *Nature Biotechnology*, 41(6), pp. 737–739. doi:10.1038/s41587-023-01824-6.

Shukla, A. *et al.* (2020) ‘Hearing loss, loneliness, and Social Isolation: A systematic review’, *Otolaryngology–Head and Neck Surgery*, 162(5), pp. 622–633. doi:10.1177/0194599820910377.

Sun, Y. *et al.* (2011) ‘Novel missense mutations in MYO7A underlying postlingual high- or low-frequency non-syndromic hearing impairment in two large families from China’, *Journal of Human Genetics*, 56(1), pp. 64–70. doi:10.1038/jhg.2010.147.

Suzuki, J. *et al.* (2017) ‘Cochlear gene therapy with ancestral AAV in adult mice: Complete transduction of inner hair cells without cochlear dysfunction’, *Scientific Reports*, 7(1). doi:10.1038/srep45524.

Tan, F. *et al.* (2019) ‘Aav-ie enables safe and efficient gene transfer to inner ear cells’, *Nature Communications*, 10(1). doi:10.1038/s41467-019-11687-8.

Tang, D. *et al.* (2023) ‘A narrative review of lifestyle risk factors and the role of oxidative stress in age-related hearing loss’, *Antioxidants*, 12(4), p. 878. doi:10.3390/antiox12040878.

Tao, Y. *et al.* (2018) ‘Delivery of adeno-associated virus vectors in adult mammalian inner-ear cell subtypes without auditory dysfunction’, *Human Gene Therapy*, 29(4), pp. 492–506. doi:10.1089/hum.2017.120.

Tertrais, M. *et al.* (2019) ‘Viral transfer of mini-otoferlins partially restores the fast component of exocytosis and uncovers ultrafast endocytosis in auditory hair cells of otoferlin knock-out mice’, *The Journal of Neuroscience*, pp. 1550–18. doi:10.1523/jneurosci.1550-18.2018.

Trapani, I. *et al.* (2013) ‘Effective delivery of large genes to the retina by dual AAV vectors’, *EMBO Molecular Medicine*, 6(2), pp. 194–211. doi:10.1002/emmm.201302948.

Usher syndrome National Institute of Deafness and Other Communication Disorders. Available at: https://www.nidcd.nih.gov/health/usher-syndrome (Accessed: 29 June 2023).

van Beelen, E.S. *et al.* (2022) ‘Efficient viral transduction in fetal and adult human inner ear explants with AAV9-PHP.B vectors’, *Biomolecules*, 12(6), p. 816. doi:10.3390/biom12060816.

Verdera, H.C., Kuranda, K. and Mingozzi, F. (2020) ‘AAV vector immunogenicity in humans: A long journey to successful Gene Transfer’, *Molecular Therapy*, 28(3), pp. 723–746. doi:10.1016/j.ymthe.2019.12.010.

Verdoodt, D. *et al.* (2021) ‘Transduction efficiency and immunogenicity of viral vectors for cochlear gene therapy: A systematic review of Preclinical Animal Studies’, *Frontiers in Cellular Neuroscience*, 15. doi:10.3389/fncel.2021.728610.

Wang, D. and Zhou, J. (2021) ‘The kinocilia of cochlear hair cells: Structures, functions, and diseases’, *Frontiers in Cell and Developmental Biology*, 9. doi:10.3389/fcell.2021.715037.

Wang, J. *et al.* (2022) ‘Efficient delivery of adeno-associated virus into inner ear in vivo through trans-stapes route in adult Guinea pig’, *Human Gene Therapy*, 33(13–14), pp. 719–728. doi:10.1089/hum.2021.236.

Wang, J. *et al.* (2023) ‘Gene therapy: An emerging therapy for hair cells regeneration in the cochlea’, *Frontiers in Neuroscience*, 17. doi:10.3389/fnins.2023.1177791.

Wangemann, P. and Schacht, J. (1996) ‘Homeostatic mechanisms in the cochlea’, *Springer Handbook of Auditory Research*, pp. 130–185. doi:10.1007/978-1-4612-0757-3_3.

Well, D. *et al.* (1995) ‘Defective myosin VIIA gene responsible for Usher syndrome type Ib’, *Nature*, 374(6517), pp. 60–61. doi:10.1038/374060a0.

Wersinger, E. and Fuchs, P.A. (2011) ‘Modulation of hair cell efferents’, *Hearing Research*, 279(1–2), pp. 1–12. doi:10.1016/j.heares.2010.12.018.

Whitfield, T.T. (2015) ‘Development of the inner ear’, *Current Opinion in Genetics & Development*, 32, pp. 112–118. doi:10.1016/j.gde.2015.02.006.

Wiley, L.A. *et al.* (2018) 'Assessment of adeno-associated virus serotype tropism in human retinal explants', *Human Gene Therapy*, 29(4), pp. 424–436. doi:10.1089/hum.2017.179.

World Health Organization. (2023). Deafness and hearing loss. Available at: https://www.who.int/news-room/fact-sheets/detail/deafness-and-hearing-loss (Accessed: 26 May 2023).

Wright, T.J. and Mansour, S.L. (2003) 'FGF signaling in ear development and Innervation', *Current Topics in Developmental Biology*, pp. 225–259. doi:10.1016/s0070-2153(03)57008-9.

Wu, D.K. and Kelley, M.W. (2012) 'Molecular mechanisms of inner ear development', *Cold Spring Harbor Perspectives in Biology*, 4(8). doi:10.1101/cshperspect.a008409.

Wu, P.Z. *et al.* (2019) 'Primary neural degeneration in the human cochlea: Evidence for hidden hearing loss in the aging ear', *Neuroscience*, 407, pp. 8–20. doi:10.1016/j.neuroscience.2018.07.053.

Wu, Z., Yang, H. and Colosi, P. (2010) 'Effect of genome size on AAV vector packaging', *Molecular Therapy*, 18(1), pp. 80–86. doi:10.1038/mt.2009.255.

Xiao, Q. *et al.* (2022) 'Rescue of autosomal dominant hearing loss by in vivo delivery of mini dcas13x-derived RNA base editor', *Science Translational Medicine*, 14(654). doi:10.1126/scitranslmed.abn0449.

Xue, Y. *et al.* (2022) 'Gene editing in a myo6 semi-dominant mouse model rescues auditory function', *Molecular Therapy*, 30(1), pp. 105–118. doi:10.1016/j.ymthe.2021.06.015.

Yang, Y. *et al.* (2009) 'A ferm domain autoregulates drosophila myosin 7A activity', *Proceedings of the National Academy of Sciences*, 106(11), pp. 4189–4194. doi:10.1073/pnas.0808682106.

Yoshimura, H. *et al.* (2018) 'Enhanced viral-mediated cochlear gene delivery in adult mice by combining canal fenestration with round window membrane inoculation', *Scientific Reports*, 8(1). doi:10.1038/s41598-018-21233-z.

Yoshimura, H. *et al.* (2019) 'Targeted allele suppression prevents progressive hearing loss in the mature murine model of human TMC1 deafness', *Molecular Therapy*, 27(3), pp. 681–690. doi:10.1016/j.ymthe.2018.12.014.

Yu, I.-M. *et al.* (2017) 'Myosin 7 and its adaptors link cadherins to actin', *Nature Communications*, 8(1). doi:10.1038/ncomms15864.

Zachary, S.P. and Fuchs, P.A. (2015) 'Re-emergent inhibition of cochlear inner hair cells in a mouse model of hearing loss', *Journal of Neuroscience*, 35(26), pp. 9701–9706. doi:10.1523/jneurosci.0879-15.2015.

Zanzibar commemorates World Hearing Day | WHO | Regional Office for Africa (accessed on 25 June 2023).

Zhang, K.D. and Coate, T.M. (2017) 'Recent advances in the development and function of type II spiral ganglion neurons in the mammalian inner ear', *Seminars in Cell & Developmental Biology*, 65, pp. 80–87. doi:10.1016/j.semcdb.2016.09.017.

Zhao, X. *et al.* (2022) 'Gene therapy restores auditory functions in an adult VGLUT3 knockout mouse model', *Human Gene Therapy*, 33(13–14), pp. 729–739. doi:10.1089/hum.2022.062.

Zhao, Y. *et al.* (2022a) 'Approaches and vectors for efficient cochlear gene transfer in adult mouse models', *Biomolecules*, 13(1), p. 38. doi:10.3390/biom13010038.

Zheng, J. *et al.* (2000) 'Prestin is the motor protein of cochlear outer hair cells', *Nature*, 405(6783), pp. 149–155. doi:10.1038/35012009.

Zincarelli, C. *et al.* (2008) 'Analysis of AAV serotypes 1–9 mediated gene expression and tropism in mice after Systemic Injection', *Molecular Therapy*, 16(6), pp. 1073–1080. doi:10.1038/mt.2008.76.